eman ta zabal zazu

Universidad del País Vasco

Euskal Herriko Unibertsitatea

Design of chitosan-based materials for food applications

Iratxe Zarandona Rodríguez

Department of Chemical and Environmental Engineering

Donostia-San Sebastián 2022

eman ta zabal zazu

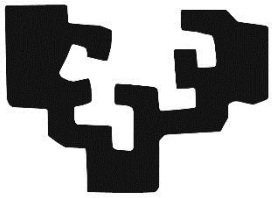

Universidad del País Vasco

Euskal Herriko Unibertsitatea

Design of chitosan-based materials for food applications

Iratxe Zarandona Rodríguez

Supervisors:

Koro de la Caba & Pedro Guerrero

Department of Chemical and Environmental Engineering

Donostia- San Sebastián, 2022

Maite nautenei,

"Investigar es ver lo que todo el mundo ha visto, y pensar lo que nadie más ha pensado"

Albert Szent-Györgyi

"Caminante, son tus huellas
el camino y nada más;
Caminante, no hay camino,
se hace camino al andar."

Antonio Machado

Agradecimientos

Escribiendo las últimas líneas de la tesis, me vienen a mi memoria mil recuerdos de esta etapa, que ha sido a partes iguales bonita e intensa. Durante estos 4 años he reído, llorado, me he caído y he vuelto a levantarme, pero, sobre todo, he aprendido mucho profesional y personalmente.

No podría terminar esta tesis sin agradecer el apoyo que he recibido a todas esas personas que me han acompañado en esta aventura.

Primero de todo quería agradecer a Koro de la Caba y Pedro Guerrero, mis directores de la tesis. Ha sido un placer haberos conocido y poder aprender tanto de vosotros. Gracias por la confianza que depositasteis en mí, por el trabajo y la dedicación que habéis puesto en mi tesis y por ser buenos guías. Sin vosotros este trabajo no hubiera sido lo mismo.

Además, quería agradecer a todas esas personas que me han acogido en sus laboratorios y arropándome como una más de su grupo.

A Maite Dueñas y Ana Isabel Puertas, de la Facultad de Química, por descubrirme el mundo de la microbiología. Gracias por tener la paciencia de enseñarme un trabajo tan bonito y meticuloso.

A Juan Maté y Carmen Barba, por acogerme tan bien en vuestro grupo en la Universidad Pública de Navarra (UPNA) y enseñarme sobre encapsulación.

A Carmen Gómez Guillén, Pilar Montero y Elvira López Caballero del Instituto de Ciencia y Tecnología de Alimentos y Nutrición (ICTAN-

CSIC), sois una inspiración. Y a todo el equipo, por arrimar el hombro en sacar adelante el gran trabajo que hicimos como si fuera propio.

A Antonio Guerrero, Carlos Bengoechea y Estefanía Álvarez, del departamento de Ingeniería Química de la Universidad de Sevilla, es cierto que Sevilla tiene un color especial, aunque fuera en pandemia. Me sentí muy arropada por todo el grupo y fue un gusto aprender de reología con vosotros.

A Senentxu Lanceros, Daniela Correia y Carlos da Silva, de la Universidade do Minho en Braga, fue un placer trabajar con vosotros. Gracias al grupo por la cálida acogida que recibí y a Ricardo Lima por su ingenio para fabricar una campana de vacío con cuatro piezas del laboratorio.

Asimismo, quería agradecer a AZTI-Tecnalia por el suministro de exopolisacaridos para emplearlos como aditivos en los films de quitosano y a Nguyen Cong Minh y Trang Si Trung de la Nha Trang University de Vietnam por suministrarnos el quitosano obtenido a partir de langostinos.

Por otro lado, quería agradecer al Gobierno Vasco, en especial al Departamento de Desarrollo Económico, Sostenibilidad y Medio Ambiente, por el contrato predoctoral (22-2018-00078), y el posterior contrato de investigación (KKKK-2021/00131). También agradecer a los servicios generales de la UPV/EHU, SGIker.

Por último, quería agradecer a todas esas personas que han estado al pie del cañón todos los días a mi lado apoyándome. A mis compañeras del grupo Biomat y a Joseba, que habéis estado para todo, sois un tesoro. A

Amaia, Fabio y Rut, por los buenos ratos que he pasado con vosotros en las horas del café y la comida, en especial a Rut, por las quedadas “equipo investigación” en las que siempre nos ocurren cosas poco comunes. A mis amigos y familia, que siempre andáis interesándoos en mis avances, aunque no entendáis ni papa. Batez ere Anderri, une onetan eta txarretan nirekin egoteagatik, nire ondoan baldintzarik gabe egoteagatik eta estualdietan lasaitzen jakiteagatik. Y por supuesto, a mis padres, por creer en mí, su apoyo infinito y su comprensión. Gracias a todos!

Summary

In the food industry, large amounts of non-biodegradable and non-renewable materials are produced for food packaging and the vast majority are single-use, leading to environmental problems specially after disposal. At the same time, biopolymers are gaining interest due to its natural character and biodegradability, becoming a raw material for the production of alternative materials. In this context, chitosan is a polysaccharide obtained from the deacetylation of chitin, extracted from biowastes from crustaceans, mollusks, fungi and insects. Due to its good mechanical properties, capacity of selective permeability to O_2 and CO_2, and antimicrobial activity, chitosan is a suitable material for food packaging applications. Therefore, the combination of chitosan with other bioactive compounds that supplement the chitosan matrix properties could be an alternative for food packaging materials to reduce the use of non-renewable and non-biodegradable materials.

In this context, the aim of this thesis was to develop chitosan-based materials processed by different methods and adding several bioactive compounds that improved the properties of the material intended for food applications.

The thesis is divided into 10 chapters. **Chapter 1** is an overview of chitosan-based films and coatings for food packaging. Processing methods and the addition of natural bioactives for active and intelligent packaging is explained in this chapter. In the next three chapters, chitosan films were prepared by solution casting, but different additives were employed in each chapter. In **Chapter 2** exopolysaccharides from bacteria extracted from deep waters were used as fillers. Physicochemical, optical, barrier and mechanical properties were evaluated to see the influence of exopolysaccharides on the functional properties of chitosan. In **Chapter 3,** cyclodextrins were used to encapsulate 2-phenyl ethanol in order to keep it stable and prevent volatilization. In **Chapter 4** gallic acid was added, which has antioxidant and antimicrobial properties, thus adding new capacities to the chitosan film. In addition to analyzing the physicochemical, mechanical and optical properties, the antioxidant and antimicrobial capacity of the material was analyzed, in order to determine the suitability of the films for active food packaging.

Taking the results of Chapter 4 into account and with the motivation to implement the materials in active food packaging applications, the shelf-life extension of horse mackerel fillets with chitosan coatings with

gallic acid was studied in **Chapter 5**. After that, in **Chapter 6,** the development of chitosan films was carried out by compression molding, using citric acid as crosslinker and aloe vera as bioactive. Then, in **Chapter 7,** pectin-chitosan hydrogels were used to prepare films by 3D printing. In order to determine the best hydrogel for 3D printing, the systems were assessed from a rheological perspective. Physicochemical and mechanical characterization of 3D printed scaffolds was carried out. , In **Chapter 8** chitosan films with Fe_3O_4 magnetic nanoparticles were prepared by solution casting and analyzed for intelligent food packaging. The films were magnetically and electronically evaluated andphysicochemical, mechanical and antimicrobial properties were measured.

Finally, general conclusions of this doctoral thesis are presented in **Chapter 9,** and the list of references cited along this work is showed in **Chapter 10**.

Objectives

The main objective of this doctoral thesis was to develop chitosan-based films and coatings, using different processing methods and supplementing with additives that enhanced the properties of the material, especially for food packaging applications.

The specific objectives of the study can be summarized as follows:

- Analyze the physicochemical, mechanical, barrier, optical, morphological and thermal properties of chitosan-based materials processed by solution casting, deeping, compression molding, and 3D printing.
- Assess the effects of the addition of exopolysaccharides, 2-phenyl ethanol, gallic acid, *Aloe vera* and Fe_3O_4 magnetic nanoparticles in the chitosan matrix for food packaging applications.
- Valorize marine resources from deep water bacteria for the extraction of exopolysaccharides and used them as fillers for chitosan films.
- Evaluate the use of cyclodextrins as encapsulation agents for 2-phenyl ethanol bioactive protection.

- Verify the shelf-life extension of horse mackerel fillets during chilling storage with different chitosan coatings supplemented with gallic acid as active compound.
- Prepare citric acid crosslinked chitosan films by compression molding and analyze the effect of crosslinking and the release of *Aloe vera.*
- Assess the effect of Fe_3O_4 magnetic nanoparticles in chitosan-pectin films for intelligent packaging.

Index

Chapter

1

Introduction

1.1. Valorization of biowaste for food application

In 2015, the United Nations Assembly approved the 2030 Agenda, a plan of action to promote sustainable development in 17 universal goals (Sustainable Development Goals, SDGs) (Agenda 2030, 2015). Among the main objectives, it pursues a transition of economic, productive and consumption models towards sustainability. In this sense, the valorization of food waste into value-added products has become a spearhead for the progression towards a circular economy.

In this context, some opportunities can be generated from by-products from the slaughter of livestock and the processing of fish. In this regard, industrial processing of livestock generates waste viscera, fat, skin, bones and feet, while industrial fishing waste is mainly composed of muscle, skin, fins, bones, viscera and scales, making these by-products rich sources of various valuable materials, such as proteins, polysaccharides, lipids, minerals, nutrients and flavors (Lee et al., 2020; Martínez-Alvarez, Chamorro, & Brenes, 2015; Meena et al., 2020). In this sense, natural polymers represent a challenging opportunity for the development of sustainable materials due to their structural and physical characteristics,

as well as their safety, availability, biocompatibility and biodegradability (Nasrollahzadeh et al., 2021).

Polysaccharides and proteins provide many possibilities for food purposes. They can be used as encapsulating agents of flavors, texturizing agents or food thickeners, as well as for food packaging or delivery of bioactive compounds since they show good barrier and mechanical properties for packaging materials (Bealer et al., 2020; Haghighi et al., 2020).

1.2. Chitosan extraction and properties

Chitosan is a copolymer of D-glucosamine and N-acetyl-D-glucosamine (Figure 1.1), obtained by the deacetylation of chitin (Rasente et al., 2016). It is nontoxic, biocompatible and biodegradable, and it can provide antimicrobial and antioxidant activities (Casadidio et al., 2019). Chitosan can be obtained from crustaceans, insects, mollusks, fungi or shrimps, although the main extraction sources are shrimp and crab exoskeleton residues, producing approximately 2000 tons of chitosan annually (Santos et al., 2020; Sharma & Tiwari, 2020).

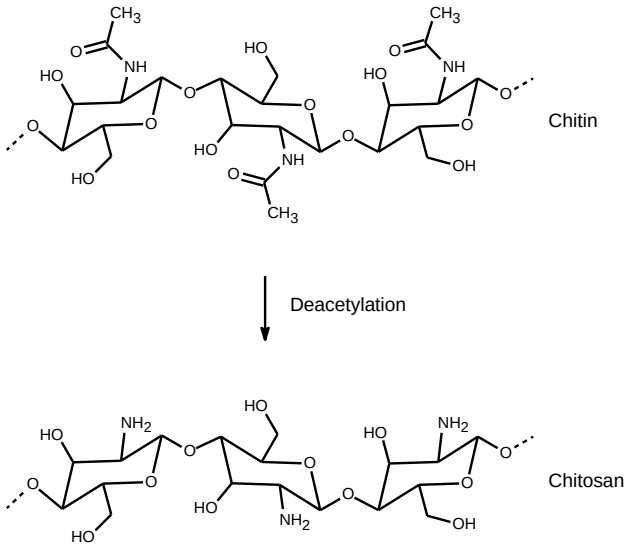

Figure 1.1. Chitin and chitosan molecular structure.

Chitin can be extracted by chemical and/or biological treatments (Figure 1.2) (Hou et al., 2016).

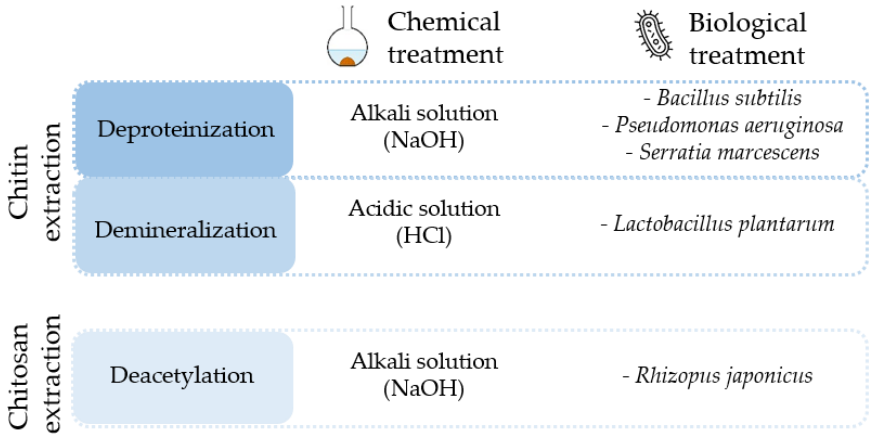

Figure 1.2. Chitin and chitosan extraction diagram.

Generally, chitin is extracted by a two-step process, including deproteinization and demineralization (Muxika et al., 2017). In the case of shell wastes, another step, depigmentation treatment, is required in order to remove color (Hou et al., 2016). Once chitin is extracted, a deacetylation process is carried out to obtain chitosan. The aggressiveness of the procedure affects the deacetylation degree of chitosan, influencing the final properties of the biopolymer (Castillo et al., 2017).

In terms of chemical treatments, the deproteinization step is carried out using an alkali solution (usually NaOH), the demineralization process is performed with an acidic solution (typically HCl), and the depigmentation process is accomplished by soaking the chitin in an alkali solution. Hereafter, an alkali solution (commonly NaOH) is used for the chitosan extraction (Baron et al., 2017; Huang et al., 2018). In the case of biological treatments, instead of chemical substances, bacteria strains are employed for deproteinization and demineralization. For instance, *Bacillus subtilis*, *Pseudomonas aeruginosa* and *Serratia marcescens*, bacterial strains that produce protease, have been tested for the deproteinization treatment, and *Lactobacillus plantarum* has been analyzed for the demineralization process to remove calcium from chitin (Sedaghat et al.,

2017). Moreover, for the chitin transformation into chitosan, *Rhizopus japonicas* has been used as a biological alternative (Zhang et al., 2017). It is worth mentioning that no depigmentation process using bacterial strains has been found.

Although chemical treatments are cheap procedures, appropriate for mass production (Shavandi et al., 2017), high concentrations and volumes of acid and alkali solutions are used at high temperatures and, thus, biological treatments could be more suitable processes from the environmental perspective. Nevertheless, they have longer production times, are more expensive, and have not been implemented for mass production; only pilot scale processes have been reported (Zhang et al., 2017).

Combination of both chemical and biological methods can also be employed. For instance, Pachapur et al. (2015) proposed a combined enzymatic deproteinization (with *Bacillus licheniformis*) followed by a chemical demineralization process, using seawater during all steps of chitin extraction. Thereby, using large amounts of freshwater and chemicals can be avoided. Furthermore, Lopes et al. (2018) compared the chitosan extraction by chemical and biological processes at pilot scale and

their environmental impact. The use of a soft alkaline treatment, and the possibility of recovery NaOH, water, and fish protein hydrolysates are some of the reported improvements to decrease the environmental impact associated to the chemical treatments. Additionally, some improvements were proposed for the biological processes in order to mitigate the environmental impacts and the costs associated to the enzyme production; in particular, employing fish protein hydrolyzed obtained in the enzymatic hydrolysis of the crustacean biomass, as peptones for bacterial growth, could be a strategy to reduce environmental loads.

Recently, a novel method for chitosan extraction has been proposed (El Knidri et al., 2016), using microwave technique for all chitosan extraction steps (demineralization, deproteinization and deacetylation). Although the method uses the same preparation conditions as chemical treatments, it needs less time than the conventional one. Indeed, this novel method reduced the deacetylation time from more than 6 h to less than 30 min, reaching the same deacetylation degree. Furthermore, chitosan structure, morphology, and chemical composition in both methods were similar.

1.3. Chitosan for food applications

Chitosan is a suitable material for applications such as food packaging due to its good mechanical properties and capacity of selective permeability to O_2 and CO_2 (Cazón & Vázquez, 2020), which play an important role for protecting food quality during transportation, storage and distribution, when food can be spoiled by chemical and microbiological processes (Sahraee et al., 2019). Owing to its antimicrobial activity, chitosan can preserve foods from foodborne pathogens (Shin, Kim, & Shin, 2019). In this regard, the most accepted mechanism of action is the electrostatic interaction between the protonated amine of chitosan and the anionic charges on the microbial surface, which results in a leakage of the cell components and, thus, in the cell necrosis (Amato et al., 2018). Therefore, chitosan is able to prevent microbial spoilage of foods, a major factor that affects shelf life and food quality. With this aim, chitosan can be applied as films or coatings (Figure 1.3). Chitosan films and coatings have been extensively assessed for non-processed food, such as fruits, vegetables, refrigerated fish and meat as well as for processed food like sausages or bread. Depending on the product, different coating techniques are used: dipping, spraying or wrapping.

Films are preformed layers that can be wrapped around the food (Gudjónsdóttir et al., 2015) or used as a pouch for foodstuff (Zhang et al., 2020c), while coatings are thin layers directly formed on food surface by immersing the product in a solution (Yu et al., 2017) or by spraying the solution (Jiang et al., 2020). In this regard, Alemán et al. (2016) studied the shelf life of fish sausages packaged with chitosan-based films and coatings. Results showed that chitosan coatings were imperceptible and able to extend sausage shelf life by 15 days, while sausages packaged with films showed a pickled appearance with lower pH values and water content, and harder texture than coated sausages. Moreover, Leceta et al. (2015) compared spraying and dipping on ready to eat baby carrots and found that both coating methods were effective to maintain the product safe against microbiological spoilage during a storage period of 15 days. A slightly better antimicrobial activity was shown for dipped samples, whereas moderately better results for weight loss and texture were presented in sprayed samples. Pea pods have also been coated by chitosan solutions, reducing the vegetable weight loss, titratable acidity, and chilling injury, compared to the untreated product (El-hamahmy et al., 2017).

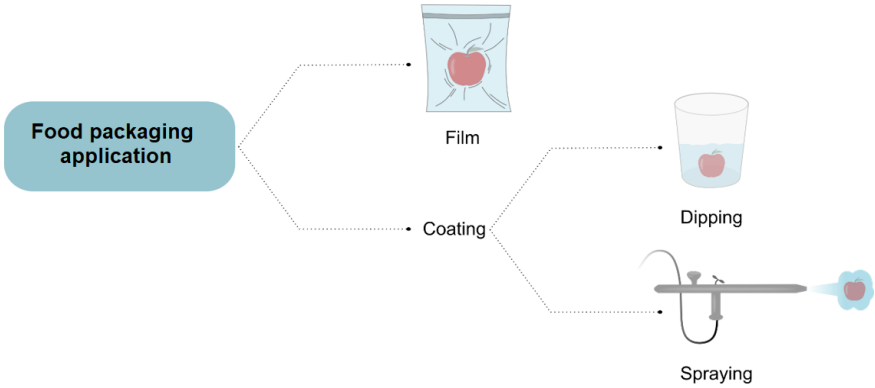

Figure 1.3. Schematic representation of chitosan applications for food packaging.

1.4. Chitosan processing and characterization

Chitosan based materials can be prepared employing two different processes known as wet or dry techniques (Figure 1.4). The wet method is the most extended process when using this polysaccharide because it is a versatile technique (Chen et al., 2018). During this process, chitosan is dissolved in acidified water since it is non-soluble in basic media (Priyadarshi et al., 2018; Zhang et al., 2019a). After heating and stirring the solutions, films can be obtained by solution casting and drying, or food coatings can be prepared by spraying or dipping (Bonilla et al., 2018; Limchoowong et al., 2016). On the other hand, few works related to dry process to prepare chitosan films have been reported in the literature. Galvis-Sánchez et al. (2018) prepared chitosan films by thermal compression. First, chitosan powder was mixed with natural deep eutectic

solvents, such as citric acid or lactic acid. The mixture was put into an oven at 80 °C for 30 min and then, an acetic acid solution was added during manual mixture. The resultant mixture was put into a hydraulic press and thermo-compressed. In another work, Guerrero et al. (2019) thermo-compressed citric acid-chitosan films at 125 °C for 2 min, using glycerol as plasticizer. Chitosan has also been compressed after blending with other polysaccharides such as starch. Valencia-Sullca et al. (2018) dispersed chitosan, starch, glycerol and polyethylene glycol in water and the mixture was melt blended at 160 °C for 30 min, until a homogeneous paste was obtained, before processing by thermal-compression.

After preparing chitosan films and coatings, material characterization must be carried out in order to know their suitability for the specific application of food packaging. Mechanical properties are one of the most important parameters of film characterization. Mechanical behavior determines whether the film is suitable for the packaging purpose since it has to support mechanical loads during the logistic process to keep the product intact and avoid food deterioration (Zhang et al., 2019b). Unmodified chitosan films are brittle due to the electrostatic interactions and hydrogen bonding between chitosan chains. Hence,

plasticizers are used to lend chitosan better mechanical properties, to provide chitosan chains with mobility and, thus, increase flexibility. Among plasticizers, glycerol has the most extended use in chitosan films (Muxika et al., 2017).

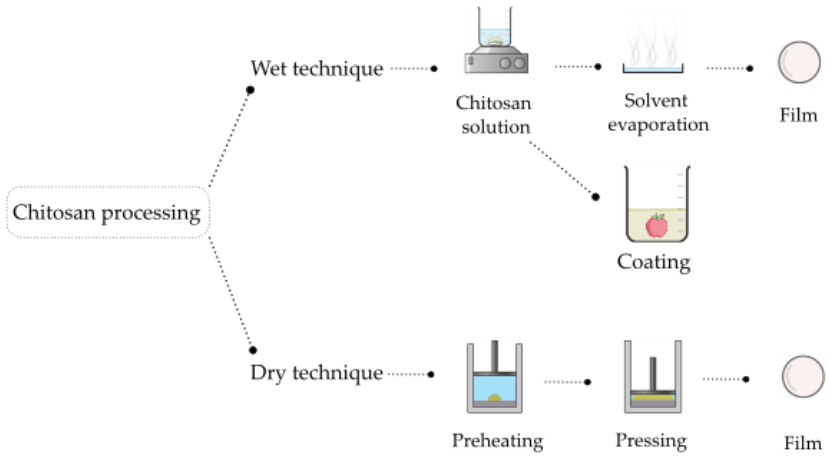

Figure 1.4. Processing techniques of chitosan for food packaging.

In relation to water-related properties, these are of interest to define which kind of product can be packaged. Since chitosan films and coatings present moderate values of water resistance due to the presence of hydrophilic groups (-OH and -NH_2) (Priyadarshi et al., 2018), chitosan properties are modified employing different additives. Wang et al. (2019) studied chitosan films enriched with anthocyanins at different concentrations (5%, 10% and 15% by weight on chitosan basis). Regarding

moisture content, this value decreased with the increase of anthocyanin concentration due to the intermolecular interactions by hydrogen bonding between anthocyanins and the hydrophilic groups of chitosan. Concerning water vapor permeability, anthocyanin-added chitosan films exhibited lower values due to the more compact structure formed as a consequence of the interactions between anthocyanin and chitosan.

1.5. Chitosan as food packaging material

1.5.1. Active packaging

1.5.1.1. Antioxidants for chitosan films and coatings

Packaging designed to extend shelf life or provide information about the quality of the product is defined as active and/or intelligent packaging (Figure 1.5). Active packaging prevents food from deterioration and from foodborne pathogens; therefore, it preserves food quality, extends food shelf life, and enhances food safety (Jha, 2020). In this sense, the oxidation of foodstuff is considered a food spoilage factor, which causes discoloration and rancidity, affecting food quality negatively (Charles et al., 2021).

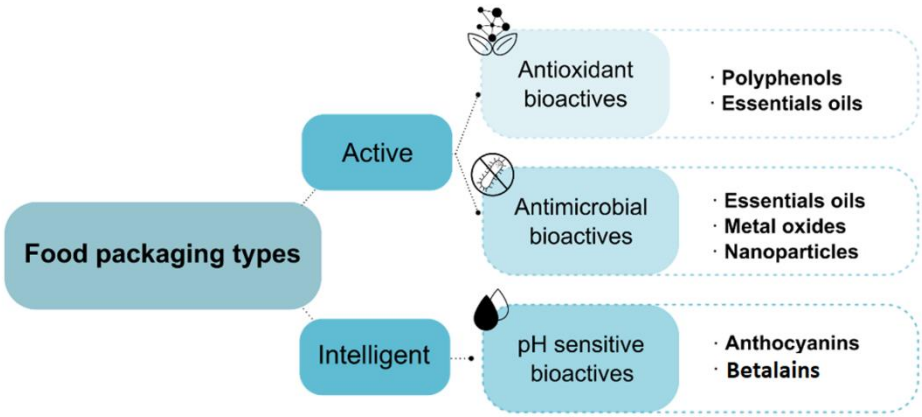

Figure 1.5. Schematic representation of different types of chitosan food packaging.

In food industry, special attention is being paid to natural antioxidant compounds (Talón et al., 2017), such as those containing polyphenols (Zhang et al., 2020b); some of these studies are summarized in Table 1.1. In this regard, rainbow trout fillets coated with chitosan-Ferulago angulata essential oil reduced the increase of thiobarbituric acid reactive substances (TBARS) during storage at 4 °C, improving fish shelf life up to 16 days (Shokri et al., 2020). Moreover, Lekjing (2016) employed clove oil, an essential oil with antimicrobial and antioxidant properties, to coat pork sausages by dipping, and microbiological, physical and chemical analyses as well as sensory evaluation were carried out. It was demonstrated that the coating inhibited the microbial growth, retarded

the lipid oxidation, and extended the shelf-life of the product during refrigerated storage. However, negative impacts were found on odor and taste qualities. Other essential oils, such as that extracted from oregano, have also been incorporated into chitosan solutions to provide coatings with active properties. Paparella et al. (2016) added oregano essential oil into chitosan solutions to coat fresh pork fillets and found that oregano had antimicrobial properties against meat spoilage bacteria, such as *B. thermosphacta* and *Pseudomonas spp.* In another study, Alsaggaf et al. (2017) analyzed the effect of edible chitosan coatings applied by immersion of Nile tilapia fillets into chitosan solutions with pomegranate peel extract, an extract that has several bioactive phytochemicals for antimicrobial or food preservative applications. Composition, microbiological, antioxidant, total nitrogen volatile base value and sensory analyses demonstrated that chitosan/pomegranate peel extract coatings were effective at extending the shelf-life of fish fillets. In addition to coatings, chitosan films with antioxidant bioactives have been used to wrap food products with the aim of prolonging food shelf-life. Serrano-León et al. (2018) wrapped chicken products using chitosan films incorporated with peanut peel extract or pink peppers by-products. Peanut peel extract contains proanthocyanidins and procyanidins, phenolic compounds with

antioxidant activity, while pink peppers by-products are composed of vitamin C, phenolic compounds, flavonoids and carotenoids. The characterization of the chicken product was carried out analyzing chicken pH and color, peroxide value, thiobarbituric acid reacting substances (TBARS) and microbiological parameters. None of the additives altered chicken pH or color, but pink pepper by-products showed greater antimicrobial and antioxidant activities than peanut peel extract.

Bioactive compounds, in spite of enhancing the antioxidant capacity, can also improve other properties of chitosan films. Eucalyptus globulus essential oil incorporated into chitosan films increased the film water resistance and the 2,2-diphenyl-1-picrylhydrazil (DPPH) free radical scavenging capacity up to 43% (Hafsa et al., 2016). Additionally, other natural antioxidants extracted from fruits discards, such as banana peel extracts, reduced water solubility, moisture content and water vapor permeability while increased the antioxidant capacity of chitosan films (Zhang, Li, & Jiang, 2020a).

Table 1.1. Chitosan-based active films and coatings.

Packaged food	Packaging	Bioactive	Bioactivity	Reference
White brined cheese	C	ZnO nanoparticles	AM	Al-Nabulsi et al., 2020
Rainbow trout fillets	C	*Ferulago augulata* essential oil	AO + AM	Shokri et al., 2020
Apples	C	Ripe banana peel extract	AO	Zhang et al., 2020a
Fresh poultry meat	F	Rosemary essential oil	AO + AM	Souza et al., 2019
Cherry tomatoes and grapes	F	Tannic acid	AO + AM	Halim et al. 2018
White shrimp (*Litopenaeus vannamei*)	C	ε-polylysine	AM	Na et al. 2018
Bread slices	F	Apricot kernel essential oil	AO + AM	Priyadarshi et al. 2018
Chicken	F	*Schinus terebinthifolius* Raddi (pink pepper) extract/peanut skin extract	AO	Serrano-León et al. 2018
Nile tilapia fillets	C	Peels of pomegranate extracts	AM	Alsaggaf et al. 2017
Grass carp (*Ctenopharyngodon idellus*)	C	Glycerol monolaurate	AM	Yu et al. 2017
Yellow croakers	C	Nisin	AM	Hui et al. 2016
Pork sausages	C	Clove oil	AO + AM	Lekjing 2016
Tomatoes	C	Iodide	AM	Limchoowong et al. 2016
Pork fillets	C	*Origanum vulgare* essential oil	AM	Paparella et al. 2016
Pacific mackerel (*Pneumatophorus japonicus*) fillets	C	Gallic acid	AO + AM	Wu et al. 2016
Chicken breast	C	*Zataria multiflora* essential oil/pomegranate juice	AO + AM	Bazargani-Gilani et al. 2015

C, coating; F, film; AO, antioxidant; AM, antimicrobial.

1.5.1.2. Antimicrobials for chitosan films and coatings

Besides antioxidant capacity, the safety of food is impaired by microbiological activity (Ebadi et al., 2019). Like antioxidants, synthetic antimicrobial compounds, such as sodium nitrite, can generate side effects and health risks for the consumer (Chang, Chen, & Tsai, 2020; De Mey et al., 2017). Therefore, the food industry seeks substitutes for these compounds from natural sources that do not compromise the sensory properties of the food (Ozaki et al., 2020). In addition to antioxidant activity, essential oils exhibit antimicrobial activity when added to chitosan formulations. For instance, rosemary essential oil inhibited foodborne pathogens, both gram-positive (*Bacillus cereus*, *Straphylococcus aureus* and *Listeria monocytogenes*) and gram-negative bacteria (*Escherichia coli*, *Salmonella enterica* and *Pseudomonas aeruginosa*), mainly due to its high content of phenolic compounds (Souza et al., 2019). On the other hand, inorganic antimicrobial materials are represented by metal oxides, that have higher thermal resistance and broader biocidal spectrum than organic antimicrobials (Al-Tayyar, Youssef, & Al-Hindi, 2020). In this regard, zinc oxide (ZnO) nanoparticles decreased initial numbers of *Escherichia coli* by 2.8 log CFU/g and 2.1 log CFU/g in white brined cheese

stored at 4 °C and 10 °C, respectively (Al-Nabulsi et al., 2020). In particular, Zn^{2+} ions can attack cell wall, leading to a leakage and, finally, to bacteria death (Yadav, Mehrotra, & Dutta, 2021).

In recent years, chitosan nanoparticles are gaining more attention, since they can improve functional properties due to their bigger contact surface, which make them more reactive and increase the relative surface of the mass (Istúriz-Zapata et al., 2020), resulting in the enhancement of antimicrobial activity (Badawy, Lotfy, & Shawir, 2020). Chitosan nanoparticles can be integrated into food formulations, such as those incorporated with cinnamon essential oil for retarding beef patties deterioration during refrigeration storage (Ghaderi-Ghahfarokhi et al., 2017). Furthermore, chitosan nanoparticles can be used to provide a sustained release of active substances (Kuai et al., 2020).

1.5.2. Intelligent packaging

Also recently and due to consumer concerns about the safety and quality of food products, smart packaging has been developed to provide information on food quality of packaged products (Wu et al., 2019). In general, most smart food packaging has been used to check the freshness of seafood, fish, meat and fruits, using quality indicators such as pH-

sensitive color change films (Merz et al., 2020). The most commonly compounds used as pH indicators are anthocyanins extracted from different food waste. Anthocyanins extracted from purple corn were used in chitosan-silver nanoparticles films, showing pH sensitive properties (Qin et al., 2019). Additionally, anthocyanins extracted from purple and black eggplant peels were incorporated into chitosan films, resulting effective for the spoilage control of milk (Yong et al., 2019).

1.6. Conclusions and future perspectives

The food processing industry generates increasing amounts of biowaste as the population grows. Integrating these wastes into the circular economy chain and outputting them as value-added products for food packaging production is an alternative to address the sustainability principles set by the European Union in the 2030 Agenda. In this context, biopolymers such as chitosan are gaining attention due to their natural abundance and the possibility of obtaining from fishing industry waste. Chitosan is produced through chemical and/or biological processes, although biological processes are more sustainable, scaling up was only possible with chemical processes.

Furthermore, chitosan is an appropriate material for food packaging, as it has good mechanical properties and selectivity to O_2 and CO_2 permeation, besides its antimicrobial capacity, which preserves food from food pathogens. Regarding the processability of the material, chitosan packaging can be prepared in different formats: dipped or sprayed coatings or wrapped films. These coatings or films can be processed by wet or dry techniques, the former being the most usual.

Food packaging can be divided into active and intelligent packaging. Active packaging helps the food to extend its shelf life, while intelligent packaging provides information concerning the condition of the food. In the case of active packaging, delaying oxidation and food pathogen bacterial growth are two of the most important parameters in extending the shelf life of food. Although chitosan already has antimicrobial capacity, additives can be used to control these two factors. Compounds of natural sources are receiving special attention, since synthetic additives can have harmful effects on human health. Essential oils, which contain polyphenols, are the most commonly used, as they possess both antioxidant and antimicrobial properties. Antimicrobial inorganic materials, such as nanoparticles, especially metal oxides, which

have a higher biocidal capacity than essential oils, are also used to reduce antimicrobial activity. In addition, it should be noted that in recent years chitosan nanoparticles, due to the smaller size and the higher surface/volume ratio, are more reactive and therefore they increase the antimicrobial capacity of the material.

On the other hand, with regard to intelligent films, packaging has been studied to control the freshness of fresh foods by means of indicators. The most studied bioactives so far are anthocyanins, which change the color of the film by acting as pH-sensitive sensors.

New opportunities are opening up in the field of nanoparticles and intelligent food packaging. The latest studies related to chitosan nanoparticles in the food industry indicate that, due to their bigger contact surface, chitosan nanoparticles can enhance functional properties compared to classical chitosan coatings and, hence, new methods for food coatings are being sought to obtain a greater surface coverage due to a greater penetration of nanoparticles. In this regard, a recent study employed aerosolisation of chitosan nanoparticles for hake fillet coating treatment, which showed that a good coating coverage was achieved with small volumes of solution, and the coating had minimal impact on

physicochemical parameters (Sullivan et al., 2020). Regarding intelligent food packaging, in addition to anthocyanins, the isolation of new indicators from other natural sources is being analyzed. In this sense, betalains have been extracted from vegetable amaranth for application in monitoring of shrimp freshness (Hu et al., 2020). Results suggested that films containing betalains showed good response to the volatile ammonia produced by the shrimp's metamorphism, changing color when the total volatile basic nitrogen slightly exceeded the limit of the standard (Hu et al., 2020).

In summary, future work will be related to sustainability and progress towards the circular economy, trying to reduce the use of polluting and health-damaging chemicals, and focusing on biodegradable materials, leading to the development of food packaging that improves product quality and food safety.

Chapter

2

Chitosan films with exopolysaccharides: Valorization of marine resources

2.1. Summary

Two *Alteromonas* sp. strains isolated from deep seawater were grown to promote the production of exopolysaccharides (EPS, E611 and E805), which were incorporated into chitosan solutions to develop films. The combination of the major marine polysaccharides (chitosan and the isolated bacterial EPS) resulted in the formation of homogenous, transparent, and colourless films, suggesting the good compatibility between the two components of the film-forming formulation. With regards to optical properties, films showed low values of gloss, in the range of 5-10 GU, indicating the formation of non-glossy and rough surfaces. Also related to the film surface, both films showed hydrophobic character, with water contact angles higher than 100 °, regardless of EPS addition. Among the two EPS under analysis, chitosan films with E805 showed better mechanical performance, leading to resistant, flexible and easy to handle films.

2.2. Introduction

Polysaccharides are widely used to develop films and coatings for food applications (Ghasemlou et al., 2011) as an alternative to plastic-based film production. In particular, chitosan is a polysaccharide extracted

from marine crustacean shells (Negm et al., 2020) and, due to its non-toxicity, antimicrobial activity and biocompatibility (Riezk et al., 2020), it is suitable as food preservative (Hu & Gänzle, 2018) applications. Recently, some research has been conducted in order to find novel functionalities of chitosan films through the incorporation of bioactive compounds of natural origin.

In addition to other marine sources, like animals, seaweeds and invertebrates, microorganisms provide glycopolymers that display a great diversity in structures and composition. These original chemical structures are frequently linked to promising biological activities (Delbarre-Ladrat et al., 2014) and, thus, represent a target for biodiscovery. In general, exopolysaccharides (EPS) are high molecular weight polymers constituted of homopolysaccharides or heteropolysaccharides, which can form linear or branched structures (Mohamed et al., 2018; Zhao et al., 2019). EPS derived from marine bacteria are currently attracting substantial attention (Selim et al., 2018). These EPS include sugar monomers, such as fructose and rhamnose (Sahana & Rekha, 2019), which are of commercial interest, and they typically contain several organic and inorganic substitutes that modulate their physicochemical properties. For

instance, the adhesive and viscous properties of EPS are attributed to the presence of uronic acids, sulphates or carboxyl groups that confer anionic character to the polymer (Wang et al., 2019).

EPS are used as thickening, gelling, stabilizing or emulsifying agents (de Oliveira, Amaral, & Burkert, 2018). Since EPS are biocompatible, biodegradable and have a good adhesion capacity to cells (Ale et al., 2020; Tabernero & Cardea, 2020), they are increasingly used in the fields of biotechnology and biomedicine, despite their cost of production is still high for most commercial applications.

The genus *Alteromonas* is ubiquitously found in marine environments, from surface coastal seawater to the deep ocean (García-Martínez et al., 2002), and represents a promising source of a wide range of metabolites, including EPS, antimicrobial and antitumoral agents. Members of this genus have a great diversity of genes involved in the synthesis of EPS (López-Pérez & Rodriguez-Valera, 2016), likely essential for cell-cell interaction and recognition, biofilm formation or nutrient uptake. It has been found that *Alteromonas* HYD-1545 secretes an EPS with high levels of uronic acids and pyruvate, showing anticoagulant and bone healing properties (Vincent et al., 1994). Moreover, the EPS from

Alteromonas macleodii subsp. *fijiensis* is currently commercialized for cosmetic purposes under the name of Abyssine(®) and it is able to reduce skin irritation against chemical, mechanical and UVB aggression. Additionally, *Alteromonas* strain 1644 secreted an EPS that is capable of binding heavy metals (Le Costaouëc et al., 2012; Finore et al., 2014).

The aim of this chapter was to analyze the compatibility between the EPS produced by *Alteromonas* strains, isolated from deep (≥ 500 m depth) seawaters, and a polysaccharide like chitosan in order to develop sustainable films from marine-derived biopolymers. In particular, these bacteria were found to produce omega-3 in a previous work (Estupiñan et al., 2020) and a further valorization of these microorganisms, together with the assessment of their compatibility with chitosan to develop films, were the main aims of the current study. Hence, EPS were incorporated into chitosan formulations, resulting in homogenous films, indicating the good compatibility between these two biopolymers derived from marine sources. Functional properties of these films, such as physicochemical, optical, barrier and mechanical properties, were assessed and related to the film structure.

2.3. Materials and methods

2.3.1. Materials

Chitosan, with a molecular weight of 375 kDa and deacetylation degree above 75 %, was supplied by Sigma-Aldrich, Spain. Acetic acid solution (1 N), and glycerol (99.0 % purity), used as solvent and as a plasticizer, respectively, were supplied by Panreac, Spain.

2.3.2. EPS production

Two *Alteromonas* strains (611 and 805), isolated from deep seawater samples (1,000 m and 500 m depth, respectively) collected in the Bay of Biscay (Estupiñán et al., 2020), were grown in MASW. For EPS production and isolation, 1 L bottles containing 600 mL of MASW were inoculated at 2 % (v/v) from a starter overnight culture, incubated at 25 °C, 190 rpm. To induce EPS production, *Alteromonas* sp. 611 culture media MASW was supplemented with an additional carbon source (3 % of sucrose, Fisher BioReagents), and shaken for 6 days (190 rpm) at 10 °C in aerobic conditions.

The crude EPS from the bacterial isolates was obtained as previously described (Rougeaux et al., 1996). In brief, cells were removed from the

medium by centrifugation at 15,000 x g for 20 min. The supernatant was centrifuged twice in order to reduce the presence of bacteria. EPS was precipitated from the clarified supernatant by addition (1:1, v/v) of cold absolute ethanol (-20 °C) (Fisher Scientific), and incubated at 4 °C overnight. The precipitate was harvested by centrifugation (12,000 × g, 30 min) and washed three times with increasing ratios of ethanol to water (50 %, 70 %, 100 %). Then, the precipitate was resuspended in deionized water, rehydrated overnight at 4 °C, and freeze-dried. The crude EPS (E611 and E805) were stored at room temperature.

The yield of EPS production was determined by gravimetry of the lyophilized crude EPS. Protein and DNA contents were measured by Quibit ®.

2.3.3. Film preparation

1 % (w/v) chitosan was dissolved in 1 % wt acetic acid solution by mechanical agitation for 45 min at room temperature. 5 wt % EPS (referred to chitosan dry mass) was added to the chitosan solution and stirring was maintained for 30 min. In order to homogenize the mixture, Ultraturrax (IKA, Germany) was used at 15,000 rpm for 90 s. Subsequently, 15 wt % glycerol (chitosan based) was added and stirring was maintained for 2 h.

Solutions were poured into Petri dishes and let dry at room temperature. The resulting films were named CH for control chitosan films, CHE611 for chitosan films supplemented with E611, and CHE805 for chitosan films with E805.

2.3.4. Film characterization

2.3.4.1. UV-vis spectroscopy

A UV-VIS-NIR Shimadzu spectrometer (Shimadzu Scientific Instruments, Kyoto, Japan) was employed to measure light transmission through the film. The absorbance range was set up from 200 to 800 nm.

2.3.4.2. Color measurements

Color measurements were collected with a CR-400 Minolta Chroma Meter colorimeter (Konica Minolta, Tokyo, Japan). CIELAB scale was used for color parameter determination: L* from 0 to 100 (from black to white), a* from – to + (from greenness to redness) and b* from – to + (from blueness to yellowness). Ten replicates were collected for each sample. Films were placed on a white patron (L*= 97.39, a*= 0.03, b*= 1.77) and the total color difference (ΔE*) was calculated as:

$$\Delta E^* = \sqrt{(\Delta L^*)^2 + (\Delta a^*)^2 + (\Delta b^*)^2}$$

2.3.4.3. Gloss measurements

Gloss values were determined by a Multi Gloss 268 Plus (Konica Minolta, Tokyo, Japan) with an incidence angle of 60 °, according to ASTM D523-18 (ASTM, 2018). Ten samples were collected for each sample at room temperature.

2.3.4.4. Water contact angle (WCA)

A Dataphysic Contact Angle System, Oca 20 model, was used for WCA measurements. A 3 μL of distilled water was dropped onto the film surface and the drop image was collected using a SCA20 software. Measurements were carried out in quintuplicate.

2.3.4.5. Water vapor permeability (WVP)

PERME™W3/0120 chamber (Labthink Instruments Co. LTD., Shandong, China) was used to measure WVP at a temperature and relative humidity of 38 °C and 90 %, respectively, according to ASTM E96-00 (ASTM, 2000). Films were cut with disc shape of 7.40 cm diameter and a test area of 33 cm^2. Tests were carried out in triplicate.

Water vapor transmission rate (WVTR) was calculated as:

$$WVTR\ \left(\frac{g}{s\ cm^2}\right) = \frac{G}{t \cdot A}$$

where G is the weight change (g), t is the time (s), and A is the film area that was tested (cm^2).

WVP was calculated by the following equation:

$$WVP\left(\frac{g}{cm\ s\ Pa}\right) = \frac{WVTR \cdot L}{\Delta P}$$

where L is the film thickness (cm) and ΔP is the partial pressure difference of the water vapor across the film (Pa).

2.3.4.6. Mechanical properties

An Instron 5967 electromechanical testing system (Instron, Massachusetts, USA) was employed for tensile tests. Tensile strength (TS), elongation at break (EAB), and elastic modulus (E) were measured. Tests were carried out with a load cell of 500 N and a crosshead rate of 5 mm/min, according to ASTM D638-14 (ASTM, 2014). Films were cut into dog bone-shaped samples of 4.75 mm × 22.25 mm. At least 5 samples for each composition were tested.

2.3.4.7. Fourier transform infrared (FTIR) spectroscopy

FTIR spectra were collected with a Nicolet Nexus FTIR spectrometer (Thermo Fisher Scientific, Massachusetts, USA) with a Golden Gate ATR

accessory. The spectra, with a resolution of 4 cm^{-1}, were acquired between 4000 and 800 cm^{-1} with 32 scans for each sample.

2.3.4.8. X-ray diffraction (XRD)

X-ray diffraction (XRD) was carried out at 40 kV and 40 mA, with Cu-Cu-Kα (λ = 1.5418 Å) as a radiation source, using a PANalytic Xpert Pro (PANalytical, Almelo, The Netherlands) equipment with a diffraction unit. Data were collected between 2 ° and 34 ° (step size = 0.026, time per step = 118 s).

2.3.4.9. Scanning electron microscopy (SEM)

A Hitachi S-4800 scanning electron microscope (Hitachi High-Technologies Corporation, Tokyo, Japan), with an acceleration voltage of 15 kV, was employed to analyze the film cross-sections. Films were placed on a metallic stub and were covered with gold under vacuum in argon atmosphere.

2.3.5. Statistical analysis

In order to determine significant differences between measurements, analysis of variance (ANOVA) was carried out with SPSS software (SPSS Statistic 24.0.0.2). Tukey's test with a statistically

significant at the $P < 0.05$ level was used for multiple comparisons among different systems.

2.4. Results and discussion

2.4.1. EPS production

In the batch experiment, an EPS production of 1.0 g/L (E805) and 0.7 g/L (E611) was observed after 96 h of culture at 10 °C, as typically found for marine EPS-producing strains (i.e., 0.5 to 4.0 g/L of EPS in the presence of glucose) (Roca et al., 2016).

2.4.2. Optical properties

The effect of EPS supplementation on chitosan film appearance was determined by UV-vis absorbance, color, and gloss measurements. In general, chitosan films were transparent and colorless with a subtle yellow color. As can be seen in Figure 2.1, there was no light absorbance in the visible range from 400 to 800 nm, indicating that control films and those with EPS were transparent. Additionally, all films absorbed UV light at 200 nm, corresponding to the carbonyl groups in chitosan (Ji et al., 2016).

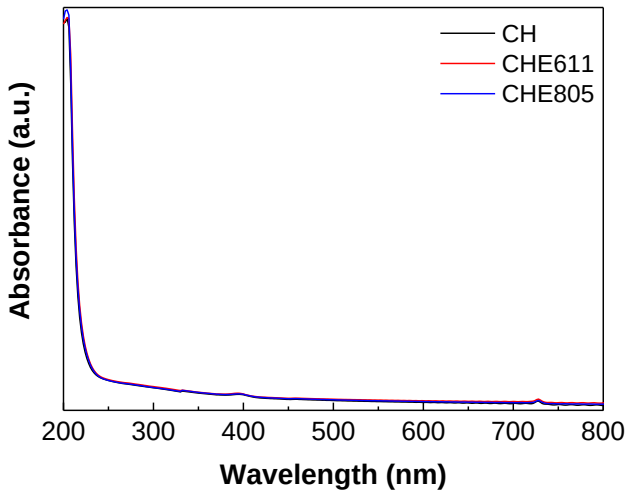

Figure 2.1. UV-vis light absorption of control (CH) and chitosan films with E805 (CHE805) and E601 (CHE601).

Regarding color, color changes were analyzed by determining L*, a* and b* parameters and results are shown in Table 2.1. E811 did not significantly ($P > 0.05$) affect the color parameters of chitosan films. However, the addition of E611 caused a significant ($P < 0.05$) increase of b* values and a* values, which became more negative ($P < 0.05$), indicating an increase of yellowness and greenness, respectively. L* values did not decrease ($P > 0.05$), indicating that CHE611 films showed high lightness. It is worth noting that these changes were not perceptible for human eye, since ΔE^* values were lower than 5 (Luchese et al., 2018); in particular, values were lower than 1 in this work. Therefore, it can be said that the

appearance of control chitosan films prevailed after the addition of EPS. Additionally, gloss values were measured and are shown in Table 2.1. All films showed very low gloss values, indicating that the film surface was very rough, since low gloss values are related to high surface roughness (Sánchez-González et al., 2010). Moreover, chitosan films supplemented with E805 were found to be even rougher since gloss values decreased from 10 to 5 GU.

Table 2.1. L*, a*, b* and ΔE* color parameters and gloss values of control (CH) and chitosan films with E805 (CHE805) and E601 (CHE601).

Films	L*	a*	b*	ΔE*	$Gloss_{60}$ (GU)
CH	95.5 ± 0.5[a]	-0.08 ± 0.03[a]	2.39 ± 0.06[a]	---	10 ± 2[a]
CHE805	96.8 ± 0.3[a]	-0.12 ± 0.03[a]	2.56 ± 0.09[a]	0.67	10 ± 2[a]
CHE611	96.6 ± 0.5[a]	-0.22 ± 0.09[b]	3.04 ± 0.40[b]	0.33	5 ± 2[b]

[a-b]Two means followed by the same letter in the same column are not significantly (P > 0.05) different through the Tukey's multiple range test.

2.4.3. Barrier and mechanical properties

Following with the analysis of film surface, the hydrophilic or hydrophobic character of chitosan films was assessed by measuring water contact angle (WCA) values. As shown in Table 2.2, control chitosan films were hydrophobic since the WCA values were greater than 90° (Grande-

Tovar et al., 2018). No significant ($P > 0.05$) difference was found for CHE805 films, while a significant ($P < 0.05$) increase was observed for CHE611 films, with values of 115°. These results are in accordance with the abovementioned gloss values, which indicated a rougher surface for CHE611 films.

In relation to water-related properties, there was no significant ($P > 0.05$) difference in WVP values with the addition of EPS (Table 2.2). Permeability values depend on adsorption, diffusion, and desorption processes. Although CHE611 films were more hydrophobic, similar values of WVP would indicate that diffusion process is more rapid in these films.

Table 2.2. Water contact angle (WCA), water vapor permeability (WVP), tensile strength (TS), elongation at break (EAB), and elastic modulus (E) of control (CH) and chitosan films with E805 (CHE805) and E611 (CHE611).

Films	WCA (°)	WVP·10^{-12} (g/cm·s·Pa)	TS (MPa)	EAB (%)	E (MPa)
CH	105 ± 2[a]	1.37 ± 0.07[a]	41.6 ± 1.0[a]	24.7 ± 2.1[a]	1193 ± 24[a]
CHE805	109 ± 1[a]	1.51 ± 0.02[a]	42.7 ± 1.5[a]	23.7 ±1.9[a]	1186 ± 29[a]
CHE611	115 ± 3[b]	1.54 ± 0.01[a]	39.5 ± 0.5[b]	16.6 ± 1.3[b]	1008 ± 26[b]

[a-b]Two means followed by the same letter in the same column are not significantly ($P > 0.05$) different through the Tukey's multiple range test.

Tensile tests were performed in order to evaluate the effect of EPS addition on tensile strength (TS), elongation at break (EAB) and elastic modulus (E). The addition of E611 caused a significant ($P < 0.05$) decrease in TS, EAB and E values, but E805 did not significantly ($P > 0.05$) change the mechanical performance of chitosan films (Table 2.2), resulting in resistant and flexible films, which were easy to handle. This behavior is in accordance with the previous analyses, which also led to similar results for control and CHE805 films, while CHE611 films showed changes in both optical and barrier properties compared to control and CHE805 films.

2.4.4. Physicochemical properties and film morphology

FTIR analysis was carried out to evaluate the interactions between chitosan and EPS. Regarding EPS (Figure 2.2a), the main characteristic bands appeared at 3300 cm^{-1}, corresponding to O-H stretching; at 1633 cm^{-1}, associated to C=O stretching; around 1400 cm^{-1}, corresponding to C-H stretching vibrations in hexoses; at 1230 cm^{-1}, associated to the presence of sulfates; at 1100 cm^{-1}, due to glycosidic linkages; and at 1000 cm^{-1}, related to C-O stretching (Sahana & Rekha, 2019). The most relevant difference between the two EPS is related to the difference in the relative intensity between the bands at 1633 and 1400 cm^{-1}. As can be seen in Figure 2.2a, the

intensity of those bands is similar for E805, indicating a higher content of hexoses, which could lead to a higher TS of CHE805 films, due to these cyclic structures that provide rigidity. Additionally, a higher EAB of CHE805 films could be due to the promotion of hydrogen bonding with the hydroxyl groups of the hexoses.

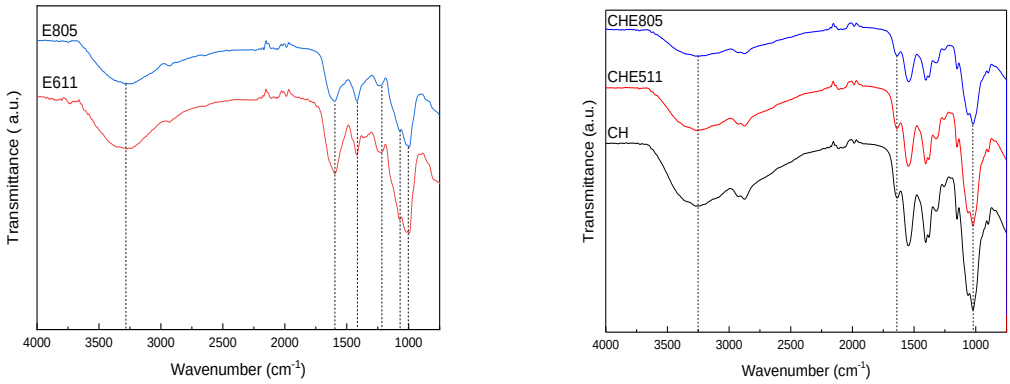

(**a**) (**b**)

Figure 2.2. FTIR spectra of (a) E611 and E805 and (b) those of control (CH) and chitosan films with E611 (CHE611) and E805 (CHE805).

When EPS were incorporated into chitosan film forming formulations, some shifts of the abovementioned characteristic bands were observed, as shown in Figure 2.2b. In particular, the band at 3300 cm^{-1} was shifted to 3250 cm^{-1}, the band at 1633 cm^{-1} to 1655 cm^{-1}, and the band at 1000 cm^{-1} to 1030 cm^{-1} for CHE805 and CHE611 films. These shifts would be indicative of physical interactions among chitosan, glycerol and

EPS, mainly by hydrogen bonding among the polar groups (hydroxyl and carbonyl groups) of the components of the film forming formulation.

Finally, XRD and SEM analyses were carried out in order to assess the film structure. The three characteristic peaks of chitosan are observed at 9 °, 12 °, and 20 ° (Di Filippo et al., 2020) for all the chitosan films under study, regardless the addition of EPS (Figure 2.3).

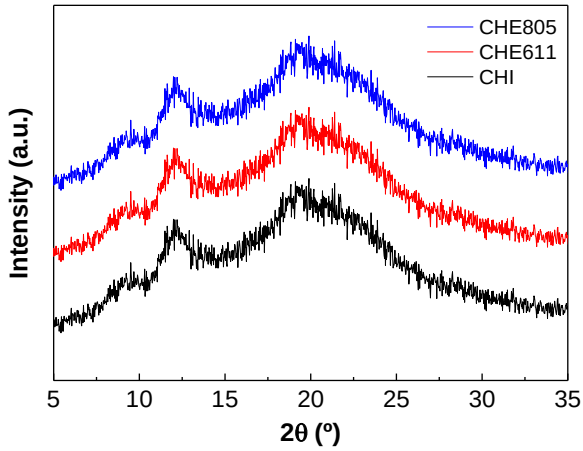

Figure 2.3. XRD patterns of control (CH) and chitosan films with E611 (CHE611) and E805 (CHE805).

Regarding SEM analysis, film cross-sections are shown in Figure 2.4. A compact structure was observed for all films, suggesting the good compatibility among the film components.

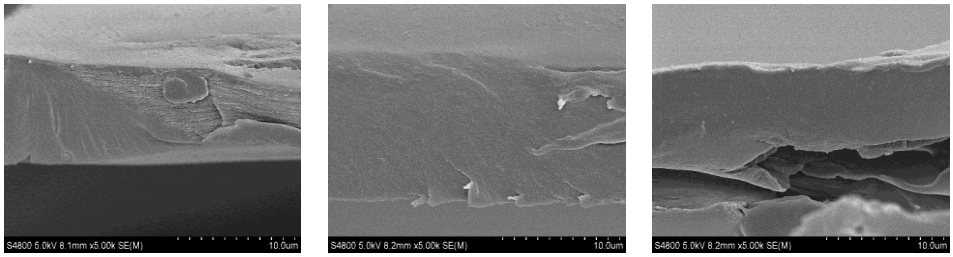

(**a**) (**b**) (c)

Figure 2.4. SEM images of cross-sections of (a) control films and chitosan films enriched with (b) E611 and (c) E805 exopolysaccharides.

2.5. Conclusions

In this work, a preliminary characterization of crude EPS (E611 and E805), produced by two deep seawater *Alteromonas* sp. strains, was carried out. All the films obtained were colorless, transparent and homogeneous. The addition of crude EPS caused an increase of the hydrophobic character of chitosan films, especially for CHE611 films, as shown by higher WCA values. However, WVP prevailed unchanged, indicating that water vapor diffusion was more rapid for CHE611. On the other hand, the addition of E805 led to a better mechanical performance compared to CHE611 films, leading to resistant and flexible films. This preliminary work indicates the good compatibility between these two marine polysaccharides from renewable resources and, thus, their potential to develop improved films. Results suggest that the valorization of natural materials from marine

sources may be of great interest for the development of potentially active films for food applications. In this regard, more assays should be conducted to analyze properties related to food applications.

Chapter

3

Active chitosan films with 2-phenyl ethanol: Encapsulation with cyclodextrins

3.1. Summary

2-phenyl ethanol is a natural compound, which have many applications due to its nice fragrance, bacteriostatic and antifungal character. However, it is difficult to keep it stable and it is highly volatile. In this chapter, chitosan films with 2-phenyl ethanol were developed and inclusion complexes with cyclodextrins (CDs) were prepared in order to have a controlled release of 2-phenyl ethanol. β-CD was selected to develop the inclusion complex since it showed higher retention yield (45 %, molar basis) than α- or γ-CDs. Chitosan films incorporated with β-CD:2-phenyl ethanol were homogeneous, transparent and colorless, and showed high mechanical resistance. Furthermore, the release results of the films without the inclusion complex indicated that 2-phenyl ethanol was evaporated during the film preparation, and only an 8 % of the total bioactive was retained in the film, while more than 90 % of 2-phenyl ethanol was retained in the films with the inclusion complex.

3.2. Introduction

The use of active compounds in films is a strategy to confer functional properties, such as antimicrobial, antioxidant or ultraviolet (UV) light barrier properties. However, many of these compounds are not

stable under the preparation, storage and/or use conditions (Hosseini, Nahvi, & Zandi, 2019; Li et al., 2019). Therefore, the use of encapsulation agents for active compounds become necessary to protect the compound from volatilization or possible reactions with external agents, and to control a sustained release (Reineccius, 2009). Among encapsulation processes, only molecular inclusion occurs at molecular level and, thus, one molecule of the active compound is trapped in the cavity of the host molecule (Reineccius, Reineccius, & Peppard, 2002). One of these host molecules is cyclodextrin, since the Food and Agriculture Organization (FAO) of the United Nations recognizes it as additive (FAO, 2019).

Cyclodextrins (CD) are cyclic oligosaccharides constituted of glucose molecules joined together by α-1,4 bonds (Szente & Szejtli, 1999). CDs are hollow truncated cone structures with an external hydrophilic character and an internal hydrophobic character (Huang et al., 2019; Simionato et al., 2019). Therefore, CD is a suitable molecule to host a variety of bioactives, including those that are non-soluble in water since interactions between cyclodextrins and guest molecules include hydrophobic forces as well as hydrogen bonding (Zhou et al., 2019).

Depending on the glucopyranose units conforming the molecule, the most common CDs are α-, β- or γ-CDs, composed of 6, 7 or 8 glucopyranose units, respectively (Prabu & Mohamad, 2020). Due to the variety of guest molecules that can host and their acceptability as food additives, CDs are widely used in food and pharmaceutical industries. Regarding food industry, CDs can be employed for different applications, such as food supplement for spaghetti, adding pumpkin oil (Durante et al., 2019); as flavor masking, reducing the high intensity of sourness, bitterness and astringency flavor in lingonberry juice (Kalanne et al., 2019); or as thermal stabilizers (Yoshikiyo et al., 2019).

CDs can be used in a variety of matrixes. Morin-β-CD complexes have been incorporated into gelatin to prepare antioxidant films (Yuan et al., 2019). In addition, antimicrobials, such as citral, have been used to prepare β-CD inclusion complexes to preserve bioactivity during melt extrusion of EVOH films (Chen et al., 2019). In order to provide films with both antioxidant and antibacterial properties, essential oils have been encapsulated into β-CD to promote cumulative release from chitosan films for food packaging applications (Adel et al., 2019). In this regard, several works have been reported in relation to the use of chitosan with CD

inclusion complexes for controlled release of bioactives such as resveratrol (Zhang et al., 2017), carvacrol (Andrade-Del Olmo et al., 2019), or gallic acid (Munhuweyi et al., 2018).

The goal of this work was to assess the effectiveness of cyclodextrin inclusion complexes as stabilizers and release controllers of 2-phenyl ethanol in chitosan films. 2-phenyl ethanol is naturally present in more than one hundred food products (Nijssen, Ingen-Visscher, & van Donders, 2016), and it is used in food industry to enhance flavor and odor. Although it has bacteriostatic and antifungal character, it is very volatile and highly susceptible to oxidation, thus, storing and keeping it stable is a troublesome (Yadav & Lawate, 2011). In order to address this challenge, 2-phenyl ethanol has been microencapsulated with methylcellulose, alginate and carboxymethyl chitosan (Qiu et al., 2019). However, to the best of our knowledge, this work assesses the effectiveness of 2-phenyl ethanol trapped into α-, β-, and γ-CDs for the first time. Additionally, chitosan films with β-CD:2-phenyl ethanol were developed and the optical, physicochemical and mechanical properties of the films were characterized. In order to assess if the addition of the inclusion complex alters the properties of the film, neat chitosan and chitosan with 2-phenyl

ethanol films were prepared. Furthermore, the release of 2-phenyl ethanol from chitosan films into a fatty food simulant was determined.

3.3. Materials and methods

3.3.1. Materials

Chitosan (CHI), with a molecular weight of 375 kDa and a deacetylation degree above 75 %, was supplied by Sigma-Aldrich, Spain. Acetic acid (1 N) and glycerol (GLY, 99.0 % purity), used as solvent and plasticizer, respectively, were supplied by Panreac, Spain. 2-phenyl ethanol and α- and β-cyclodextrins (CAVAMAX® w6 and w7, respectively), used for the development of inclusion complexes, were food grade and supplied by Wacker Chemical, Spain; while γ-cyclodextrins were provided by Roquette, France.

3.3.2. Inclusion complex preparation

The inclusion complexes of 2-phenyl ethanol were prepared according to Barba, Eguinoa, & Maté (2015) with some modifications. Firstly, 10 % (w/w) cyclodextrins were hydrated for 10 min; then, 2-phenyl ethanol was added in equimolar ratio and the mixture was mechanically stirred for 24 h. In order to obtain the dry powder, a B-191, Büchi spray-

dryer was used at the following conditions: 100 % aspirator capacity, inlet temperature of 180 °C, and pump at 4 mL/min. The powder was collected and stored in vials at -20 °C.

3.3.3. FTIR analysis of cyclodextrin complexes

Fourier-transform infrared (FTIR) spectroscopy was carried out with a Nicolet Avatar 260. Inclusion complexes (α-CD:2-phenyl ethanol, β-CD:2-phenyl ethanol, and γ-CD:2-phenyl ethanol), cyclodextrins (α-CD; β-CD and γ-CD) and 2-phenyl ethanol were milled with anhydrous KBr and the pellet was formed by compression. The spectra were recorded between 4000-800 cm^{-1} with 32 scans and a resolution of 4 cm^{-1}.

3.3.4. Retention of 2-phenyl ethanol cyclodextrin

2-phenyl ethanol was extracted from cyclodextrins by liquid-liquid extraction following the method of Charve & Reineccius (2009) with some modifications. The analysis was carried out one week after the inclusion complex was formed. 0.15 g of the inclusion complex was weighed and added into a centrifuge glass tube, and 5 mL hexane and 10 mL distilled water were added. The mixture was shaken energetically for 2 min and then, vortexed for 2 min. The samples were put into a bath at 85 °C and shacked for 30 min. The organic phase was gathered into a 50 mL flask.

For each sample, three extractions were carried out, adding the organic phase into the 50 mL flask. A fourth extraction was done to confirm that the extraction was completed. From a 1:10 solution, 1 μL was injected into a Hewlett-Packard 5890 series II gas chromatography spectrometer (Agilent Technology, Barcelona, Spain), equipped with a flame ionization detector (FID) and a Supra Wax 280 column (1.0 μm x 0.53 mm, 30 m). The gas carrier employed was helium, the injection temperature was 250 °C, the oven temperature program was started at 40 °C with a temperature ramp of 5 °C/min up to 220 °C (1 min), and the detector temperature was set at 300 °C. In order to avoid the fluctuation of the signal, an internal standard (1-heptanol) was added to the calibration standards and samples. The retention of 2-phenyl ethanol was calculated as the ratio of experimental concentration over the theoretical content.

3.3.5. Film preparation

Chitosan films were prepared by solution casting. 1 wt % chitosan was dissolved in 1 wt % acetic acid solution under stirring for 45 min. Then, 10 wt % 2-phenyl ethanol or 10 wt % β-CD:2-phenyl ethanol (based on chitosan) was added, and stirring was continued for other 30 min. Finally, 15 wt % glycerol (based on chitosan) was added into some

solutions as plasticizer and other 30 min of stirring were needed until total homogenization of the mixture. The solution was casted into Petri dishes and dried at room temperature for 48 h. In total, six compositions were analyzed: control films, named as CHI0GLY and CHI15GLY as a function of glycerol content; chitosan films with 2-phenyl ethanol, named as CHI0GLY2PE and CHI15GLY2PE; and chitosan films with β-CD:2-phenyl ethanol inclusion complex, named as CHI0GLYCD:2PE and CHI15GLYCD:2PE.

3.3.6. Film characterization

3.3.6.1. Optical properties

Color and gloss parameters of the films were analyzed. Color measurements were recorded with a CR-400 Minolta Chroma Meter colorimeter (Konica Minolta, Tokyo, Japan). Ten replicates were carried out for each sample. For the determination of color parameters CIELAB scale was used: L* from 0 to 100 (from black to white), a* from – to + (from greenness to redness), and b* from – to + (from blueness to yellowness). The films were laid on a standard white plate with color parameter values of L*= 97.39, a*= 0.03 and b*= 1.77.

Multi Gloss 268 Plus (Konica Minolta, Tokyo, Japan) was used for the determination of gloss with an incidence angle of 60° according to ASTM D523-18 (ASTM, 2018). For each composition, ten samples were assessed at room temperature.

Light-barrier capacity of films was measured by using a UV-VIS-NIR Shimadzu 3600 spectrophotometer (Shimadzu Scientific Instruments, Kyoto, Japan) in the range of 200-800 nm.

4.2.6.2. Physicochemical properties

A Nicolet Nexus FTIR spectrometer (Thermo Fisher Scientific, Messachusetts, USA) with a Golden Gate ATR sampling accessory was used for collecting FTIR spectra. The spectra were acquired between 4000 and 800 cm^{-1} with 32 scans for each sample and a resolution of 4 cm^{-1}.

A PANalytic Xpert Pro (PANalytical, Almelo, The Netherlands) X-ray diffraction (XRD) equipment was employed with a diffraction unit at 40 kV and 40 mA. A Cu-Kα (λ = 1.5418 Å) was employed as radiation source and the data were collected between 2° and 34° (step size = 0.026, time per step = 118 s).

3.3.6.3. Mechanical and barrier properties

In order to determine the tensile strength (TS), elongation at break (EAB) and elastic modulus (E), an Instron 5967 electromechanical testing system (Instron, Massachusetts, USA) was used. Films were cut into dog bone-shaped samples of 4.75 mm × 22.25 mm and tests were carried out according to ASTM D638-14 (ASTM 2014). A load cell of 500 N was used and tensile tests were carried out with a crosshead rate of 1 mm/min. Five replicates were tested for each sample.

Water vapor permeability (WVP) was tested with a PERME™ W3/0120 chamber (Labthink Instruments Co. Ltd., Shandong, China) in a controlled humidity environment, according to ASTM E96-00 (ASTM, 2000). Film discs were cut with a diameter of 7.40 cm and a test area of 33 cm^2. The temperature and relative humidity were set up at 38 °C and 90 %, respectively. Three replicates for each sample were reported for the WVP analysis.

3.3.6.4. Bioactive release

Film pieces (1 cm x 2 cm) were submerged into 8 mL of 95 % ethanol solution, used as a fatty food simulant (Liang et al., 2017), for 4 days under continuous stirring (200 rpm) at room temperature. Aliquots were

collected at different times (30 min, 1 h, 2 h, 4 h, 8 h, 1 d, 2 d, 3 d, and 4 d). The bioactive release was analyzed by using a UV-VIS-NIR Shimadzu 3600 spectrophotometer (Shimadzu Scientific Instrument, Kyoto, Japan). 2-phenyl ethanol concentration was calculated by means of a calibration curve from 0.1 to 10.0 μg/ mL at the maximum wavelength absorbance (207 nm). Measurements were carried out in triplicate.

3.3.7. Statistical analysis

In order to determine significant differences among the samples, analysis of variance (ANOVA) was carried out with SPSS software (SPSS Statistics 25.0). For multiple comparisons, Tukey's multiple range test was used with a statistically significance at the $P < 0.05$ level.

3.4. Results and discussion

3.4.1. Characterization of cyclodextrin inclusion complexes

FTIR spectroscopy was used in order to characterize α-, β-, and γ-cyclodextrin inclusion complexes with 2-phenyl ethanol. As can be seen in Figure 3.1, the O-H stretching vibration band is observed around 3390 cm^{-1}, indicative of the hydroxyl groups of cyclodextrin (Salih et al., 2020). The C-O-C stretching vibrations are observed at 1158 cm^{-1}, associated to the

oligosaccharide structure, and the bands at 1080 and 1030 cm^{-1} correspond to the C-C stretching vibrations of the cyclodextrin ring carbons (Han et al., 2019).

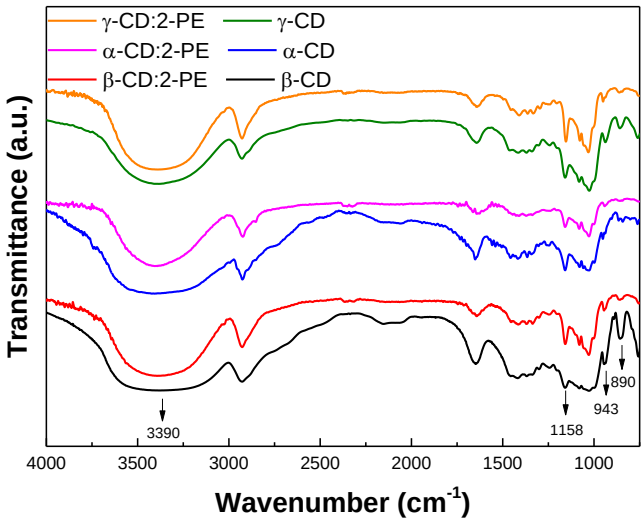

Figure 3.1. FTIR spectra of α-, β-, and γ-cyclodextrin (CD) inclusion complexes.

Additionally, the characteristic band of the α-pyranyl vibration in cyclodextrin appeared at 943 cm^{-1} and the characteristic band of α-(1,4) glucopyranose in cyclodextrin appeared at 890 cm^{-1} (Yuan et al., 2013). As can be seen, there was no chemical interaction between the cyclodextrin and 2-phenyl ethanol. However, some characteristic bands of cyclodextrin were shifted in the inclusion complex spectra. The O-H stretching vibration displaced from 3383 cm^{-1} for β-cyclodextrin to 3393 cm^{-1} for the

inclusion complex. Furthermore, C-O-C stretching vibration band moved slightly to lower wavenumbers, from 1158 cm^{-1} for β-cyclodextrin to 1157 cm^{-1} for the inclusion complex. The shift of these bands suggested physical interactions between cyclodextrins and 2-phenyl ethanol (Xiao et al., 2019).

3.4.2. Retention yield of 2-phenyl ethanol

The retention yield of 2-phenyl ethanol for α-, β-, and γ-cyclodextrin inclusion complexes was determined. The highest value was observed for β-clyclodextrin inclusion complex (45 %), followed by γ-cyclodextrin (40 %) and finally, α-cyclodextrin (32 %). These relative low retention values can be related to the fact that 2-phenyl ethanol has only one hydroxyl group to get attached to the cyclodextrin and, thus, the interactions could be weaker. Regarding the differences in retention values, those differences can be associated to the cavity size of CDs. While α-cyclodextrin cavity is the smallest (5.7 Å) to host 2-phenyl ethanol, γ-cyclodextrin cavity is too big (9.5 Å) and, therefore, the interactions between the host and the guest were weaker. However, β-cyclodextrin cavity (7.8 Å) was big enough to host 2-phenyl ethanol and small enough to facilitate physical interactions between them (Ciobanu et al., 2013; Decock et al., 2008). Taking the above into consideration, chitosan films were prepared with the inclusion

complex with the highest retention yield; therefore, β-cyclodextrin:2-phenyl ethanol inclusion complexes were incorporated into chitosan film forming solutions.

3.4.3. Optical properties of films

All films were transparent and colorless. Regarding CIELab color parameters (Table 3.1), all films presented L* values close to 100, indicating high lightness of the films, a* parameter had slightly negative values, while b* parameter showed positive values, as also shown in other works for chitosan films (Pereira, Queiroz de Arruda, & Stefani, 2015). Considering the ΔE* value referred to CHI0GLY, the films did not show differences for the naked eye, since ΔE* values were lower than 1 (Uranga et al., 2019). Furthermore, statistical analysis concluded that there were no significant ($P > 0.05$) difference among samples for L*, a* and ΔE* parameters, only a slight difference for b* value, which was not relevant. Therefore, the addition of glycerol, 2-phenyl ethanol, or the inclusion complex did not affect the film color. Regarding gloss values (Table 3.1), there was a slight increase ($P < 0.05$) with the addition of 2-phenyl ethanol or the inclusion complex, but there was no significant ($P > 0.05$) difference among the films with 2-phenyl ethanol, regardless the presence of CDs.

For an incidence angle of 60°, values greater than 70 gloss units (G.U.) are considered glossy surfaces (Villalobos et al. 2005); therefore, the values measured in this work indicated that chitosan films were not glossy. Furthermore, since gloss and surface roughness are inversely correlated; lower values of gloss are related to rougher surfaces (Luchese et al., 2018; Valencia-Sullca et al., 2016); therefore, the gloss values indicated that chitosan film surface was rough.

Table 3.1. Color (L*, a*, b* and ΔE* parameters) and gloss values for chitosan films.

Film	L*	a*	b*	ΔE*	$Gloss_{60}$ (G.U.)
CHI0GLY	96.9 ± 0.5^{a}	-0.03 ± 0.06^{a}	2.5 ± 0.2^{a}	---	14 ± 2^{a}
CHI15GLY	96.6 ± 0.4^{a}	-0.11 ± 0.08^{a}	3.1 ± 0.3^{b}	0.6^{a}	16 ± 1^{a}
CHI0GLY2PE	96.7 ± 0.3^{a}	-0.08 ± 0.09^{a}	2.8 ± 0.2^{a}	0.3^{a}	$18 \pm 2^{a,b}$
CHI15GLY2PE	96.8 ± 0.3^{a}	-0.11 ± 0.07^{a}	2.9 ± 0.2^{b}	0.4^{a}	20 ± 2^{b}
CHI0GLYCD:2PE	96.4 ± 0.3^{a}	-0.10 ± 0.04^{a}	2.9 ± 0.2^{b}	0.6^{a}	20 ± 1^{b}
CHI15GLYCD:2PE	96.4 ± 0.7^{a}	-0.11 ± 0.08^{a}	2.9 ± 0.2^{b}	0.6^{a}	20 ± 1^{b}

$^{a-b}$Two means followed by the same letter in the same parameter are not significantly ($P > 0.05$) different through the Tukey's multiple range test.

Additionally, ultraviolet-visible (UV-vis) spectroscopy was carried out and results are shown in Figure 3.2. As can be seen, films were transparent since there was no absorption at 600 nm (Uranga et al., 2019). Furthermore, there was no absorption in the visible range from 400 to 800 nm, although chitosan films absorbed UV light, especially below 250 nm,

probably due to some chromophores present in chitosan (Leceta et al., 2013). In this regard, UV light barrier properties provide films with value-added properties, which can reduce lipid oxidation in food products and extend food shelf life (Fasihi et al., 2019).

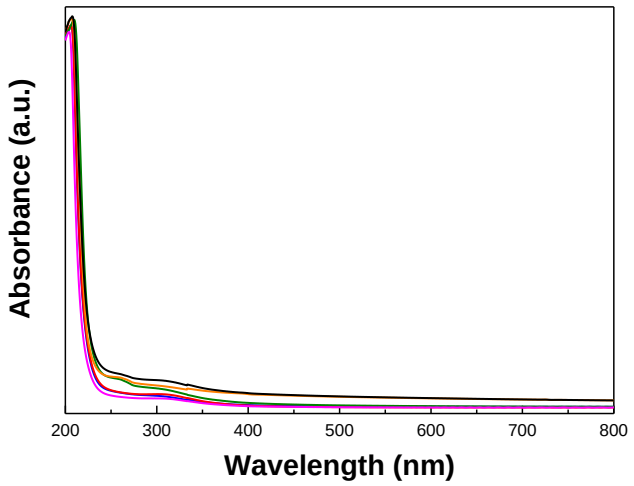

Figure 3.2. UV-vis light absorption of chitosan films: CHI0GLY, blue line; CHI15GLY, red line; CHI0GLY2PE, green line; CHI15GLY2PE, pink line; CHI0GLYCD:2PE, orange line; and CHI15GLYCD:2PE, black line.

3.4.4. Physicochemical properties of films

In order to assess the interactions among the components of the films, FTIR analysis was carried out and the FTIR spectra of chitosan films are shown in Figure 3.3. The characteristic bands of chitosan appeared at 1630 cm^{-1} (amide I band), associated to C=O stretching; at 1530 cm^{-1} (amide

II band), related to N-H bending; and at 1310 cm^{-1} (amide III band) assigned to C-N stretching (Mauricio-Sánchez et al., 2018). Moreover, O-H stretching band and C-O-C absorption band were observed at 3250 cm^{-1} and around 1080 cm^{-1}, respectively (Branca et al., 2016).

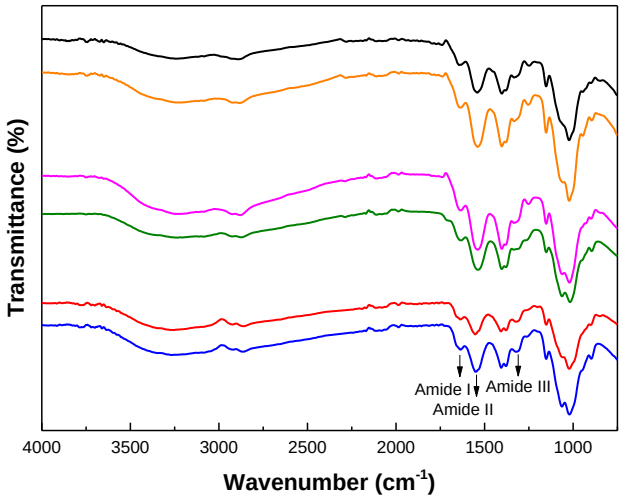

Figure 3.3. FTIR spectra of chitosan films: CHI0GLY, blue line; CHI15GLY, red line; CHI0GLY2PE, green line; CHI15GLY2PE, pink line; CHI0GLYCD:2PE, orange line; and CHI15GLYCD:2PE, black line.

No new band was observed between the control spectra and the spectra corresponding to the films with 2-phenyl ethanol, with or without CDs, indicating that no chemical reaction occurred. However, some band displacements were observed when β-CD:2-phenyl ethanol was incorporated into chitosan films; in particular, for O-H and N-H stretching

band from 3264 to 3214 cm^{-1}, for amide II band from 1546 to 1538 cm^{-1}, and for amide III band from 1324 to 1332 cm^{-1}. This suggests physical interactions, such as hydrogen bonding or electrostatic interactions among the components of the films (Roy & Rhim, 2020). Additionally, a similar behavior was observed with the addition of glycerol since O-H and N-H stretching band shifted from 3214 to 3243 cm^{-1} and amide II band from 1538 to 1540 cm^{-1} due to hydrogen bonding with glycerol.

In order to determine the structure of the films, XRD analysis was carried out (Figure 3.4).

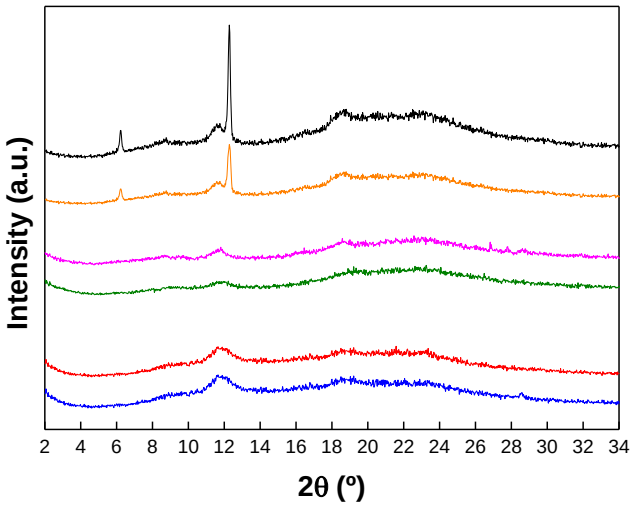

Figure 3.4. XRD diffractograms of chitosan films: CHI0GLY, blue line; CHI15GLY, red line; CHI0GLY2PE, green line; CHI15GLY2PE, pink line; CHI0GLYCD:2PE, orange line; and CHI15GLYCD:2PE, black line.

Films without the inclusion complex present two broad peaks, one at 11.7° and another one around 21.3°, characteristic of chitosan (Pang & Zhitomirsky, 2005). These broad peaks indicate the amorphous character of chitosan films. Regarding the films with the inclusion complex, two sharp peaks appeared at 6.2° and 12.3°, characteristic of β-CD (Campos et al., 2019; Menezes et al., 2016).

This indicates that CDs maintained certain degree of crystallinity after the incorporation into chitosan matrix. However, the intensity of these peaks was different for the films with and without glycerol, which could be attributed to the change in molecular organization of the cyclodextrin (Campos et al., 2018). Since glycerol is a small molecule, it can penetrate between chitosan chains, decreasing intramolecular interactions among chitosan chains and facilitating the interactions of chitosan with the additives incorporated into the film forming formulation (Zarandona et al., 2020). As shown by FTIR results, the intermolecular interactions with cyclodextrin molecules occurred by hydrogen bonding, which changed the chitosan film structure due to the heterogeneous nucleation effect between the inclusion complex and chitosan (Li, & Zhen, 2017) and, as a consequence, the film mechanical behavior also changed.

3.4.5. Mechanical and barrier properties

In order to assess the effect of structure changes in the mechanical behavior, tensile tests were performed and TS and EAB values were measured and shown in Table 3.2. As expected, films plasticized with glycerol showed higher EAB values and lower TS and E values, indicating more flexible and less rigid films due to the increase of free volume (Rivero et al., 2016). Regarding the addition of 2-phenyl ethanol, it was observed that this compound did not significantly ($P > 0.05$) change TS or EAB values with respect to the corresponding control film, probably due to the 2-phenyl ethanol evaporation during film preparation when CDs were not used. However, an increase of E values was noticed, indicating a higher rigidity, probably due to the interactions among chitosan and the remaining amount of 2-PE. The most significant change was observed for TS values when the inclusion complex was incorporated into formulations; in particular, TS value significantly ($P < 0.05$) increased from 34.5 to 48.8 MPa for the chitosan films with the inclusion complex but without glycerol. In accordance, E values also increased and EAB values decreased. This behavior can be related to the interactions among chitosan and CD, as shown by FTIR analysis, which would lead to a more compact

network, increasing resistance and rigidity, but decreasing flexibility (Siripatrawan & Vitchayakitti, 2016; Sun et al., 2014). It is worth noting that TS values above 40 MPa are higher values than those found for commercial packaging films, such as PP or LDPE (Honarvar et al., 2017, Lomate, Dandi, & Mishra, 2018).

Table 3.2. Tensile strength (TS), elongation at break (EAB), elastic modulus (E) and water vapor permeability (WVP, $g \cdot cm^{-1} \cdot s^{-1} \cdot Pa^{-1}$) of chitosan films.

Film	TS (MPa)	EAB (%)	E (MPa)	WVP·10^{12} ($g \cdot cm^{-1} \cdot s^{-1} \cdot Pa^{-1}$)
CHI0GLY	34.5 ± 2.2^{a}	9.2 ± 2.2^{b}	$1511 \pm 163^{a,b}$	1.08 ± 0.04^{a}
CHI15GLY	32.4 ± 3.1^{a}	16.4 ± 3.1^{a}	1374 ± 125^{a}	1.04 ± 0.02^{a}
CHI0GLY2PE	39.5 ± 3.6^{a}	7.8 ± 1.6^{b}	2205 ± 114^{c}	0.89 ± 0.04^{b}
CHI15GLY2PE	33.7 ± 3.4^{a}	12.3 ± 3.4^{a}	1687 ± 72^{b}	0.82 ± 0.01^{b}
CHI0GLYCD:2PE	48.8 ± 3.2^{b}	7.4 ± 2.2^{b}	2639 ± 173^{d}	0.83 ± 0.03^{b}
CHI15GLYCD:2PE	37.5 ± 4.1^{a}	8.1 ± 2.3^{b}	1960 ± 84^{c}	0.85 ± 0.02^{b}

$^{a\text{-}c}$Two means followed by the same letter in the same parameter are not significantly ($P > 0.05$) different through the Tukey's multiple range test.

Regarding water vapor permeability (WVP), there was no significant difference ($P > 0.05$) between the chitosan films without 2-phenyl ethanol. However, the addition of the active compound significantly ($P < 0.05$) decreased WVP values, probably due to the interactions with chitosan (Salami et al., 2020), as shown by FTIR, and also due to the increase of crystallinity, as observed by XRD. Although WVP

values found in this work are lower than those measured for chitosan films in other works (Priyadarshi et al., 2018), these values are still higher than those shown by commercial films (Honarvar et al., 2017, Lomate, Dandi, & Mishra, 2018).

3.4.6. Release of 2-phenyl ethanol

The release of 2-phenyl ethanol from chitosan films with 2-phenyl ethanol and from chitosan films with β-cyclodextrin:2-phenyl ethanol was carried out in order to compare the delivery trend during the immersion into 95 % ethanol for 4 days (Figure 3.5). Regarding CHI0GLY2PE films, it is worth noting that some bioactive content was lost before the analysis, probably during film preparation due to the high volatility of the compound and, as a result, a maximum release of 8 % was achieved. However, chitosan films with the inclusion complex retained the bioactive inside β-cyclodextrin after film preparation. An improvement of 2-PE retention through its encapsulation with methylcellulose, alginate sodium and carboxymethyl chitosan has also been observed in other works (Qiu, Tian, Yin, Zhou, & Zhu, 2019). In this work, 2-phenyl ethanol was released after 4 h of immersion into 95 % ethanol. The fast release of 2-phenyl

ethanol could be explained due to the weak interactions with β-cyclodextrin, since 2-phenyl ethanol has only one hydroxyl group.

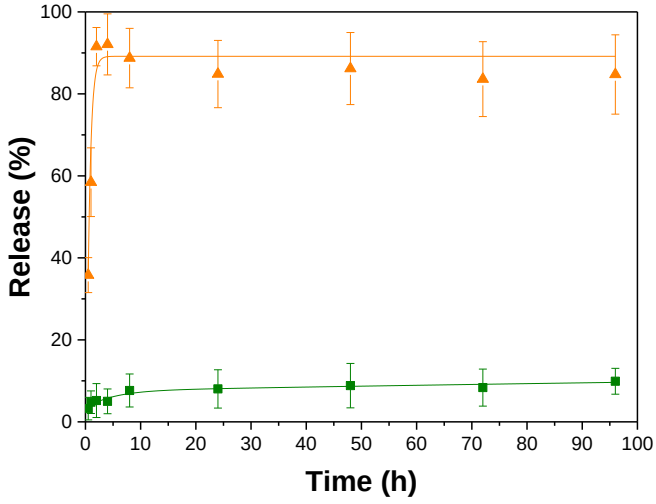

Figure 3.5. Bioactive release from chitosan films: CHI0GLY2PE, green line; CHI0GLYCD:2PE, orange line.

3.5. Conclusions

This work showed the good capacity of cyclodextrins to form inclusion complex with 2-phenyl ethanol. Specifically, β-cyclodextrin showed the highest retention yield. The films obtained were homogeneous, transparent and colorless. Moreover, the addition of the inclusion complex into chitosan film forming solutions led to chitosan films with improved properties. In particular, tensile strength reached values up to 48 MPa. The tensile strength increase was related to the

physical interactions between chitosan and the inclusion complex, which were corroborated by FTIR and XRD analyses, which indicated the crystalline structure of chitosan films with the inclusion complex. Finally, the release of 2-phenyl ethanol into 95 % ethanol was carried out in films with and without β-cyclodextrin. Results suggested that the bioactive was evaporated during film preparation for the films without the inclusion complex. In contrast, the films with the inclusion complex preserved the bioactive inside the inclusion complex. These results indicated that CDs were effective to avoid the loss of bioactive compounds during film preparation.

Chapter

4

Active chitosan films with gallic acid: Antioxidant and antimicrobial activities

4.1. Summary

Chitosan films with antioxidant and antimicrobial properties were prepared by the incorporation of gallic acid as a bioactive. The films obtained were homogeneous, transparent and colorless with high mechanical resistance. Results indicated that films had antimicrobial activity against *E. coli*, especially those films plasticized with 15 wt % glycerol and containing 20 wt % gallic acid, which showed the biggest inhibition halo. Additionally, gallic acid-incorporated chitosan films exhibited a great antioxidant activity with DPPH scavenging capacity values of 99 % and a bioactive release of 33 % after 4 days, suggesting the potential suitability of these modified chitosan films as active films for food purposes.

4.2. Introduction

Phenolic compounds are well-known antioxidants that can be derived from biowastes, contributing to their valorization (Crizel et al., 2018; Liudvinaviciute et al., 2019; Mirón-Mérida et al., 2019). In recent years, the use of chitosan with different antioxidants has been assessed. Polyphenols extracted from blueberry or grape skin pomace have been incorporated into chitosan film forming formulations in order to develop bioactive films for food packaging, obtaining easy to handle films that

show antioxidant activity proportional to the total phenolic content (Kurek et al., 2019). Additionally, antioxidant and antimicrobial chitosan films have been prepared with naringin, resulting in UV-barrier films that prevent food oxidation by UV light (Iturriaga et al., 2014). Furthermore, eggplant and sweet potato extracts have been added to the chitosan matrix to develop both active and intelligent films since sweet potato extract is rich in anthocyanins, which show pH-sensitive color changes (Yong et al., 2019 a, b). In addition, curcumin, a di-phenolic compound with antioxidant and antimicrobial activities, among others, has provided chitosan films with enhanced water vapor and UV barrier properties, leading to suitable materials for active food packaging (Roy & Rhim, 2020).

Regarding phenolic compounds, gallic acid (GA) is a natural phenolic compound, found as a secondary metabolite in blueberries, apples, grapes and tea, which has shown antioxidant, antimicrobial, antimutagenic, anti-inflammatory and anticancer properties (Brewer 2011; Raspo, Gomez, & Andreatta, 2018; Rui et al., 2017). Like other phenolic compounds, GA can interact with chitosan through physical interactions, such as hydrogen bonding and electrostatic and hydrophobic forces, and/or chemical reactions, contributing to enhance the mechanical

properties of chitosan films, in addition to its antioxidant activity (Wang et al. 2019). Additionally, GA can be chemically bound to chitosan using reagents like carbodiimide (Zhang et al., 2019); however, dark and opaque films are obtained as a result of the grafting reaction. Moreover, harsh conditions and/or the use of environmentally disadvantageous or even toxic reagents are usually required in these reactions. In this context, the aim of this work was to enhance functional properties and biological activity of chitosan films by the incorporation of GA without the addition of further chemical agents.

In this chapter, chitosan films prepared with gallic acid as a bioactive compound were characterized as a function of the concentrations of gallic acid and glycerol, used as a plasticizer. Hence, optical properties, such as color and gloss, were analyzed due to the fact that the film appearance is a relevant aspect for the customer willingness to buy a product. In order to evaluate the interactions between the components of the film forming formulations, Fourier transform infrared (FTIR) spectroscopy was carried out. Additionally, the mechanical behavior of the films was analyzed and related to the film microstructure observed by scanning electron microscopy (SEM). Finally, the film bioactivity, including antioxidant and

antimicrobial properties, was assessed in order to evaluate the suitability of these films for food or pharmaceutical applications

4.3. Materials and methods

4.3.1. Materials

Chitosan (CHI), with a molecular weight of 375 kDa and deacetylation degree above 75 %, was supplied by Sigma-Aldrich, Spain. Acetic acid solution (1 N) and glycerol (GLY, 99.0 % purity), used as solvent and plasticizer, respectively, were supplied by Panreac, Spain. Gallic acid (GA, ≥ 98.0 % purity), employed as a bioactive compound, was supplied by Merck, Spain.

4.3.2. Film preparation

Chitosan films were prepared by solution casting as described by Leceta, Guerrero, Ibarburu, Dueñas, & de la Caba (2013), with some modifications. First, 1 % (w/v) chitosan was dissolved in 1 wt % acetic acid solution and maintained at room temperature under continuous stirring for 45 min. After that, 10 or 20 wt % gallic acid (based on chitosan) was added and stirring was continued for other 30 min. Finally, 15 wt % glycerol (based on chitosan) was added as plasticizer and other 30 min of

stirring were needed until total homogenization of the mixture. The solution was casted into Petri dishes (33 g per dish) and left to dry at room temperature for 48 h. Control films without gallic acid were prepared and designated as CHI0GLY0GA and CHI15GLY0GA as a function of glycerol content. The films prepared with gallic acid were designated as CHI0GLY10GA, CHI0GLY20GA, CHI15GLY10GA, and CHI15GLY20GA as a function of glycerol and gallic acid contents, whose concentrations were selected considering the results of previous works (Leceta et al., 2013) and solubility in water, respectively. All films were conditioned in a climatic chamber (Alava Ingenieros, Madrid, Spain) at 25 °C and 50% relative humidity before testing.

4.3.3. Film characterization

4.3.3.1. Color and gloss measurements

Color measurements were performed using a CR-400 Minolta Chroma Meter colorimeter (Konica Minolta, Tokyo, Japan). CIELAB scale was employed for the determination of color parameters, with L* from 0 to 100 (from black to white), a* from - to + (from green to red), and b* from - to + (from blue to yellow). Moreover, saturation and color appearance were determined by Chrome and Hue parameters. Before measuring

samples' color, calibration was carried out with a standard white plate. Standard values for the white calibration plate were $L^* = 97.39$, $a^* = 0.03$, and $b^* = 1.77$. Ten replicates were done for each sample.

Gloss was determined at the incidence angle of 60°, according to ASTM D523-18 (ASTM, 2018), with a Multi Gloss 268 Plus gloss meter (Konica Minolta, Tokyo, Japan). Ten measurements were taken for each sample.

4.3.3.2. Fourier transform infrared (FTIR) spectroscopy

FTIR spectra of the films were collected by means of a Nicolet Nexus FTIR spectrometer (Thermo Fisher Scientific, Massachusetts, USA) with a Golden Gate ATR sampling accessory. 32 scans were collected for each sample at a 4 cm^{-1} resolution between 4000 and 800 cm^{-1}.

4.3.3.3. Mechanical properties

An Instron 5967 electromechanical testing system (Instron, Massachusetts, USA), equipped with a load cell of 500 N, was used to determine the tensile strength (TS), elongation at break (EAB) and elastic modulus (E). Tensile tests were carried out according to ASTM D638-14

(ASTM, 2014). Five specimens for each sample were cut into bone-shaped samples of 4.75 mm × 22.25 mm and the crosshead rate was 1 mm/min.

4.3.3.4. Scanning electron microscopy (SEM)

A Hitachi S-4800 scanning electron microscope (Hitachi High-Technologies Corporation, Tokyo, Japan), with an acceleration voltage of 15 kV, was used to record surface and cross-section images. Films were set on a metallic stub and covered with gold under vacuum in argon atmosphere.

4.3.3.5. Antioxidant activity

Antioxidant activity was measured according to Fernández-Pan, Maté, Gardrat, & Coma (2015), with some modifications. Samples were immersed into a 95 % ethanol solution during 4 days and an aliquot of 2 mL was mixed with 2 mL of DPPH solution (75 μM). The mixture was stirred and the absorbance at 570 nm was measured after the solution was settled for 30 min. The antioxidant activity, given as the inhibition value (I), was calculated as follows:

$$I\ (\%) = \frac{A_c - A_{sample}}{A_c} \cdot 100$$

where A_c is the absorbance of DPPH solution and A_{sample} is the absorbance of the sample solution with DPPH.

At the same time, the pieces of films were weighed before being immersed into the 95 % ethanol solution (W_0) and after 4 days of immersion (W_f) for the mass loss measurement:

$$Mass\ loss\ (\%) = \left[1 - \left(\frac{W_f}{W_0}\right)\right] \cdot 100$$

4.3.3.6. Bioactive release

Pieces of films (1 cm x 2 cm) were immersed into a 95 % ethanol solution (30 mL) during 4 days at room temperature with continuous stirring (200 rpm). Aliquots of 4 mL were collected at 30 min, 1 h, 2 h, 4 h, 8 h, 1 d, 2 d, 3 d, and 4 d and replaced with fresh 95 % ethanol solution in order to keep the initial volume. Aliquots were analyzed with a UV-VIS-NIR Shimadzu 3600 spectrophotometer (Shimadzu Scientific Instruments, Kyoto, Japan) at the maximum wavelength absorbance for gallic acid (272.5 nm). So as to calculate the concentration of gallic acid, a calibration curve was carried out from 0.1 to 10 μg/mL. Measurements were carried out in triplicate.

4.3.3.7. Antimicrobial activity

In order to test the antimicrobial capacity of chitosan films against both Gram-negative and Gram-positive bacteria, *Escherichia coli* DH5α *(E. coli)* (Hanahan, 1983) and *Lactobacillus sakei* AC11 (*L. sakei*), lactic acid bacteria isolated from the ropy slime of the surface of a vacuum-packed sliced cooked ham, were used. *E. coli* was grown in Luria Bertani (LB) broth at 37 °C with shaking (220 rpm) and *L. sakei* in de Man Rogosa and Sharpe broth (MRS, Pronadisa, Spain) at 30 °C under an atmosphere containing 5 % of CO_2.

The antibacterial activity of the films was tested by using a disk diffusion assay as described by Zivanovic, Chi, and Draughon (2005) with some modifications. Chitosan films were cut as discs of 15 mm diameter and sterilized under UV light. Films were placed on the surface of LB and MRS agar and covered by a thin layer of agar. After 4 h at room temperature for the diffusion of gallic acid into the agar, plates were spread with 0.1 mL of inoculum containing $10^5 – 10^6$ CFU/mL of bacteria. The plates were incubated overnight, as described above, and they were optically examined for the diameter of inhibition in the surrounded area

of the films. Two inhibition halo diameters were measured for each sample and three replicates were tested for each sample.

4.3.4. Statistical analysis

In order to determine significant differences between samples, analysis of variance (ANOVA) was done with SPSS software (SPSS Statistic 24.0.0.2). Tukey's test with a statistically significance at the $P < 0.05$ level was considered for multiple comparisons among different systems.

4.4. Results and discussion

4.4.1. Optical properties

Color parameters are shown in Table 4.1. As can be observed, values were very similar; therefore, the addition of glycerol and gallic acid at different concentrations did not affect the film color, in contrast to other works in which dark and opaque films are obtained for chitosan films with gallic acid (Zhang et al., 2019). The films were colorless, in agreement with the color values obtained, since a* and b* values were close to zero. Regarding Chrome (C*) and Hue (h*) parameters, which are related to the saturation and color appearance, respectively, C* showed values around 2.5 for chitosan films without GA and around 5.0 for films with GA,

indicating that the film color saturation was low. For h* values, all samples showed similar color appearance, with values around 93, indicating that the color of the films was greenish-yellowish.

Film gloss can be related to the film roughness: the lower the gloss, the higher the roughness. Since glossy and smooth surfaces are considered when gloss values at 60° incidence angle are above 70 gloss units (G.U.) (Etxabide et al., 2017), the gloss values obtained in this work, all of them bellow 50, indicated rough surfaces (Table 4.1). Similar gloss values (bellow 50 G.U.) have been found for chitosan films with phenolic compounds (Pastor et al., 2013). It is worth noting that films without glycerol had higher values than those with glycerol, indicating smoother surfaces, and that the addition of gallic acid increased ($P < 0.05$) the film smoothness, irrespective of gallic acid content ($P > 0.05$), suggesting interactions between chitosan and gallic acid, which affected the film surface structure.

In contrast, there was no significant ($P > 0.05$) difference in the gloss values for glycerol-plasticized samples, indicating the key role of glycerol in these systems. In fact, glycerol is a small molecule that interacts with chitosan, decreasing intramolecular interactions among chitosan chains

and facilitating the interactions of chitosan with the additives incorporated into the film forming formulation.

4.4.2. Physicochemical properties

FTIR spectra of the films are shown in Figure 4.1. As can be observed, there was a wide band in the range from 3000 to 3670 cm^{-1} related to O-H and N-H stretching vibrations (Leceta et al., 2018). This band, centered around 3260-3250 cm^{-1}, shifted to lower wavenumbers (≈ 3200 cm^{-1}) for the films without glycerol and the highest content of gallic acid (CHI0GLY20GA). However, the main differences between the control films and the films with gallic acid were found in the interval from 1650 cm^{-1} to 1250 cm^{-1}. In this spectral range, two bands appeared around 1640 cm^{-1} and 1540 cm^{-1}, assigned to the amide I and amide II bands of chitosan, respectively (Roy & Rhim, 2020). In particular, the band corresponding to amide II was shifted depending on glycerol or gallic acid addition. For the films without glycerol, the increase in gallic acid concentration shifted this band to lower wavenumbers, specifically from 1544 cm^{-1} for CHI0GLY0GA to 1532 cm^{-1} for CHI0GLY20GA.

Table 4.1. Color (L*, a*, b*, C* and h*) and gloss values for chitosan films.

Film	L*	a*	b*	C*	h*	$Gloss_{60}$ (G.U.)
CHI0GLY0GA	96.4 ± 0.9^{a}	$-0.17 \pm 0.07^{c,d}$	2.86 ± 0.26^{a}	2.9 ± 0.3^{a}	93.4 ± 1.1^{b}	28 ± 4^{a}
CHI0GLY10GA	95.2 ± 0.5^{b}	-0.32 ± 0.04^{b}	4.99 ± 0.48^{b}	5.0 ± 0.5^{b}	93.7 ± 0.2^{b}	46 ± 8^{b}
CHI0GLY20GA	95.1 ± 0.4^{b}	-0.35 ± 0.04^{b}	5.63 ± 0.62^{c}	5.6 ± 0.6^{c}	93.5 ± 0.6^{b}	41 ± 3^{b}
CHI15GLY0GA	96.9 ± 0.4^{a}	-0.14 ± 0.02^{d}	2.47 ± 0.08^{a}	2.5 ± 0.1^{a}	93.3 ± 0.4^{b}	19 ± 7^{c}
CHI15GLY10GA	94.9 ± 0.4^{b}	-0.21 ± 0.05^{c}	5.94 ± 0.68^{c}	6.0 ± 0.7^{c}	92.0 ± 0.4^{a}	17 ± 3^{c}
CHI15GLY20GA	95.6 ± 0.6^{b}	-0.43 ± 0.03^{a}	4.89 ± 0.14^{b}	4.9 ± 0.1^{b}	95.0 ± 0.3^{c}	22 ± 5^{c}

$^{a-d}$Two means followed by the same letter in the same column are not significantly ($P > 0.05$) different through the Tukey's multiple range test.

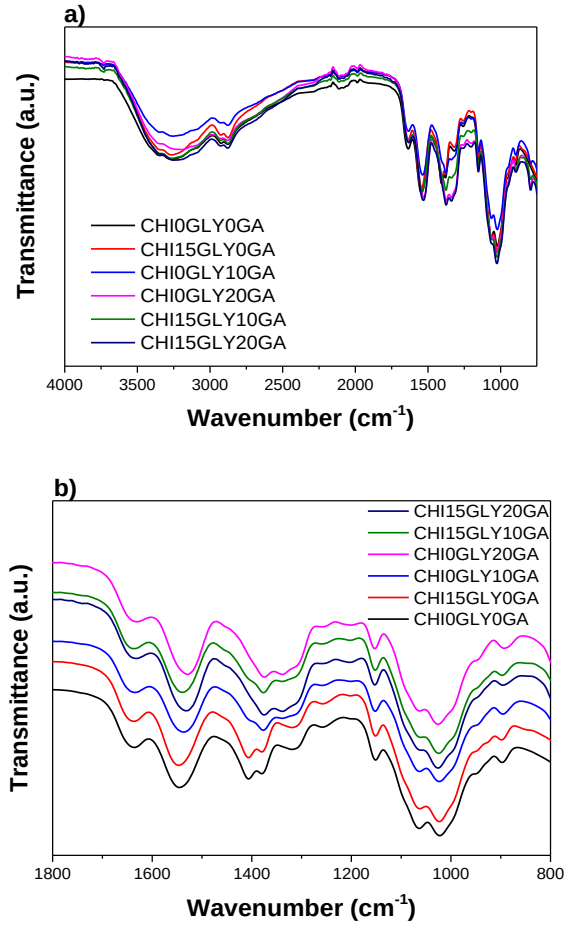

Figure 4.1. FTIR spectra a) from 4000 to 750 cm^{-1} and b) from 1800 to 800 cm^{-1} for chitosan (CHI) films as a function of glycerol (GLY) and gallic acid (GA) content.

When glycerol was added, the band was slightly shifted to higher wavenumbers, from 1544 cm^{-1} for CHI0GLY0GA to 1546 cm^{-1} for CHI15GLY0GA, and this band was shifted to lower wavenumbers when gallic acid was incorporated into glycerol-containing films. Additionally, the band associated to the C-O stretching vibration, which appears at 1310

cm^{-1} in gallic acid (Božič, Gorgieva, & Kokol, 2012), shifted to 1340 cm^{-1} for gallic acid-incorporated films, suggesting the interactions between gallic acid and chitosan.

4.4.3. Mechanical properties and film microstructure

Tensile strength (TS), elongation at break (EAB) and elastic modulus (E) values of chitosan films are presented in Table 4.2.

Table 4.2. Tensile strength (TS), elongation at break (EAB) and elastic modulus (E) values of chitosan films.

Film	TS (MPa)	EAB (%)	E (MPa)
CHI0GLY0GA	24 ± 5^{a}	10.8 ± 2.1^{b}	$1449 \pm 125^{b,c}$
CHI0GLY10GA	$41 \pm 3^{b,c}$	4.8 ± 0.6^{a}	2440 ± 222^{d}
CHI0GLY20GA	$40 \pm 3^{b,c}$	6.9 ± 1.4^{a}	2491 ± 191^{d}
CHI15GLY0GA	34 ± 4^{b}	15.6 ± 1.9^{c}	1083 ± 56^{a}
CHI15GLY10GA	43 ± 3^{c}	$13.8 \pm 2.5^{b,c}$	$1312 \pm 153^{a,b}$
CHI15GLY20GA	51 ± 4^{d}	10.9 ± 1.1^{b}	1726 ± 88^{c}

$^{a\text{-}c}$Two means followed by the same letter in the same column are not significantly ($P > 0.05$) different through the Tukey's multiple range test.

As can be observed, the addition of gallic acid increased ($P < 0.05$) both TS and E values for the films with and without glycerol. The most resistant films were those prepared with glycerol and with 20 wt % gallic acid (CHI15GLY20GA), which showed a TS value of 51 MPa, value higher than that found for commercial films, such as PP (30 MPa) and LDPE (22

MPa) (Amri, Husseinsyah, & Hussin, 2013; Bula, Klapiszewski, & Jesionowski, 2019). This behavior can be associated to the chemical structure of gallic acid, which is an aromatic compound that confers rigidity to the film (Zhao et al., 2018). Accordingly, the most flexible films were those plasticized with glycerol and without gallic acid (CHI15GLY0GA). EAB values decreased ($P < 0.05$) when gallic acid was incorporated, suggesting the interaction between the carboxylic group of gallic acid and the amino group of chitosan (Raspo, Gomez, & Andreatta, 2018; An, Kang, & Li, 2019), which would reduce the flexibility of the films.

Regarding film microstructure, cross-section images are shown in Figure 4.2, which indicated a good compatibility among the components of the films. Furthermore, when glycerol was added, a less compact structure was observed due to the plasticization effect of glycerol, which reduced the intramolecular interactions among chitosan chains while increased intermolecular interactions between chitosan and glycerol.

4.4.4. Antioxidant activity and bioactive release

Mass loss values measured after immersion into ethanol for 4 days were lower than 25 %, as can be seen in Table 4.3.

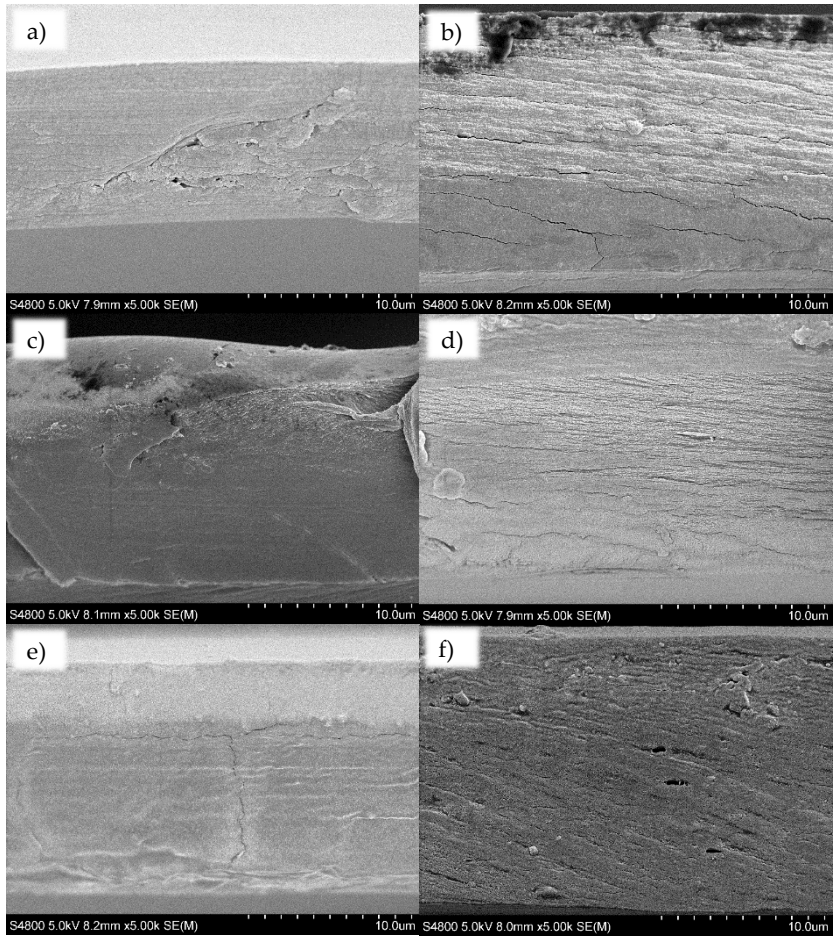

Figure 4.2. SEM images of cross-section (x5.0k) for a) CHI0GLY0GA, b) CHI15GLY0GA, c) CHI0GLY10GA, d) CHI15GLY10GA, e) CHI0GLY20GA, and f) CHI15GLY20GA films.

Films plasticized with glycerol showed higher ($P < 0.05$) mass loss values than those without glycerol, indicating that some glycerol was dissolved and suggesting that chitosan-glycerol interactions were physical interactions, probably by hydrogen bonding. Moreover, when gallic acid content increased, mass loss values decreased ($P > 0.05$) for both

plasticized and non-plasticized films. This behavior would corroborate the interactions between chitosan and gallic acid, as shown by FTIR results.

Table 4.3. DPPH inhibition and mass loss percentages for chitosan films.

Film	Mass loss (%)	DPPH inhibition (%)
CHI0GLY0GA	18 ± 1[a]	51.9 ± 2.1[a]
CHI0GLY10GA	15 ± 2[a]	96.3 ± 0.5[b]
CHI0GLY20GA	13 ± 2[a]	96.4 ± 0.2[b]
CHI15GLY0GA	24 ± 1[b]	51.4 ± 0.1[a]
CHI15GLY10GA	22 ± 2[b]	96.2 ± 0.1[b]
CHI15GLY20GA	20 ± 2[b]	96.4 ± 0.1[b]

[a-b]Two means followed by the same letter in the same column are not significantly ($P > 0.05$) different through the Tukey's multiple range test.

Regarding the antioxidant capacity, all the films prepared with gallic acid had similar ($P > 0.05$) values of DPPH radical scavenging capacity, around 96 %, while the films without gallic acid showed an antioxidant activity of 51 %. These values are higher than those found in recent works for chitosan films grafted with gallic acid (Zhang et al., 2019), probably due to the fact that the degree of crosslinking in this work was lower due to the absence of coupling agents and the use of mild conditions during the film preparation.

The results shown in Table 4.3 indicated that glycerol did not affect the antioxidant capacity of gallic acid-modified chitosan films and, thus, bioactive release measurements were carried out for glycerol-plasticized films with 10 and 20 wt % gallic acid. As can be seen in Figure 4.3, values between both films were not significantly different ($P > 0.05$) before 24 h, but they are ($P < 0.05$) from 24 h to 96 h, when the accumulative release was around 33 %, indicating that certain content of gallic acid reacted with chitosan and, thus, could not be released.

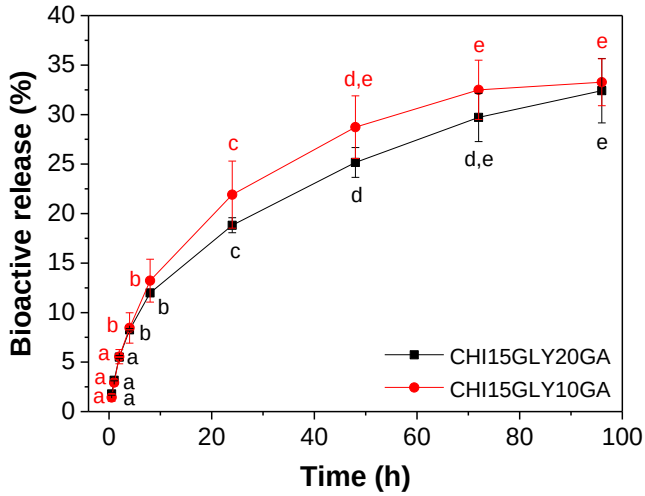

Figure 4.3. Gallic acid release profile from chitosan films into 95 % ethanol solution. [a-e]Two means followed by the same letter in the same column are not significantly ($P > 0.05$) different through the Tukey's multiple range test.

Therefore, it is worth noting that gallic acid can act as a bioactive since it can be released from chitosan films and provide them with antioxidant capacity, but also a notable amount of gallic acid can be preserved in the film, leading to films with significantly higher tensile resistance.

4.4.5. Antimicrobial activity

No inhibition zone was observed for chitosan films without GA, in accordance with previous works (Chen et al., 2019; Lun'kov et al., 2018; Raghavendra et al., 2016). However, in the films prepared with 10 and 20 wt % gallic acid, an inhibition halo was observed for *E. coli*, regardless of glycerol addition, as can be observed in Figure 4.4. In contrast, no inhibition zone was found for *L. sakei*.

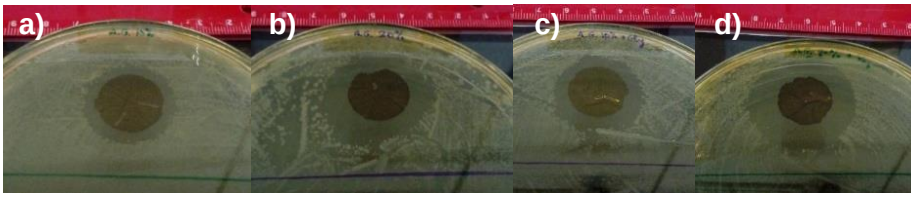

Figure 4.4. Images of the inhibition halo for a) CHI0GLY10GA, b) CHI0GLY20GA, c) CHI15GLY10GA, and d) CHI15GLY20GA films against *E. coli*.

As can be seen in Table 4.4, the inhibition halo diameters were higher for the films prepared with a higher gallic acid content. Furthermore, for the same gallic acid content, the inhibition capacity was slightly higher for the films prepared with glycerol; therefore, the best results were found for the films prepared with 15 wt % glycerol and 20 wt % gallic acid. Although glycerol itself does not have any antimicrobial effect (Sabbah et al., 2019), results suggested that glycerol facilitated the diffusion of gallic acid, improving the antimicrobial activity of gallic acid-modified chitosan films.

Table 4.4. Inhibition halo against *E. coli* and *L. sakei* for chitosan films.

Film	Inhibition halo diameter (mm)	
	E. coli	***L. sakei***
CHI0GLY0GA	nd	nd
CHI0GLY10GA	24 ± 3^{c}	nd
CHI0GLY20GA	27 ± 3^{b}	nd
CHI15GLY0GA	nd	nd
CHI15GLY10GA	$25 \pm 2^{b,c}$	nd
CHI15GLY20GA	30 ± 3^{a}	nd

nd = not detected. $^{a\text{-}c}$Two means followed by the same letter in the same column are not significantly ($P > 0.05$) different through the Tukey's multiple range test.

4.5. Conclusions

The addition of gallic acid into chitosan film forming formulations led to transparent and colorless films with tensile strength values higher

than 40 MPa. FTIR analysis showed some changes in the frequency at which the main functional groups appeared, depending on glycerol and acid gallic concentration, indicating interactions among the polar groups of chitosan and the additives incorporated into the film forming formulation. Furthermore, films showed antioxidant and antimicrobial activity. In particular, 33 % of gallic acid was released from the film, suggesting that a certain amount of gallic acid could react with chitosan and could not be delivered. Beside antioxidant activity, films showed antimicrobial capacity against *E. coli*, especially those films plasticized with glycerol and with the highest content of gallic acid (CHI15GLY20GA), which had the greatest inhibition halo diameter. This behavior suggests the potential use of these materials as bioactive films for food or pharmaceutical applications.

Chapter

5

Active chitosan coatings with gallic acid: Extension of fish shelf life

5.1. Summary

Atlantic horse mackerel (*Trachurus trachurus*) fillets were coated by gallic acid and chitosan solutions, including chitosan nanoparticles, and fish quality and shelf life were assessed during chilled storage for 13 days. All chitosan-containing coatings decreased microorganisms' growth in more than 2 log cycles up to late storage stages; however, those with chitosan nanoparticles resulted to be more effective, probably due to a greater contact surface with fish muscle. Furthermore, the lowest total volatile basic nitrogen (TVB-N) values, as well as pH values below 7, were found for horse mackerel fillets coated by those solutions with chitosan nanoparticles. Additionally, horse mackerel fillets coated by solutions with chitosan nanoparticles also showed the lowest thiobarbituric acid reactive substances (TBARS) values, maybe owing to a more sustained release of gallic acid. In this regard, it is worth noting that, although gallic acid solution showed no antimicrobial activity, this prevented lipid oxidation and, therefore, preserved color and texture during the chilling storage.

5.2. Introduction

Atlantic horse mackerel (*Trachurus trachurus*) has great popularity worldwide due to its nutritional value and its extended use as raw material for sushi, tataki or sashimi preparation, among others. Nevertheless, due to its content of unsaturated lipids, sensitive to oxidation, horse mackerel is highly perishable, and keeping fish quality during the supply chain is a challenge (Karoui & Hassoun, 2017; Sone et al., 2019). Like other fish products, horse mackerel is susceptible to rapid *post-mortem* spoilage due to biochemical reactions, handling, or storage conditions (Ezquerra-Brauer et al., 2016; Olatunde & Benjakul, 2018). In this concern, refrigerated storage is the common method for preservation in order to inhibit microbial growth and enzymatic degradation processes, maintaining fish quality (Miranda et al., 2018).

Furthermore, there is a growing interest in investigating active materials with antimicrobial and antioxidant capacities, considering shelf life enhancement as well as food safety and quality (Kumar, Mukherjee & Dutta, 2020). With this aim, natural polymers, such as chitosan, are commonly used to prepare coatings (Irawan et al., 2019). In this regard, recent studies have concluded that the use of chitosan-based coatings

delayed bacterial growth and inhibited lipid oxidation in refrigerated *Nemipterus japonicus*fillets, extending food shelf life for more than 10 days (Ebadi et al., 2019).

In this context, edible coatings are gaining more and more interest to retard fish protein degradation, lipid oxidation, and avoid discoloration and moisture loss due to their efficacy and harmless nature (Huang et al., 2020; Zhang et al., 2019). In this chapter, chitosan coatings were prepared by dipping process and their effects on the shelf life of fresh horse mackerel fillets stored at 4 °C for ready to eat products was assessed. Furthermore, chitosan nanoparticles have been employed with the aim of promoting a longer shelf life extension, due to their bigger contact surface, which could improve functional properties with respect to common chitosan coatings (Istúriz-Zapata et al., 2020). Besides, taking the previous results in chapter 5 into account, gallic acid was used as bioactive compound. To the best of our knowledge, there is no information about the effect of chitosan and/or gallic acid coatings (alone or in combination) or forming nanoparticles, during the horse mackerel storage.

In this chapter, horse mackerel fillets were coated by dipping and stored at 4 °C; bacterial counts, physicochemical properties, and texture

were analyzed during a period of 13 days in order to determine the quality of the fillets and shelf life.

5.3. Materials and methods

5.3.1. Materials

Chitosan, with a molecular weight of 375 kDa and a deacetylation degree of 75 %, and sodium tripolyphosphate (TPP, technical grade, 85 % purity) were supplied by Sigma-Aldrich, Spain. Acetic acid solution (1 N), used as a solvent, was supplied by Panreac, Spain, and gallic acid (≥ 98.0 % purity), employed as a bioactive compound, was supplied by Merck, Spain.

5.3.2. Preparation and characterization of coating solutions

With the aim of assessing the quality and shelf life of Atlantic horse mackerel (*Trachurus trachurus*) fillets, 4 coating solutions were prepared: i) 0.1 % (w/v) gallic acid solution, designated as GA; ii) 1 % (w/v) chitosan solution, named as Ch; iii) 1 % (w/v) chitosan solution with 10 wt % gallic acid (based on chitosan), identified as GACh; and iv) a solution with chitosan nanoparticles and 10 wt % gallic acid (based on chitosan),

designated as GAChNP. The pH was adjusted to 5.5 for all the solutions, which were kept at 4 °C ± 1 until use.

In order to prepare GA solution, 0.1 g gallic acid was dissolved in 100 mL distilled water at room temperature under continuous stirring until total solubilisation. For the preparation of Ch solution, 1 g chitosan was dissolved in 100 mL of 1wt % acetic acid solution and stirred for 45 min at room temperature. After that, gallic acid (10 wt % based on chitosan weight) was added to Ch solution and kept under continuous stirring for 30 min until total homogenization. Finally, the GAChNP solution was prepared by dissolving 1 g chitosan in a 3 wt % acetic acid solution under continuous stirring overnight at room temperature; afterward, 10 wt % gallic acid (chitosan-based) was added and stirring was maintained for 1 h. Subsequently, a TPP solution (3.3 mg/mL) was added, drop by drop, under continuous stirring for 30 min, and it was sonicated for 5 min in a pulsed mode, with a 60 s stop every min, and 80% amplitude using a Q700 sonicator (Qsonica, Newton, CT, EEUU, max 700 W) with a 12.7 mm diameter probe (sample was placed in an ice bath to avoid overheating).

A Zetasizer Nano Series Nano-ZS90 (Malvern Panalytical, UK) was used to assess particle size (expressed as z-average) and Zeta potential of GAChNP solution, which were 286 ± 5 nm and 27 ± 1 mV, respectively.

5.3.3. Fish storage trial

5.3.3.1. Sample preparation

Fresh Atlantic horse mackerel was acquired at a specialized local market. Fish was cleaned, cut in fillets, and stored frozen at -80 °C. Proximate analysis of the raw muscle was carried out showing the following results: 79.2 ± 0.2 % moisture, 20 ± 1 % total protein, 1.33 ± 0.04 % ash and 0.7 ± 0.2 % total fat.

24 h before the fish fillet coating, horse mackerel fillets were taken out from the store at -80 °C and thawed in a cold chamber at 4 ± 1 °C. The fillets were randomly divided in 5 batches: control fillets without coating and fillets coated by the 4 solutions prepared. Fillets were immersed into solutions and slightly shaken for 2 min. In order to remove the excess of coating, fillets were placed in a strainer and, then, they were stored at 4 °C. For fish quality assessment, the coating day was set as day 0, and samples were taken at days 3, 6, 9, and 13 for analyses.

5.3.3.2. Muscle water content

The water content of the horse mackerel muscle and the different samples along the storage period were determined according to AOAC official methods 934.01 (AOAC, 2000). Three replicates were performed for each batch.

5.3.3.3. Mass loss

Three horse mackerel fillets for each batch were weighed during the storage trial and results were expressed as mass loss percentage (%) with respect to the initial mass.

5.3.3.4. Protein viscosity

5 g of horse mackerel muscle were homogenized with 5 % NaCl in a 1:5 ratio. A CVO rotary rheometer (Bohlin Instruments Ltd, Gloucestershire, UK) coupled to a cone-plate (cone angle 4°, gap 0.15 mm) was used for viscosity determination. The analysis was performed at 4 °C and the values obtained were provided by the mean of 15 replicates.

5.3.3.5. Total volatile basic nitrogen (TVB-N)

10 g of horse mackerel muscle were homogenized with 90 mL of a 6% perchloric acid solution for protein precipitation. The mixture was

filtrated with a Whatman no. 1 filter and the volume was adjusted to 100 mL. The filtrate was alkalinized with 20 % NaOH and distilled in a Tecator AB device (model 1002, Kjeltec Systems, Sweden). The distillate was collected on a 0.3 % boric acid solution and titrated with a 0.05 N HCl solution. Three replicates were performed for each sample and the average value was expressed as mg total volatile basic nitrogen per 100 g of sample.

5.3.3.6. pH

Fillet samples were mixed with distilled water in a 1:10 (w/v) concentration. pH was measured with a pHM 93 pH meter (MeterLab, Denmark) by triplicate.

5.3.3.7. Microbiological assays

To assess the role of the coating during storage, 10 g of Atlantic horse mackerel were weighed by taking different portions of at least 5 horse mackerel fillets, and put into sterile bags (Sterilin, Stone, Staffordshire, UK), combined with 90 mL of buffered 0.1% peptone water (Oxoid, Basingstoke, UK), and shaken for 1 min in a Stomacher blender (model Colworth 400, Seward, London, UK). Appropriate dilutions were prepared for the following microorganism determinations: (i) total viable

bacteria (TVB) on spread plates of Iron Agar, IA (Scharlab, Barcelona, Spain) 1% NaCl, incubated at 15 °C for 3 days; (ii) total aerobic mesophiles on pour plates of Plate Count Agar, PCA (Oxoid), incubated at 30 °C for 72 h; (iii) Pseudomonas on spread plates of Pseudomonas Agar Base (Oxoid) with added CFC (Cetrimide, Fucidine, Cephalosporine) supplement for Pseudomonas spp. (Oxoid), incubated at 25 °C for 48 h; (iv) H_2S-producers organisms, as black colonies, on spread plates of Iron Agar, incubated at 15 °C for 3 days; (v) luminescent bacteria on spread plates of Iron Agar 1% NaCl, incubated at 15 °C for 5 days; (vi) Enterobacteriaceae on double-layered plates of Violet Red Bile Glucose Agar (VRBG, Oxoid), incubated at 30 °C for 48 h; and (vii) lactic acid bacteria on double-layered plates of MRS Agar (Oxoid), incubated at 30 °C for 72 h. The day when the jacked fillets were coated was considered as day 0. Microbiological counts were expressed as the log of the colony-forming units per gram (log CFU/g) of sample. All analyses were performed at 0, 3, 6, 9, and 13 days by duplicate.

5.3.3.8. Color parameters

A Konica Minolta CM-3500d colorimeter (Osaka, Japan) was employed for fish color measurements. CIELAB color scale was used in

order to determine L* from black (0) to white (100), a* from green (-) to red (+), and b* from blue (-) to yellow (+). The values given are the mean of fifteen replications for each batch.

5.3.3.9. Texture parameters

The hardness of horse mackerel fillets was measured by a TA.XTplus texture analyser (Stable Micro Systems, Surrey, UK). Fillets were placed on the flat plate of the texturometer and compression was applied with a 5 mm diameter plunger (P/5S) connected to a 30 kN load-cell at a deformation rate of 0.5 mm/s. Eight replicates were carried out to calculate the mean value of hardness.

5.3.3.10. Thiobarbituric acid reactive substances (TBARS)

Horse mackerel fillets (15 g) were homogenized with 35 mL of 7.5 % w/v trichloroacetic acid (TCA). The mixture was centrifuged at 5000 rpm for 20 min and filtered through Whatman no. 1 paper. The filtrate was reacted with thiobarbituric acid in a 1:1 ratio and left to incubate at 90 °C for 15 min. Then, absorbance was measured at 532 nm in a spectrophotometer (Shimadzu CPS-240, Japan). 1,1,3,5-tetraethoxypropane (TEP) was used as standard for the calibration curve.

Results were stated as mg of malonaldehyde (MAD) per kg of sample. 3 replicates were carried out for the TBARS test.

5.3.4. Statistical analysis

With the purpose of determining the significant differences between measurements, analysis of variance (ANOVA) was carried out by means of SPSS software (SPSS Statistic 25.0). Tukey's multiple range test was used for multiple comparisons among different systems with a statistical significance at the $P< 0.05$ level.

5.4. Results and discussion

5.4.1. Muscle water content, mass loss values, and protein viscosity

During fish storage, muscle protein denaturation can occur and influences water holding capacity (Zhang et al., 2020). The initial muscle water content in fish samples was 79 %, as shown in Figure 5.1A. This value did not significantly ($P > 0.05$) change within the first 9 days of storage for coated samples. At the end of the storage period analyzed, muscle water content showed a 2% decrease for control samples and a 5% decrease for coated samples. This higher decrease of muscle water content for coated samples could be related to the hydrophilic nature of the

coatings used in this study and, thus, to their affinity for water molecules, causing a certain muscle protein dehydration (da Rocha et al., 2018).

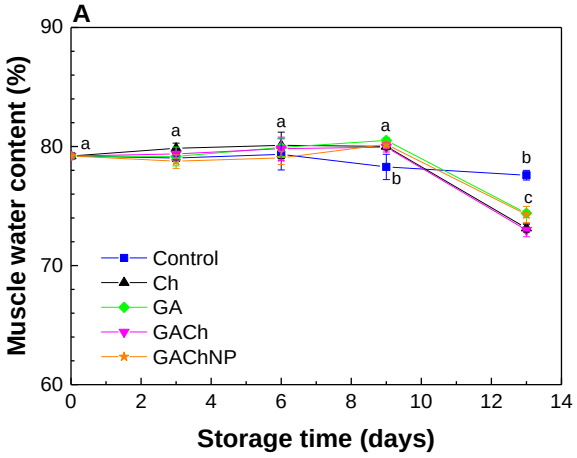

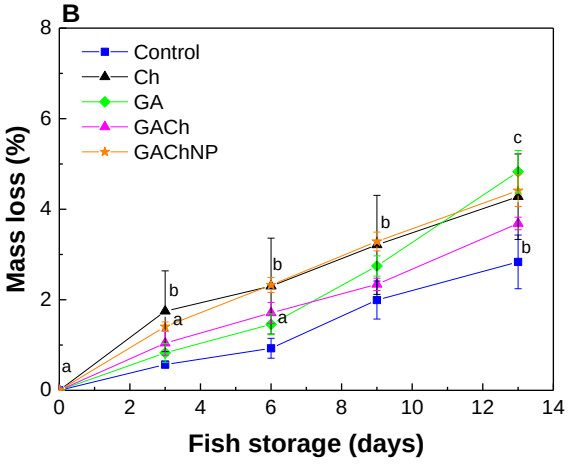

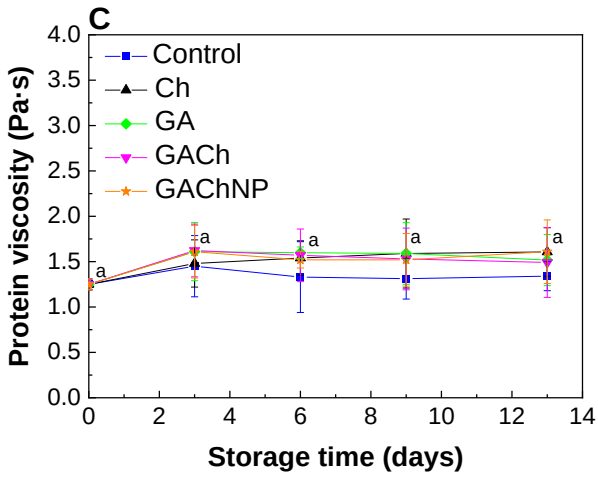

Figure 5.1. Effects of coatings on A) muscle water content, B) mass loss, and C) protein viscosity of Atlantic horse mackerel fillets stored at 4 °C for 13 days.

In accordance with the higher decrease of muscle water content that was observed at the end of storage time for coated samples, these showed also slightly higher mass loss that the control sample for the whole storage, although mass loss values were lower than 5 % for all the samples analyzed, as can be seen in Figure 5.1B. These subtle changes coincided with the values of protein viscosity, which were not significantly ($P > 0.05$) different among all coated samples during storage, as can be seen in Figure 5.1C. All these findings indicate a minimum loss of muscle protein functional quality during the storage.

5.4.2. TVB-N and pH values

TVB-N values are indicative of the activity of spoilage bacteria in fish (Lu et al., 2013) and, therefore, these values were measured for the coated fish fillets. As can be seen in Figure 5.2, fish fillets had a value of 15.3 mg TVB-N/100 g at the beginning of the analysis. This content increased during storage and exceeded 35 TVB-N/100 g, the limit value established by EU regulations (EUR-Lex-32005R2074, 2005), before the day 7 of storage for control samples.

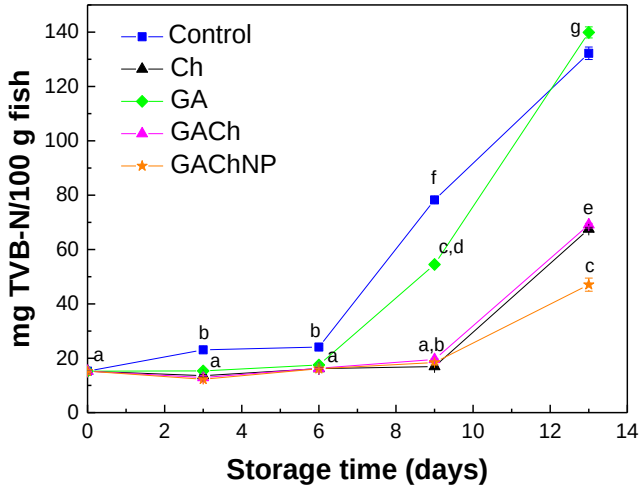

Figure 5.2. Effects of coatings on total volatile basic nitrogen (TVB-N) values of Atlantic horse mackerel fillets stored at 4 °C for 13 days.

Although horse mackerel fillets coated with GA solutions showed a significant ($P < 0.05$) enhancement, since the limit value was reached

between the day 7 and the day 8 of storage, the best results ($P < 0.05$) were found for all samples coated with chitosan solutions or nanoparticles. Regardless of gallic acid incorporation into the solution, TVB-N values were below the limit value up to the day 10 of storage for the films coated with Ch and GACh solutions, indicating a 3 day-extension in fish shelf life. Interestingly, GAChNP coatings showed a greater improvement of fish preservation up to the day 11 of storage, providing fish fillets with 4 day-extension of shelf life. This greater effect of GAChNP coatings could be related to a more sustained release of gallic acid from chitosan nanoparticles.

The change of pH values during storage showed a similar profile to that observed for TVB-N values. As can be seen in Figure 5.3, the increase of pH of fish fillets was significantly ($P < 0.05$) more rapid for control samples and for those coated with gallic acid solution; specifically, pH changed from 6.8 at day 0 to 8.2 at the end of the storage period. This increase of pH indicated the presence of non-desirable alkaline compounds derived from microbial activity (Quitral et al., 2009). Taking into account that pH 7 is considered the limit value for acceptable quality (Reyes et al., 2015), control and GA samples became non-acceptable before

the day 7 of storage, as also shown by TVB-N analysis. However, fish coated by Ch and GACh solutions did not reach the pH limit value up to day 10 and this was extended until the end of the storage for the samples coated by the solution with chitosan nanoparticles (GAChNP).

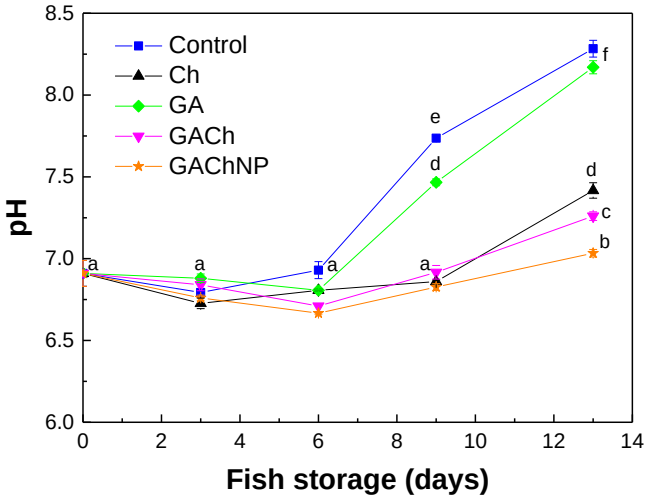

Figure 5.3. Effects of coatings on pH values of Atlantic horse mackerel fillets stored at 4 °C for 13 days.

5.4.3. Microbiological analyses

Figure 5.4 shows the microorganisms evolution during storage. Initially, the load of total aerobic mesophiles in the Atlantic horse mackerel was 4.4 log CFU/g (Figure 5.4B). Rodriguez et al., (2005) reported 3 log CFU/g in freshly caught horse mackerel. Counts in Iron Agar, which

reflects the psychrotrophic flora of fish (Otero et al., 2019), were lower in 1 log unit than those found in PCA. This fact may be due to an increase in the mesophilic flora of contamination during the handling and preparation of the fillets. At this point, the count of ubiquitous pseudomonas was 2.5 log CFU/g (Figure 5.4C), similar to the count of lactic bacteria (Figure 5.4F). In this initial stage of chilled storage, H_2S-producer organisms (Figure 5.4D), mainly *Shewanella putrefaciens*, spoiler organisms in chilled seafood (López-Caballero et al., 2001), were below the detection limit, as well as enterobacteria (Figure 5.4E), which indicates a good hygienic handling of the raw material. Luminescent colonies, as indicators of *Photobacterium phosphoreum* (López-Caballero et al., 2002), were not detected, possibly due to the sensitivity of this bacterium to freezing (Bøknæs et al., 2000).

As storage progressed, the Control batch registered an exponential growth in practically all the microorganisms studied that could be observed until at least day 9. A similar behavior was found in GA batch, with comparable or even higher counts than the Control (e.g., *Enterobacteriaceae*) (Figure 5.4E). However, the production of basic compounds was somewhat slower in GA than in the Control batch (Figure

5.2), which could be of great interest in horse mackerel storage. Applied as dipping solutions, Wu et al. (2016) described that gallic acid (5% w/v) inhibited in 2 log cycles the growth of total microorganisms in vacuum-packed Pacific mackerel(*Pneumatophorus japonicus*) fillets at day 6 of storage at 4 °C. The role of gallic acid as an antimicrobial compound has been also described against isolated bacteria. Gallic acid (250 mg/mL), as the main antimicrobial substance from ethanolic extracts of the Leguminosae *Caesalpinia mimosoides* Lamk, showed antimicrobial activity against *Salmonella typhi* (Gram-negative, G-) and *Staphylococcus aureus* (Gram-positive, G+)(Chanwitheesuk et al., 2007). In this regard, Sarjit et al (2015) studied the activity of gallic acid (7.8-1000 μg/mL) against 12 strains of *Campylobacter* (*C. jeuni* and *C. coli*). These authors found that the acid exerted a bacteriostatic or bactericidal activity related to a loss of calcium ions from the susceptible strains. In the present work, no inhibitory effect ($P > 0.05$) on microbial growth due to acid gallic was observed at the tested concentration. This could be due to the low concentration used (0.1 % w/v) in this study.

The chitosan coatings (Ch batch) decreased ($P < 0.05$) the growth of microorganisms with reductions even greater than 2 log cycles (e.g. total

counts, aerobic mesophiles, *Enterobacteriaceae*), effect that could be also observed up to late stages of storage. Chitosan-based coatings prevented the increase of bacteria during the storage of cod patties (López-Caballero et al., 2005), prawns (Arancibia et al., 2015a), and salmon (Gómez-Estaca et al., 2019). Especially striking is the effect of chitosan on H_2S-producers, with counts below the detection limit (< 2 log CFU/g) during the whole period, while Control and GA batches exceed 8 log CFU/g (Figure 5.4D). The antimicrobial effect of this cationic polymer has been widely described, among others, by the interaction of the positively charged amino groups of chitosan with the negatively charged cell membranes, causing the leakage of protein material as well as other intracellular compounds (Alishahi and Aïder, 2012; Arancibia et al., 2015b). The limiting effect of pH (as chitosan is dissolved in acetic acid) also was mentioned by these authors, but it is not relevant in the present work since the pH of the coatings was adjusted to 5.5.

As shown in Figure 5.4, chitosan also maintained its inhibitory effect on microbial growth when combined with gallic acid, since GACh and GAChNP also registered significantly ($P < 0.05$) lower counts than Control batch. In the present work, the reduction of microbial counts cannot be

attributed to the presence of gallic acid in the coatings, since this compound neither prevented at all the growth of microorganisms, as previously mentioned, nor increased the chitosan activity, but just kept it. In contrast, Wu et al. (2016) found that chitosan (1.5% w/v) - gallic acid (5% w/v) coatings extended the shelf life of vacuum-packed Pacific mackerel by 5-6 days, compared to uncoated fish, and the effect of these compounds was superior together (synergistic effect) than in separate way. These authors also reported that the microbial counts of fish dipped in gallic acid (5% w/v) were lower than in the control batch during chilled storage, but higher than those in plain chitosan-coated fish. Different gallic acid and chitosan concentrations in dipping solutions could be the reason for the apparent divergence in results with respect to the present work.

The three chitosan containing batches evolved similarly during storage (Figure 5.4). Despite this, chitosan seemed to be more effective to inhibit the microbial growth when it is in nanoparticles form. Thus, GAChNP registered 1.5 log cycle lower than Ch for TVB counts at day 3 (Figure 5.4A), while differences of ≈1 log cycle (lower in GAChNP compared to Ch) in P*seudomonas* spp. at day 6 were found (Figure 5.4C), which was also reflected in a lower ($P < 0.05$) aerobic mesophilic counts in

GAChNP (Figure 5.4B). Likewise, differences ($P < 0.05$) in 0.5-1 log cycle counts could be observed between GACh and GAChNP batches, especially in *Enterobacteriaceae* at day 9 (3.8 *vs* 2 log CFU/g, respectively). Probably the chitosan nanoparticles allow a greater contact surface of the polymer with the fish muscle, even penetrating into it, to exert its activity. In this connection, a synergistic effect between chitosan (1-1.5% w/v) nanoparticles and fennel essential oil (1% v/v) was described to reduce counts of mesophilic and psychrotrophic organisms during modified atmosphere packaging (MAP) storage of Great sturgeon (*Huso huso*) fillets compared to the effect of both compounds separately (Maghami, Motalebi & Anvar, 2019). Moreover, these authors reported that chitosan nanoparticles and fennel, alone or in combination, did not reduce the genus *Pseudomonas* spp.

From 9 days onwards, Control and GA batches showed evident signs of spoilage, reaching 9 log CFU/g in several bacterial groups. In this regard, Zheng et al (2020) reported counts in Spanish mackerel of 8.7 log CFU/g in PCA at day 9 of chilled storage. In the present work, storage was prolonged to establish the role of chitosan coatings in the late stages of storage. At 13 days, all the batches were spoiled and raised similar counts

(Figure 5.4).Oucif et al. (2018) also observed counts that exceed 8 and 9 log CFU/g at 11 days in total aerobes and psychrotrophs, respectively, during the chilled storage of horse mackerel. The genus *Pseudomonas* predominated during horse mackerel storage, with counts that exceeded 9 log CFU/g at the end of the period ($P < 0.05$). This group predominated at the end of the storage in salmon (Gómez-Estaca et al., 2019) and shrimp (Arancibia et al., 2015a).

As mentioned previously, the incidence of *S. putrefaciens* in chitosan-coated batches was negligible ($P < 0.05$) (Figure 5.4D). López-Caballero et al. (2006) described the sensitivity of *S. putrefaciens* to chitosan coatings on shrimp during chilled storage. As shown in Figure 5.4F, the lactic bacteria were not found in high concentration, registering values around 4 log CFU/g in the chitosan-coated batches at day 9 ($P < 0.05$). Chitosan could favor the growth of this group due to the acidification by acetic acid in which it is dissolved (López-Caballero et al., 2006), but this fact was not clearly observed in the present study (Figure 5.4). In this connection, Arancibia et al. (2015a) observed that the increase in lactic acid bacteria counts during chilled storage of chitosan-coated prawns was not significant.

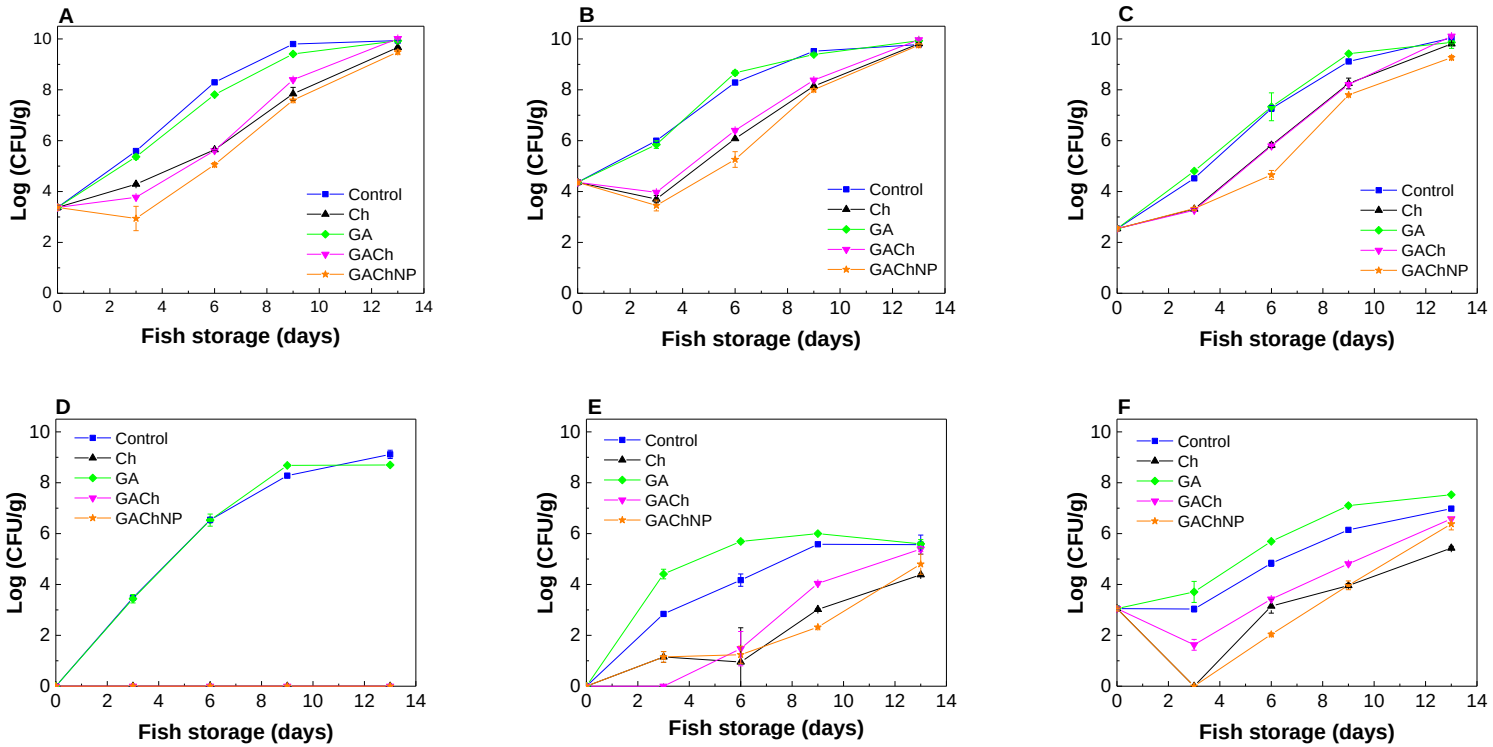

Figure 5.4. Microbial counts (log CFU/g) in Atlantic horse mackerel stored at 4 °C: A) total viable bacteria (TVB), B) total aerobic mesophiles, C) *Pseudomonas* spp., D) H_2S-producing microorganisms, E) *Enterobacteriaceae*, F) lactic acid bacteria.

Some authors stated that chitosan is more effective against Gram+ bacteria than Gram- (Arancibia et al., 2015a), due to the characteristics of the Gram- wall, with the presence of the bilayer lipopolysaccharides that hinder the action of antimicrobial compounds on bacteria. This fact cannot be corroborated here, since the inhibition rate of microbial growth in the chitosan-coated batches respect to the Control was similar for lactic bacteria and *Enterobacteriaceae*, as an example of G+ and G- organisms, respectively. Moreover, chitosan coatings inhibited H_2S-producers organisms but not the growth of pseudomonas, both G- bacteria.

5.4.4. Color and texture parameters

Physicochemical changes during fish storage are known to cause changes in fish appearance and texture and, thus, surface color and hardness were measured in order to analyze the effect of the coatings under study. In particular, L*, a*, and b* color parameters are shown in Figure 5.5. As can be seen in Figure 5.5A, L* value did not significantly ($P > 0.05$) change during storage, keeping the horse mackerel fillets lightness. The presence of chitosan and/or gallic coating on the fillet induced a slight increase in lightness ($P > 0.05$), being even higher when coated with GaChNP.

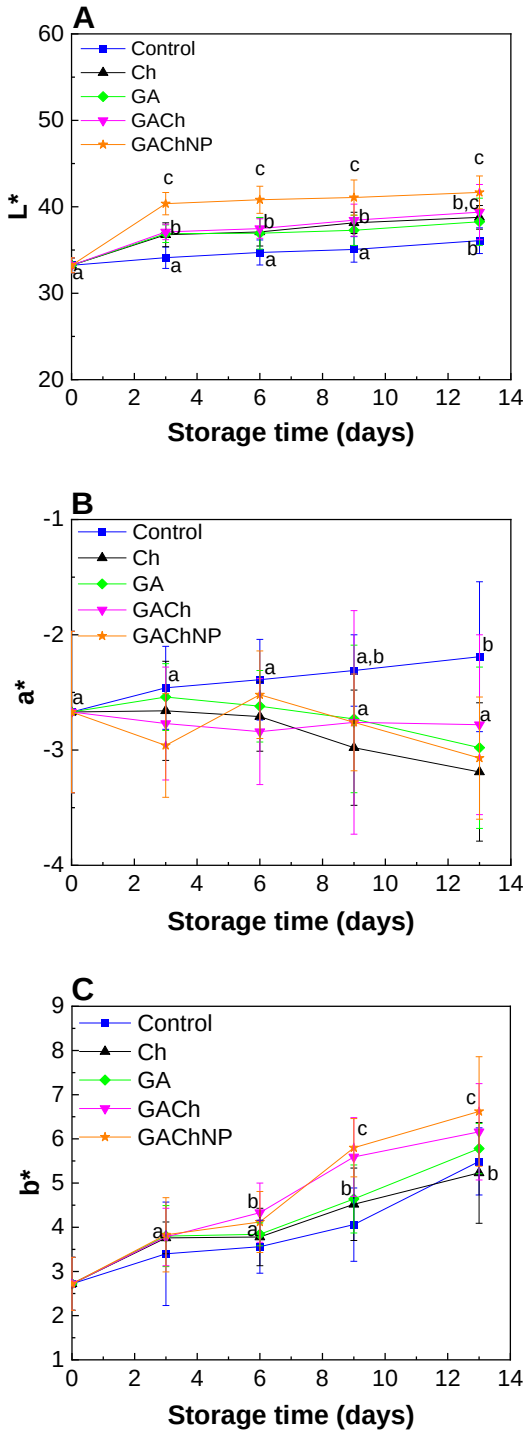

Figure 5.5. Effects of coatings on A) L*, B) a*, and C) b* color parameters of Atlantic horse mackerel fillets stored at 4 °C for 13 days.

Concerning a* parameter (Figure 5.5B), the samples showed mean values in the range from -3.5 to -2.0, similar to those found in the work of Cai et al. (2018). While coated fillets did not present any significant ($P > 0.05$) change of a* values during storage, control films showed a significant ($P < 0.05$) increase of a* parameter from day 9 of storage. Similarly, b* parameter also increased ($P < 0.05$) from day 9 for control fillets, as well as for coating samples, as shown in Figure 5.5C. This yellowing effect, related to the increase of volatile amines, as previously shown by TVB-N values, was similar to that found in other works where chitosan solutions were used to coat tilapia (Yang et al., 2019) and grass carp fillets (Cai et al., 2018).

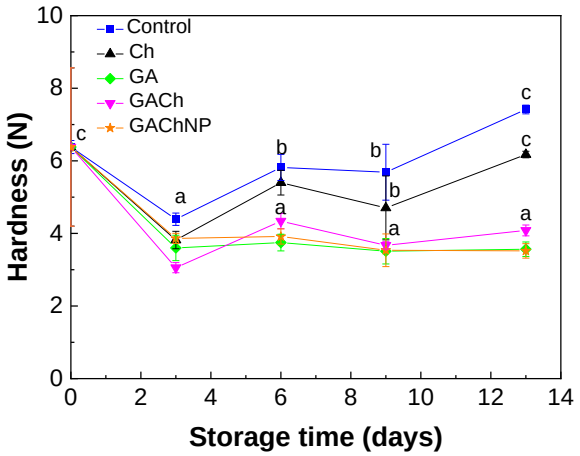

Figure 5.6. Effects of coatings on hardness of Atlantic horse mackerel fillets stored at 4 °C for 13 days.

Additionally, physicochemical changes affected slightly fish texture. As can be seen in Figure 5.6, the mean hardness values obtained are in a narrow range from 3.0 to 7.5 N, similar to those obtained for chitosan-coated sierra (*Scomberomorus sierra*) fish fillets (Ramírez-Guerra et al., 2018).

The increase in hardness during storage is in accordance with the increase of mass loss shown in Figure 5.1B. However, in the first three days of storage all samples showed a significant ($P < 0.05$) drop in hardness, which tended to increase thereafter in both control and Ch lots. The texture softening in fish fillets during chilled storage is well known, and mainly attributed to protein deterioration by the action of endogenous cathepsins and, in a second stage, more advanced in chilled storage by the action of exogenous proteases, due to microorganisms (Huss, 2013; Yu et al., 2017). Such a muscle degradation effect during storage was not clearly evidenced by any significant drop in protein viscosity values, as described before. Gallic acid-containing coatings led to significantly ($P < 0.05$) softer textures, which are linked to the phenol content and its capacity to hold water molecules, as also shown in smoked sea bass fillets with resveratrol-incorporated chitosan coatings (Martínez et al., 2018).

5.4.5. Thiobarbituric acid reactive substances (TBARS)

TBARS analysis quantifies the presence of lipids' secondary oxidation substances, which major component is malondialdehyde (MDA) (Lee et al., 2019). Since lipids present in fresh fish are highly prone to oxidation, causing changes in fish quality attributes, TBARS index was determined and values are shown in Figure 5.7. Considering that the acceptability limit for TBARS is around 2 mg MDA/kg fish (Binsi et al., 2016), it can be said that control samples reached this limit at day 3 of storage and chitosan-coated fish (Ch) exceeded the limit value, probably one day later. Interestingly, the samples coated by gallic acid-containing chitosan did not reach this value up to day 12, indicating that lipid oxidation was 2-fold extended due to the antioxidant activity of gallic acid (Zarandona et al., 2020). It is worth noting that GAChNP coating showed a significant ($P < 0.05$) increase of TBARS values at the beginning of storage, but the lowest TBARS mean value at the end of storage, suggesting the sustained release of gallic acid from chitosan nanoparticles (Jahromi et al., 2020; Lamarra et al., 2017), as also shown by TVB-N and pH results in Figures 5.2 and 5.3, respectively. Therefore, further research

is needed in order to control the gallic acid delivery from nanoparticles to improve its antioxidant effect.

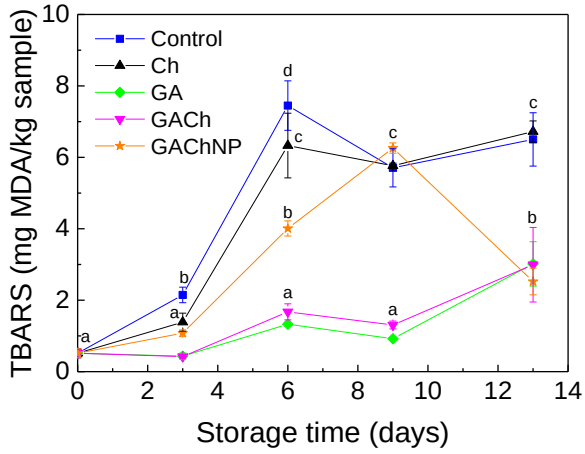

Figure 5.7. Effects of coatings on TBARS of Atlantic horse mackerel fillets stored at 4 °C for 13 days.

5.5. Conclusions

Chitosan coatings protected horse mackerel fillets from quality deterioration sincethe microbial growth was delayed and the production of volatile amines remained constant up to the last day of storage, as shown by TVB-N and pH values. Although gallic acid showed no antimicrobial effect, gallic acid-containing coatings in the amounts added prevented from lipid oxidation during the chilled storage of horse mackerel fillets. However, the sustained release of gallic acid from

chitosan nanoparticles should be more in-depth analyzed in order to enhance the antioxidant activity of chitosan coatings during food storage.

Chapter

6

Active chitosan films with *Aloe vera:* Compression molded films

6.1. Summary

Thermocompression was employed to prepare citric acid-crosslinked chitosan films with *Aloe vera* (AV) as bioactive compound. Films were easy to handle and mechanical properties did not change with the addition of AV up to 10 wt %, although both TS and EAB decreased for the films with 15 wt % AV, indicating that high AV contents would hinder intermolecular interactions among the formulation components. Maillard reaction occurred between chitosan and citric acid at the processing temperature used (115 °C), while physical interactions took place with AV, as shown by FTIR analysis. All films were insoluble but displayed hydration and limited swelling due to both physical and chemical interactions promoted by AV and citric acid, respectively. A slow AV release, governed by a Fickian diffusion controlled mechanism, and an increase of surface hydrophilicity were observed.

6.2. Introduction

Chitosan films are widely processed by solution casting (Muxika et al., 2017), but thermocompression is another suitable option due to its simplicity and high productivity and capacity to produce films at industrial scale (Valencia-Sullca et al., 2018). The conditions employed in

the above-mentioned processes, such as pH, temperature, and pressure, influence the final material properties (Ochoa-Yepes et al., 2019). To the best of our knowledge, few studies have reported chitosan films processed by thermocompression. Among them, Galvis-Sánchez et al. (2018) prepared chitosan films with four natural deep eutectic solvents as plasticizers, and Matet et al. (2013) used acetic acid as crosslinker, while Guerrero et al. (2019) used citric acid. Furthermore, the addition of a crosslinking agent helps to enhance functional properties. In this sense, citric acid can be added to react with amine and hydroxyl groups of chitosan and to enhance the mechanical properties and water resistance of the resulting films (Kanatt & Makwana, 2020; Oryan et al., 2018).

In this chapter, in addition to citric acid, used as crosslinker, *Aloe vera* (AV) was utilized as bioactive compound. AV is a perennial herb containing over 75 active ingredients, such as phenolics, sugars, amino acids, saponins and minerals (Tapeh, Baei & Keshel, 2021). Due to its physiologically active components, it has antioxidant, anti-inflammatory and antibacterial properties, providing active properties to chitosan films (Kanatt & Makwana, 2020; Tapeh et al., 2021).

In this context, the aim of this chapter was to prepare chitosan films by thermocompression, using citric acid as crosslinker and *Aloe vera* as bioactive. The effect of AV concentration on the structure and thermal and physicochemical properties of the films was assessed, as well as the bioactive release.

6.3. Materials and methods

6.3.1. Materials

Chitosan was extracted from shrimp shells in Nha Trang University, Vietnam. H_2O_2, NaOH, acetic acid, anhydrous citric acid and glycerol (with a purity of 99.01 %) were supplied by Panreac (Barcelona, Spain). *Aloe vera* (AV) powder was supplied by Agora Valencia SL (Valencia, Spain).

6.3.2. Extraction and characterization of chitosan

Chitosan was obtained according to Minh et al. (2017) with some modification. Chitosan was ground (100 mesh) and then soaked in NaOH solution (0.6 wt %) for 14 h at room temperature. Subsequently, H_2O_2 solution (0.6 wt %) was added and kept for 18 h at room temperature.

Finally, the solid chitosan product was collected on filter cloth, washed by distilled water to neutral pH, and dried at 60 °C for 12 h.

The ash content in chitosan was determined by burning the samples at 600 °C in a muffle furnace. Additionally, protein content was measured by using the standard micro-Biuret protein assay using bovine serum albumin standards. Furthermore, the average molecular weight (M) of chitosan was determined according to a previous study (Rinaudo, 2006). Typically, 100 mg of chitosan was dissolved completely in a mixture of 0.1 M acetic acid and 0.2 M NaCl solution. The intrinsic viscosity [μ] of chitosan was determined by an Ubbelohde viscometer at 25 °C, and M of chitosan was calculated according to the Mark–Houwink equation:

$$[\mu] = K \cdot M^{a}$$

where K is 1.81×10^{-3} and a is 0.93.

The degree of deacetylation (DD) of chitosan was determined based on a previous work (Minh et al., 2019). Typically, 100 mg of chitosan were dissolved in 20 mL of 85% H_3PO_4 solution at 60 °C for 40 min. Then, 1 mL of the above solution was diluted in deionized water and kept at 60 °C for 2 h. After being cooled down to room temperature, samples were

measured by UV spectroscopy at 210 nm. DD was calculated according to the following equation:

$$DD = 100 \cdot \left[1 - \frac{GlcNAc}{GlcNAc + GlcN}\right]$$

where GlcNAc refers to N-acetyl glucosamine and GlcN to glucosamine.

6.3.3. Film preparation

Compression molded chitosan films were prepared as described by Guerrero et al. (2019) with some modifications. 3 g of chitosan were weighed and mixed with 20 wt % citric acid (based on chitosan weight) and 0, 5, 10, or 15 wt % AV (based on chitosan weight). In order to facilitate mixture flowing during the compression process, 9 mL of deionized water were added and, finally, 15 wt % glycerol (based on chitosan weight) was added as plasticizer. All reagents were manually mixed and stored in a plastic bag during 24 h at room temperature to hydrate the dough. Four film systems were analyzed: i) control films without *Aloe vera* (control), ii) chitosan films with 5 wt % *Aloe vera* (5AV), iii) chitosan films with 10 wt % *Aloe vera* (10AV), and iv) chitosan films with 15 wt % *Aloe vera* (15AV).

The hydrated dough was placed between two aluminum plates, put into the press (Specac, Spain), previously heated up to 115 °C for 30 s, and pressed at 0.5 MPa for 2 min.

6.3.4. Film characterization

6.3.4.1. Fourier transform infrared (FTIR) spectroscopy

FTIR spectra were collected with a Nicolet Nexus FTIR spectrometer (Thermo Fisher Scientific, Massachusetts, USA) with a Golden Gate ATR accessory. The spectra, with a resolution of 4 cm^{-1}, were acquired between 4000 and 800 cm^{-1} with 32 scans for each sample.

6.3.4.2. Color measurement

Color parameters of the films were measured using a CR-400 Minolta Chroma Meter (Konica Minolta, Spain) portable colorimeter. Ten samples were analyzed for each composition. CIELAB scale was used to measure color parameters: L*=0 (black) to L*=100 (white), -a* (greenness) to +a* (redness) and –b* (blueness) to +b* (yellowness). Films were placed on a white patron (L*=97.39, a*=0.03, b*=1.77)

6.3.4.3. Water contact angle

Water contact angle (WCA) of films was measured by a Dataphysics Contact angle OCA (DataPhysics, Spain) equipment. 3 μL distilled water was dropped onto the film surface and the drop image was captured using a SCA20 software. Five replicates were carried out for each system.

6.3.4.4. Degradation degree

Degradation degree (DD) of chitosan films with *Aloe vera* was calculated on samples conditioned in a climatic chamber (Angelantoni, Spain) at 25 °C and 50% relative humidity. Samples (W_0) were immersed in PBS (pH 7.4) at 37 °C for 2 and 7 days (W_d). Samples were dried with paper and conditioned in the climatic chamber at 25°C and 50 % RH until they reached a constant weight. The results were taken in triplicate for each system and were calculated as follows:

$$DD\ (\%) = \frac{W_0 - W_d}{W_0} \cdot 100$$

6.3.4.5. Swelling measurements

Swelling test for chitosan films with *Aloe vera* was carried out by gravimetric method. Samples of each system were immersed into PBS (pH 7.4) and weighed before (W_0) and after immersion (W_h) every 30 min for

the first 3 h. Thereafter, measurements were carried out at 24 h and 48 h. Three replicates were taken for each system and swelling degree (S) was calculated by the following equation:

$$S\ (\%) = \frac{W_h - W_0}{W_0} \cdot 100$$

6.3.4.6. *Aloe vera* release

AV powder was dissolved in PBS (pH 7.4) at 37 °C. The absorbance of AV solution as a blank solution was read by a UV-VIS Multiskan SkyHigh (Thermo Fisher, Spain) spectrophotometer at 255 nm. The ratio of the AV release was determined by the calibration curve from 10 to 1000 ppm (μg/mL), and the theoretical total release was calculated from the determination of the accumulative release percentage. In order to determine AV release, film pieces (1 cm x 2 cm) were immersed into 10 mL of PBS (pH 7.4) at 37 °C for 9 days. Aliquots (2 mL) were collected at different times (1 h, 24 h, 3 d, 7 d and 9 d) and replaced with an equal volume of fresh PBS. Results were taken in triplicate for each system.

In order to analyze the mechanism of the *Aloe vera* release, Korsmeyer-Peppas model was used, since this model is the most

comprehensive semi-empirical equation to study the release from a polymeric matrix (Bruschi, 2015):

$$M_t/M_\infty = k \cdot t^n$$

where M_t/M_∞ is the ratio of AV released at time t, k is the release velocity constant and n is the release diffusion coefficient, related to the AV release mechanism.

6.3.4.7. Thermo-gravimetric analysis (TGA)

A Mettler Toledo TGA/SDTA 851 thermo-balance was used to measure the thermal stability of the samples. Dynamic scans from 25 to 900 °C were carried out at a constant rate of 10 °C/min under nitrogen atmosphere to avoid thermo-oxidative reactions.

6.3.4.8. Differential scanning calorimetry (DSC)

A Mettler Toledo DSC 822 was used to perform differential scanning calorimetry. Samples of around 3 mg were heated from -50 °C to 300 °C at a heating rate of 10 °C/min under nitrogen atmosphere to avoid oxidative reactions.

6.3.4.9. X-ray diffraction (XRD)

X-ray diffraction (XRD) analysis was carried out at 40 kV and 40 mA by means of a PANalytic Xpert Pro (PANalytical, Almelo, The Netherlands) equipment with a diffraction unit and Cu-Kα (λ = 1.5418 Å) as a radiation source. Data were collected from 2° to 40° (step size = 0.026, time per step = 118 s).

6.3.4.10. Scanning electron microscopy (SEM)

Scanning electron microscopy (SEM) was used to visualize cross-section and surface morphologies of the samples. For that purpose, a Hitachi S-4800 scanning electron microscope (Hitachi High-Technologies Corporation, Tokyo, Japan) was used with an acceleration voltage of 15 kV. Samples were placed in a metallic stub and coated with gold under vacuum in argon atmosphere.

6.3.4.11. Mechanical properties

Mechanical properties were measured with an Instron 5967 electromechanical testing system (Instron, Spain). According to ASTM D638-14 (ASTM, 2014), tests were carried out with a load cell of 500 N and

a crosshead rate of 1 mm/min. Films were cut into bone shaped samples of 4.75 mm x 22.25 mm. Five samples were measured for each system.

6.3.5. Statistical analysis

With the purpose of determining the significant differences between measurements, analysis of variance (ANOVA) was carried out by means of SPSS software (SPSS Statictic 25.0). Tukey's multiple range test was used for multiple comparisons among different systems with a statistical significance at the $p < 0.05$ level.

6.4. Results and discussion

6.4.1. Physicochemical properties

The characteristics of chitosan are shown in Table 6.1. Chitosan was white in color and highly soluble in diluted acetic acid. Chitosan had high purity with a low protein content and a low mineral content. The degree of deacetylation was not affected by the mild conditions used to produce chitosan.

The FTIR spectra of chitosan and AV to determine the characteristic bands of each compound are shown in Figure 6.1A. The spectrum of chitosan showed some characteristic bands: a broad band between 3000-

3600 cm^{-1}, associated to O-H and N-H vibrations; a band at 2877 cm^{-1}, associated to aliphatic C-H stretching; a band at 1648 cm^{-1}, attributed to C=O stretching; a band at 1585 cm^{-1}, associated to NH_2 bending; two bands at 1421 cm^{-1} and 1376 cm^{-1}, assigned to CH_3 deformation; and some bands in the range from 1150 to 891 cm^{-1}, corresponding to C-O-C stretching absorption of the glycosidic ring of chitosan (Barbosa et al., 2019; Mauricio-Sánchez et al., 2018).

Table 6.1. Characteristics of the chitosan extracted from shrimp shells.

Solubility (%) of 1 wt % chitosan in 1% acetic acid	99.7 ± 0.1
Minerals (%)	0.36 ± 0.02
Protein (%)	0.41 ± 0.04
Degree of deacetylation (%)	89 ± 2
Viscosity (cP)	92 ± 7
Molecular weight (kDa)	135 ± 4

Regarding *Aloe vera*, it showed a wide band between 3000-3600 cm^{-1}, associated to O-H vibrations of phenolic groups, particularly to anthraquinines such as aloin (Isfahani, Tavanai, & Morshed, 2017; Torres-Giner et al., 2017). The band at 1639 cm^{-1} is attributed to C=O stretching and the bands in the region between 1150-848- cm^{-1} are assigned to C-O-C and stretching vibrations related to polysaccharides and sugars present in *Aloe vera* (Bajer, Janczak, & Bajer, 2020; Prajapati, Das, & Mondal, 2020).

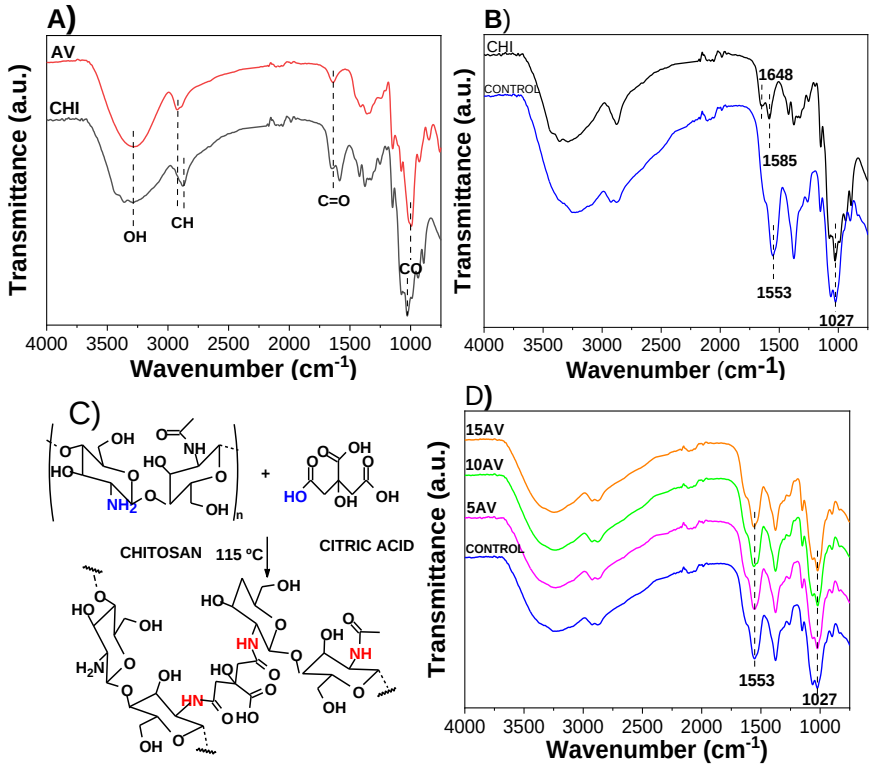

Figure 6.1. FTIR spectra of A) neat chitosan (CHI) and *Aloe vera*(AV) powders. B) FTIR spectra of chitosan (CHI) powder and compression molded chitosan film (control). C) Crosslinking reaction between chitosan and citric acid. D) FTIR spectra of compression molded chitosan films without *Aloe vera*(control) and with 5wt % *Aloe vera*(5AV), 10 wt % *Aloe vera*(10AV) and 15 wt % *Aloe vera*(15AV).

In order to assess the crosslinking effect between chitosan and citric acid, the spectra of chitosan powder and chitosan film with citric acid (control) are shown in Figure 6.1B. The bands related to C-O glycosydic linkage of chitosan at 1151, 1063 and 1023 cm^{-1} are presented in both spectra. New bands were detected in control films due to the reaction of carboxyl groups of citric acid with the amino groups of chitosan forming

an amide linkage (Gawish et al., 2012). The largest difference between both spectra was detected in the range of 1300-1700 cm^{-1}. In the chitosan spectrum, C=O and NH_2 bands appeared at 1648 and 1585 cm^{-1}, respectively; however, when citric acid was added, NH_2 band was more pronounced and shifted to 1553 cm^{-1}, while C=O band appeared as a small shoulder. Therefore, due to the crosslinking reaction between chitosan and citric acid (Figure 6.1C), the amino group of chitosan was transformed from primary to secondary amine (Guerrero et al., 2019).

The interactions among the components of the film led to a chromatic change when *Aloe vera* concentration increased (Table 6.2). Control films had a yellowish color, showed by a positive value of b* parameter, due to the occurrence of Maillard reaction at the working temperature, 115 °C (Leceta et al., 2013).When *Aloe vera* was added, film color changed to a darker yellow, supported by the increase in b* value, especially for films with 10 and 15 wt% AV. In accordance, ΔE value indicated bigger color differences, visible to the human eye, for 10AV and 15AV films. This color change can be attributed to the anthranquinones like aloin, transformed into aloe emodin and other substances during thermal processing (Chang et al., 2006). Aloe emodin is a phenolic

compound with anti-inflammatory, antioxidant and antibacterial activities (Rahman, Carter, & Bhattarai, 2017).

Table 6.2. L*, a*, b* and ΔE color parameters of compression molded chitosan films without *Aloe vera* (control) and with 5 wt % *Aloe vera* (5AV), 10 wt % *Aloe vera* (10AV), and 15 wt % *Aloe vera* (15AV).

	L*	a*	b*	ΔE
Control	92.7 ± 0.3[a]	-1.68 ± 0.05[a]	13.4 ± 1.1[a]	---
5AV	92.6 ± 0.3[b]	-1.51 ± 0.05[a]	14.9 ± 0.9[a]	1.54
10AV	92.4 ± 0.2[a]	-1.51 ± 0.19[a]	19.1 ± 2.8[b]	5.71
15AV	92.2 ± 0.5[a]	-1.31 ± 0.06[b]	18.9 ± 1.1[b]	5.51

[a-b]Two means followed by the same letter in the same column are not significantly ($p > 0.05$) different according to the Tukey's multiple range test.

In order to determine the effect of AV on film surface hydrophobicity or hydrophilicity, water contact angle (WCA) was measured and results are presented in Table 6.3. Control film showed a WCA of 83°, indicative of the film surface hydrophobicity. However, a significant decrease ($p < 0.05$) was observed when *Aloe vera* concentration increased, reaching values of 68° for 15AV films. Since many of the components of *Aloe vera* have hydrophilic character, WCA results suggested that these polar groups of *Aloe vera* were oriented towards the film surface.

Table 6.3. Water contact angle (WCA) and hydrolytic degradation (HD) of compression molded chitosan films without *Aloe vera* (control) and with 5 wt % *Aloe vera* (5AV), 10 wt % *Aloe vera* (10AV), and 15 wt % *Aloe vera* (15AV).

Film	WCA (°)	HD (%)	
		Day 2	Day 7
Control	83 ± 1[a]	21.2 ± 0.9[a]	21.2 ± 0.3[a]
5AV	78 ± 1[b]	21.5 ± 0.5[a]	21.7 ± 0.2[a]
10AV	75 ± 3[b]	22.2 ± 0.3[a]	23.1 ± 0.2[b]
15AV	68 ± 2[c]	22.3 ± 0.2[a]	23.4 ± 0.3[b]

[a-c]Two means followed by the same letter in the same column are not significantly ($p > 0.05$) different according to the Tukey's multiple range test.

Regarding hydrolytic degradation, the values after 2 and 7 days immersed in water at 37 °C are shown in Table 6.3. At day 2, a HD value between 21 and 22 % was achieved for all films, with no significant differences ($p > 0.05$) among samples. These values could be related to the glycerol migration, since glycerol is crosslinked by hydrogen bonding with chitosan and *Aloe vera*, while chemical crosslinking provides polymeric networks with resistance to degradation. After 7 days, HD was between 21 and 23 %, indicating that films maintained their integrity and the crosslinking among the components of the films was successful. Additionally, there was a significant increase ($p < 0.05$) of mass loss for 10AV and 15AV films, which can be attributed to the release of non-crosslinked *Aloe vera* at high concentrations.

Also swelling tests were performed and results are shown in Figure 6.2A. It is worth noting that all samples kept their structure after 3000 min of immersion in PBS at 37 °C. In the first 30 min, swelling increased fast up to 33 %. After 60 min, swelling reached the equilibrium with values of 40 %, indicating that a compact structure was formed due to the interactions among the film components, which reduced the free hydrophilic moieties, preventing the absorption of large amounts of water (Deshmukh et al., 2021). The swelling capacity decreased when AV was added; however, no relevant differences among the films with AV were observed. This would indicate that the reaction between chitosan and citric acid would lead to a more compact network, hindering the swelling capacity of the films. It is worth noting that all films were insoluble in an aqueous environment, but displayed hydration and limited swelling. These characteristics are possible due to the presence of both physical and chemical crosslinks in the network formed. The release kinetics of bioactive compounds from a polymeric matrix is mainly dictated by the physicochemical properties of the system and the interactions between polymer, solvent and the bioactive agent. Crosslinked polymers make the penetration of water more difficult and, thus, these materials become useful for the sustained release of bioactive compounds. Therefore,

controlling the rate of water diffusion is an effective strategy to control the release of the bioactive compound.

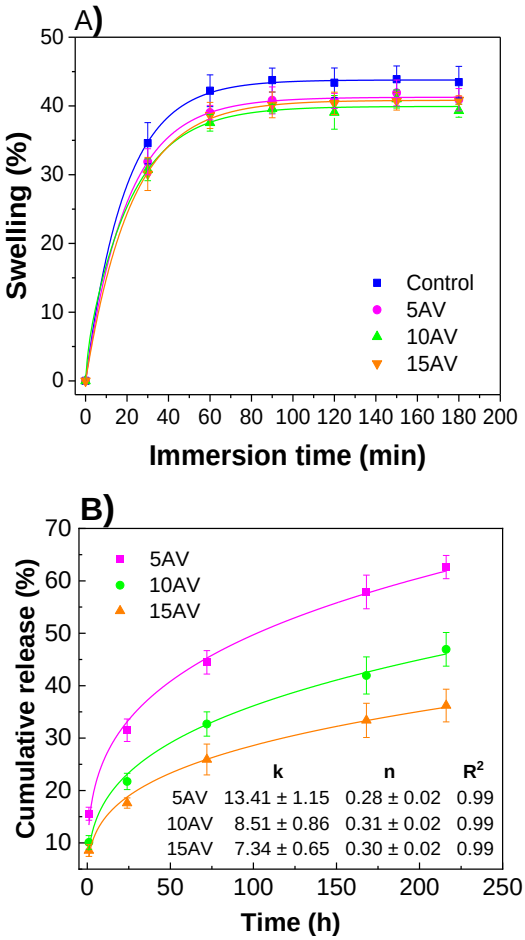

Figure 6.2. A) Swelling curves and B) release of *Aloe vera* from compressed molded chitosan films without *Aloe vera* (control) and with 5 wt % *Aloe vera* (5AV), 10 wt % *Aloe vera* (10AV) and 15 wt % *Aloe vera* (15AV).

Considering hydrophilic matrices with limited swelling, the mechanism of the bioactive release is controlled by the penetration velocity of the dissolution medium. When the bioactive compound is in

contact with biological fluids, eventual dissolution of a small fraction of the active agent can occur, followed by hydration and progressive gelling of macromolecules, forming a high viscosity layer that increases in thickness with time. This gelled layer controls the penetration of water and constitutes a barrier to prevent the fast release of the active agent by diffusion.

The release of *Aloe vera* from chitosan films was analyzed in PBS media at 37 °C and the cumulative release during 9 days is presented in Figure 6.2B. As can be seen, the release of *Aloe vera* was slow, since 63, 47 and 36 % of *Aloe vera* was released from 5AV, 10AV and 15AV, respectively, at the end of the experiment (9 days). Therefore, a more sustained release of AV occurred with the increase of AV content. These results are in in accordance with the physical interactions of AV with the amine groups of chitosan, as corroborated by phenolic –OH stretching in FTIR spectra, which would hinder the release of AV molecules. Moreover, the chemical reaction between chitosan and citric acid led to a more compact network, preventing a high swelling due to steric hindering and diminishing the interaction with AV. Therefore, *Aloe vera* release is

governed by swelling and interactions between the components of the film forming formulation.

Cumulative release profiles give valuable information and indication about the release kinetics and mechanisms. In order to assess the release mechanism, Korsmeyer-Peppas model was considered. Results were fitted to the semi-empirical equation of Korsmeyer-Peppas model, which stablishes an exponential relationship between time and release (Figure 6.2B) with correlation coefficients (R^2) of 0.99 for all the systems analyzed. The diffusion exponent in the Korsmeyer-Peppas model (n) can change depending on the release main mechanism: $n < 0.5$ indicates a diffusion controlled (Fickian) release mechanism, $0.5 < n < 1$ indicates a non-Fickian diffusion and erosion release mechanism, and $n > 1$ indicates a non-Fickian erosion controlled release mechanism (Tan, Zhong, & Langrish, 2020). Considering that n values shown in Figure 6.2B inset are 0.28, 0.31 and 0.30 for 5AV, 10AV and 15AV films, respectively, all films presented a Fickian diffusion controlled release mechanism, in which swelling and relaxation of chitosan chains were involved (Li, Wang, & Kong, 2020). It is worth noting that the low swelling degree of the films, shown in Figure 6.2A, led to a sustained release. Furthermore, these results

are in agreement with those studies that indicate that release at temperatures higher than the T_g of the material are associated to the Fickian diffusion mechanism, while release at temperatures close to or slightly lower than T_g shows non-Fickian diffusion (Gomes et al., 2019).

6.4.2. Thermal properties

Thermo-gravimetric analysis (TGA) and differential scanning calorimetry (DSC) were carried out in order to study the changes occurred by the temperature effect. Regarding TGA, weight loss curves and derivative thermo-gravimetric curves are presented in Figure 6.3A. As can be observed, three main weight loss steps are presented. The first one, around 100 °C, can be related to the loss of moisture. In the case of 10AV and 15AV films, weight loss started at a higher temperature, around 110 °C, which can be attributed to the interactions observed by FTIR, that could form a leaner structure and, thus, more energy was needed to release water. The second step, around 228 °C, can be attributed to the evaporation of glycerol (Leceta et al., 2013) and to the thermal depolymerization of *Aloe vera*'s hemicellulose, lignin and cellulose (Balaji, & Nagarajan, 2017). The third step, the main mass loss, occurred around 304 °C and can be assigned to the chitosan degradation step (Andonegi et

al., 2020) and to the degradation of α-cellulose present in *Aloe vera* (Balaji, & Nagarajan, 2017).

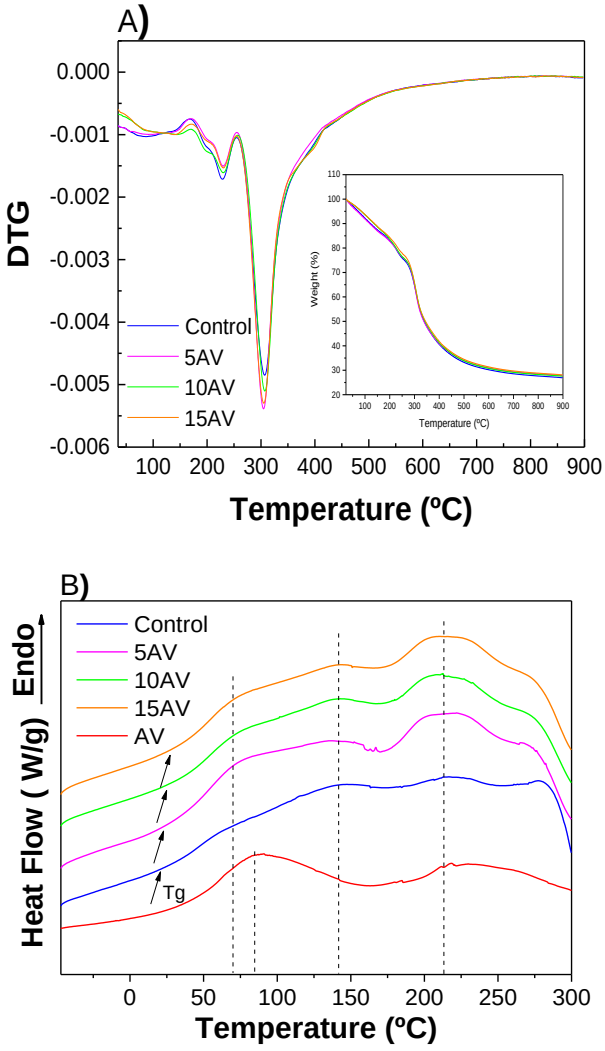

Figure 6.3. A) Thermo-gravimetric analysis (TGA) curves (inset) and derivative thermo-gravimetric (DTG) curves and B) Differential scanning calorimetry (DSC) analysis of compression molded chitosan films without *Aloe vera* (control) and with 5wt % *Aloe vera* (5AV), 10 wt % *Aloe vera* (10AV) and 15 wt % *Aloe vera* (15AV).

Concerning DSC analysis, results are shown in Figure 6.3B. *Aloe vera* sample showed two endothermic peaks, related to the sample moisture at 91 °C and at 218 °C, associated to the water entangled into the *Aloe vera* components (Pereira et al., 2011). All samples presented three endothermic peaks: the first peak at 74 °C can be related to film moisture; the second peak at 141 °C corresponds to the entrapped water linked to the film components by hydrogen bonding, since a tighter structure was formed and more energy was needed to release water; the last peak at 209 °C was associated to the melting point of citric acid and to the hemicellulose, lignin and cellulose present in *Aloe vera*, since this peak is more pronounced for the films containing *Aloe vera* than for control films.

It is worth noting that the displacement of the melting point of citric acid from 153 (neat citric acid) to 209 °C indicated that citric acid was crosslinked to chitosan. Furthermore, glass transition temperature (T_g) increased from 21 °C (control) to 27 °C (15AV), indicating that the material stiffness increased (Dehouche et al., 2020).Likewise, it can be assumed that *Aloe vera* interacted with the other components of the film.

6.4.3. Film structure and mechanical properties

In order to study the influence of *Aloe vera* in the structure of compressed molded chitosan films, XRD analysis was performed and XRD patterns are shown in Figure 6.4. Control films showed two broad diffraction peaks at around 2θ = 10.5° and 19°, corresponding to the characteristics peaks of chitosan (Liu et al., 2013; Ma et al., 2019). When *Aloe vera* concentration was increased, the intensity of the diffraction peaks decreased. The interactions between chitosan and *Aloe vera* could difficult the mobility of chitosan chains and, thus, hindered the crystallization process.

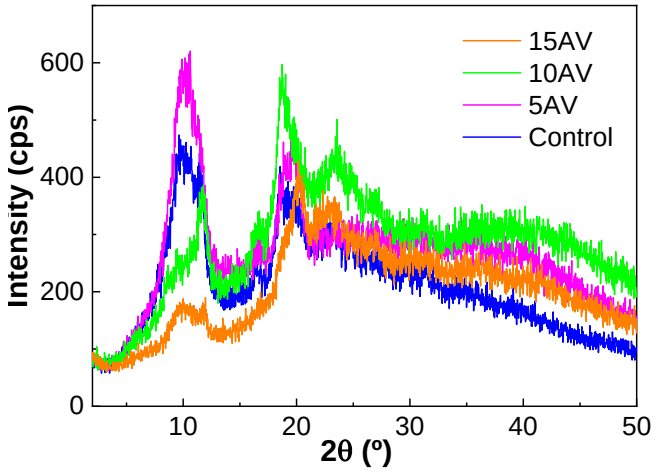

Figure 6.4. Diffractograms of compressed molded chitosan films without *Aloe vera* (control), 5wt % *Aloe vera* (5AV), 10wt % *Aloe vera* (10AV) and 15wt % *Aloe vera* (15AV).

In agreement to XRD results, SEM images (Figure 6.5) showed cross-section images of chitosan films. As can be seen, a compact structure was observed in control films, indicating a good compatibility between the components of the films. When *Aloe vera* was added, a structure formed by overlapping layers was observed, suggesting that film structure changed by the interactions of *Aloe vera* with the components of the films, as shown by FTIR analysis.

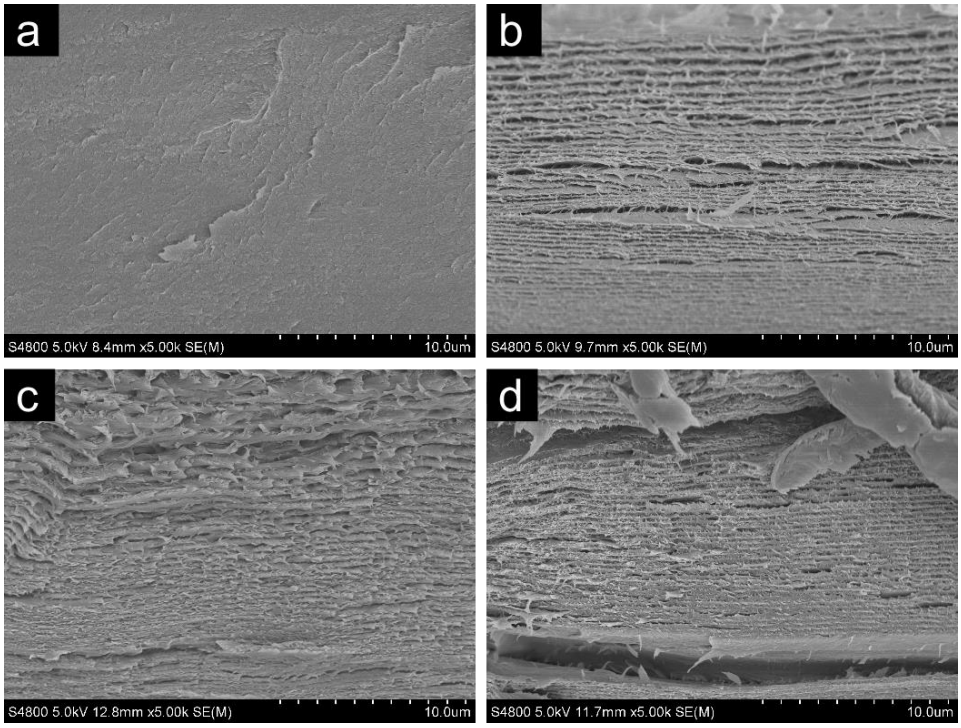

Figure 6.5. SEM images of cross-sections of compressed molded chitosan films: A) without *Aloe vera* and with B) 5wt % *Aloe vera* (5AV), C) 10wt % *Aloe vera* (10AV), and D) 15wt % *Aloe vera* (15AV).

Table 6.4. Tensile strength (TS), elongation at break (EAB) and elastic modulus (E) of compressed molded chitosan films without *Aloe vera* and with 5wt % *Aloe vera* (5AV), 10wt % *Aloe vera* (10AV), and 15wt % *Aloe vera* (15AV).

Films	TS (MPa)	EAB (%)	E (MPa)
Control	17.91 ± 0.95[a]	15.66 ± 1.46[a]	909.18 ± 83.55[a]
5AV	16.20 ± 1.03[a]	14.93 ± 0.51[a,b]	949.89 ± 66.74[a]
10AV	15.65 ± 1.98[a]	13.11 ± 2.02[a,b]	857.86 ± 54.43[a,b]
15AV	12.33 ± 1.74[b]	12.60 ± 1.87[b]	770.71 ± 58.53[b]

[a-b]Two means followed by the same letter in the same column are not significantly ($p > 0.05$) different according to the Tukey's multiple range test.

Regarding mechanical properties, tensile strength (TS), elongation at break (EAB), and elastic modulus (E) are shown in Table 6.4 in order to assess the effect of AV content in the mechanical behavior of chitosan films. No significant differences ($p > 0.05$) were observed in EAB, TS, or E values when *Aloe vera* was added up to 10 wt %. However, EAB and TS values showed a decrease for 15AV films. These results would indicate the hindrance effect of *Aloe vera* at high concentration (15AV film), avoiding intermolecular interactions between the components of the film forming formulations and, thus, decreasing the TS values (Gutiérrez & González, 2017; Pinzon, Garcia, & Villa, 2018). Moreover, the decrease of EAB when *Aloe vera* content increased was related to the lack of plasticizing effect of *Aloe vera* (Pinzon, Garcia, & Villa, 2018). As shown by previous analyses,

mechanical properties also showed that the highest AV content under study did not lead to improvements.

6.5. Conclusions

Chitosan films with *Aloe vera* were successfully processed by thermocompression. The crosslinking reaction between the amino groups of chitosan and the carboxyl groups of citric acid was confirmed by FTIR analysis. It is worth noting that crosslinked chitosan films maintained their integrity after 9 days in PBS at 37 °C. In addition, the formed structure was compact, limiting the swelling capacity of the films. In this regard, films presented a Fickian diffusion controlled release mechanism, in which swelling and relaxation of chitosan chains were involved, leading to a sustained release of *Aloe vera*. Although further assessments are required, this work showed the potential of citric-acid crosslinked chitosan films.

Chapter

7

Pectin-chitosan hydrogels: 3D printed chitosan films

7.1. Summary

Chitosan-pectin hydrogels were prepared and their rheological properties were assessed in order to select the best system to develop films by 3D printing. Hydrogels showed a weak gel behavior with shear thinning flow properties, caused by the physical interactions formed between both polysaccharides, as observed by FTIR analysis. Since systems with high concentration of pectin showed aggregations, the system composed of 2 wt % chitosan and 2 wt % pectin (CHI2PEC2) was selected for 3D printing. 3D printed films showed good shape accuracy, and SEM and XRD analyses revealed a homogeneous and amorphous structure. Moreover, films were stable and kept their shape and size after a cycle of compression sweeps. Their integrity was also maintained after immersion in PBS at 37°C, showing a high swelling capacity, suitable for being used as mats for moisture absorption from food.

7.2. Introduction

Hydrogels from natural polymers are gaining notoriety; in particular, polysaccharides and proteins are applied as bioinks for 3D printing (Baniasadi et al., 2021; Kim, Lee & Kim, 2020; Li et al., 2021). Among them, chitosan, the only natural cationic polysaccharide, due to

its positive charge in acidic media, has the ability to interact with negatively charged biomolecules by electrostatic interactions that affect mucoadhesion, hemostatic activity, antimicrobial activity, cell permeation capacity and cytocompatibility (Croisiee&Jérôme, 2013).

However, chitosan presents challenges in 3D printing, since it is too soft to self-support its structure and would collapse or deform due to its own weight (Hann et al., 2019; Hinton et al., 2015). Consequently, in order to overcome these drawbacks, chitosan can be combined with other polymers to promote physical and/or chemical crosslinking (Berger et al., 2004; Liu et al., 2019). Although physically crosslinked materials show lower mechanical strength compared to chemically crosslinked ones, physically crosslinked hydrogels exhibit shear thinning behavior and facilitate flow through the needle of the 3D printer (Hernandez, Souza, &Appel, 2021). In this regard, chitosan bioinks, reinforced with other biopolymer such as gelatin, have been successfully printed, controlling the stability of the scaffolds as a function of the gelatin content (Fischetti et al., 2020).

In this chapter, pectin has been selected to reinforce chitosan hydrogels. Pectin is an anionic heteropolysaccharide, extracted from

citrus fruits, with gelling properties (Abid et al., 2017; Demir et al., 2021). Depending on the esterification degree, pectin can be classified as high or low methoxy pectin (Mahendiran et al., 2021). Pectin is highly available, biodegradable and non-toxic (Indurkar et al., 2021; Ma et al., 2021). Moreover, the mixture of chitosan and pectin forms a polyelectrolyte complex mainly conformed by electrostatic interactions between the amino groups of chitosan and the carboxylic groups of pectin (de Souza et al., 2019).

The aim of this chapter was to prepare chitosan-pectin hydrogels with different concentrations in order to select the optimal composition for 3D printing and analyze the properties of the printed film. To accomplish this challenge, chitosan-pectin hydrogels were assessed from a rheological perspective. The hydrogel that fitted 3D printing requirements was selected, 3D printed, and the resulting films were physicochemically and mechanically characterized.

7.3. Materials and methods

7.3.1. Materials

Chitosan, with a molecular weight of 375 kDa and a deacetylation degree ≥ 75 %, was supplied by Sigma-Aldrich, Spain. High

methoxylated pectin, with a molecular weight of 472 kDa and an esterification degree of 58 %, was kindly supplied by CEAMSA, Spain. Acetic acid solution (1 N), used as solvent, was supplied by Panreac, Spain.

7.3.2. Hydrogel preparation

Chitosan-pectin systems were obtained by mixing chitosan and pectin solutions, previously prepared. On the one hand, the required amount of pectin was dissolved in water by stirring at 67 °C to obtain a 3 % (w/v) aqueous solution. This solution was left at 4 °C for 24 h before any further processing or characterization. This system was designated as CHI0PEC3. On the other hand, a certain amount of chitosan was dissolved in a 1 % acetic acid aqueous solution for 30 min under stirring to obtain a 2 % (w/v) chitosan solution designated as CHI2PEC0. Then, the corresponding volumes of both solutions were mixed at 7,000 rpm for 10 min (Ultraturrax UT25, IKA, Germany) to achieve the binary systems depicted in Table 7.1. The resulting binary systems were stored at 4 °C for 24 h until further processing or characterization.

Table 7.1. Denotation and composition of chitosan-pectin systems.

	System designation	Chitosan concentration (w/v %)	Pectin concentration (w/v %)
Single systems	**CHI2PEC0**	2.0	0.0
	CHI0PEC3	0.0	3.0
Binary systems	**CHI2PEC2**	2.0	2.0
	CHI2PEC3	2.0	3.0
	CHI1.5PEC3	1.5	3.0
	CHI1PEC3	1.0	3.0

7.3.3. Rheological characterization of the hydrogel

A Haake MARS rheometer (Thermo Fisher Scientific, Germany) coupled with a Universal Temperature Control (UTC) unit (Thermo-Scientific, Germany) was used for rheological characterization of chitosan-pectin hydrogels. The geometry used was a serrated plate-plate geometry, with a diameter of 35 or 60 mm, depending on the consistency of the system, and a gap between plates of 1 mm.

Stress sweep tests were initially carried out from 0.01 Pa to 1000 Pa at a constant frequency (1 Hz) to determine the critical stress and critical

strain that define the linear viscoelastic range (LVR) of the systems. Then, frequency sweep tests were performed from 0.01 to 10 Hz within the LVR of each system. Elastic modulus (G′), viscous modulus (G′′), and loss tangent (tanδ) were obtained. A power law correlation between G′ and the frequency was calculated using the following equation to model the frequency dependence of G′:

$$G' = a \cdot \omega^b$$

where ω is the frequency, a is a coefficient that represents the magnitude of G′ at a frequency of 1 Hz, and b is a power law exponent that describes the dependence of the slope of G′ on frequency.

Both dynamic tests were performed at two different temperatures (25 °C and 4 °C) to simulate the potential behavior of the systems studied during extrusion and on the 3D printer bed after deposition.

Regarding temperature sweep tests from 25 to 80 °C, a constant frequency of 1 Hz and a heating rate of 3 °C/min were set. Thermal treatments were always performed within the LVR, as stress was kept constant at a stress lower than the critical stress determined.

Shear flow tests were accomplished with a step-by-step increase of the shear rate ($\dot{\gamma}$) over the range of 0.01 - 100 s^{-1}, and the steady state was

obtained at each shear rate. Flow data were fitted to the model developed by Williamson for shear-thinning materials:

$$\eta = \frac{\eta_0}{1 + (\lambda\dot{\gamma})^{1-n}}$$

where η_0 is the zero-shear rate viscosity, λ is a characteristic time for the onset of the shear-thinning region and 1-n is the slope of this region. The parameter n represents the flow index of the power law region.

Moreover, an empirical viscosity during 3D printing was determined calculating the maximum shear rate at the nozzle using the Weissenberg-Rabinowitsch-Mooney equation, assuming that printing takes place at shear rates within the power law region:

$$\dot{\gamma}_W = \frac{8\,V}{D} \cdot \left(\frac{3n+1}{4n}\right)$$

where V is the 3D printing velocity, D is the nozzle diameter, and n is the flow index.

Once the gap was achieved, all samples were left for 5 min before running the test to allow residual stress to relax and to stabilize sample temperature. At least three replicates were tested for each system.

7.3.4. Characterization of CHI2PEC2 hydrogel

7.3.4.1. Fourier transform infrared (FTIR) spectroscopy

FTIR spectra were collected with a Nicolet Nexus FTIR spectrometer (Thermo Fisher Scientific, Massachusetts, USA) with a Golden Gate ATR accessory. The spectra, with a resolution of 4 cm^{-1}, were acquired between 4000 and 800 cm^{-1} with 32 scans for each sample.

7.3.4.2. Mucoadhesion study

Mucoadhesive properties of the chitosan-pectin hydrogel were determined by means of a TA.XT.Plus Texture Analyzer equipped with a 5 kg load cell, a gel mucoadhesion accessory (A/GMP), and a mucoadhesion rig (A/MUC). The maximum force required to separate the hydrogel from the membrane (maximum detachment force) and the total amount of force involved in the film withdrawal from the membrane (work of adhesion) were calculated by triplicate with a disc soaked in 1% porcine stomach's mucin in a phosphate buffered saline (PBS) at 37 °C.

7.3.4.3. Texture profile analysis (TPA)

Texture profile analysis of the chitosan-pectin hydrogel was carried out with a TA-XT plus Texture Analyzer equipped with a 5 kg load cell and an aluminum cylinder of 50 mm diameter (P/50). Samples were compressed twice until 20% of the original height and with a delay time of 5 s and activation force of 0.1 g. The operating speed was set at 1 mm/s and three replicates were collected for CHI2PEC2 hydrogel. Hardness, adhesiveness, and cohesion were determined by using the software Exponent 8,0,5,0.

7.3.5. 3D printing of CHI2PEC2 hydrogel

CHI2PEC2 films were printed using a syringe-based extrusion 3D DomoBIO printer (Domotek, Spain). The film design, a cylindrical mesh with 21 mm of diameter, 1.5 mm height and infill of 100 %, was accomplished with Cura (UltimakerCura 4.6.1) software. A syringe with the ink was placed into the cartridge with the printing temperature fixed at 25 °C. The syringe was placed in the cartridge at 25 °C for 30 min before printing to have a homogeneous temperature distribution. The hydrogel was printed in the following conditions: G18 nozzle (inside diameter of 0.84 mm), dosing distance of 0.17 mm, 2.8 mm/s printing

speed, and 120 mm/s non-printing speed. After printing, the film was dried by evaporation of the water at room temperature.

7.3.6. CHI2PEC2 film characterization

7.3.6.1. Swelling measurements

In order to perform the swelling test, a gravimetric method was followed. Printed samples were weighed (W_0) and subsequently immersed into 70 mL of PBS (pH = 7.4). After immersion, the samples were weighed (W_h) every 2 min for the first hour, then every 10 min for the second hour and every hour for the next 3 hours. Thereafter, measurements were carried out in triplicate at 24 h, 30 h, 48 h, 54 h, 72 h and 7 days. The swelling degree (S) was calculated by the following equation:

$$S\ (\%) = \frac{W_h - W_0}{W_0} \cdot 100$$

7.3.6.2. Degradation degree (DD)

Degradation degree (DD) was performed with films (W_0) immersed in PBS (pH 7.4) at 37 °C for days 1, 3, 7, 11, 15, 18 and 21 (W_d). After immersion, samples were left to dry until reaching constant weight. Three replicates were tested and DD was calculated as follows:

$$DD\ (\%) = \frac{W_0 - W_d}{W_0} \cdot 100$$

7.3.6.3. Compression test

Chitosan-pectin printed films were compressed using a TA.XT plusC Texture Analyzer equipped with a 5 kg load cell and an aluminum cylinder of 50 mm diameter (P/50). Before testing, samples were kept in a chamber at room temperature and 100% relative humidity for 48 h. A cyclic compression test was performed with five sweeps since films recovered their initial height at the end of the compression. 1 mm/s crosshead speed and activation force of 5 g were set as compression conditions. The test was carried out at room temperature and the load was applied until 80% of the film initial height was compressed. Data were analyzed with Exponent 8,0,5,0 software.

7.3.6.4. Scanning electron microscopy (SEM)

Scanning electron microscopy (SEM) was used to visualize cross-section and surface morphologies of the samples. For that purpose, a Hitachi S-4800 scanning electron microscope (Hitachi High-Technologies Corporation, Tokyo, Japan) was used with an acceleration voltage of 15

kV. Samples were placed in a metallic stub and coated with gold under vacuum in argon atmosphere.

7.3.6.5. X-ray diffraction (XRD)

X-ray diffraction (XRD) analysis was carried out at 40 kV and 40 mA by means of a PANalyticXpert Pro (PANalytical, Almelo, The Netherlands) equipment with a diffraction unit and Cu-Kα (λ = 1.5418 Å) as a radiation source. Data were collected from 2° to 40° (step size = 0.026, time per step = 118 s).

7.3.7. Statistical analysis

With the purpose of determining the significant differences between measurements, analysis of variance (ANOVA) was carried out by means of SPSS software (SPSS Statictic 25.0). Tukey's multiple range test was used for multiple comparisons among different systems with a statistical significance at the $p < 0.05$ level.

7.4. Results and discussion

7.4.1. Rheological characterization

7.4.1.1. Linear viscoelastic properties

Rheological properties of chitosan-pectin systems were characterized to determine the most suitable hydrogel composition for 3D printing. Frequency sweep tests were performed at 4 and 25 °C to confirm chitosan-pectin gel formation and observe the time dependence of the systems (Figure 7.1). Regardless of the temperature used during the test (25 or 4 °C), the single system containing only chitosan (CHI2PEC0) showed a predominantly viscous response, with the loss modulus (G´´) greater than storage modulus (G´) in the low frequency regime (Figure 7.1a and 7.1c), and a crossover point at high frequency (i.e., at 8.60 Hz and 6.45 Hz for 25 °C and 4 °C, respectively). This difference in the crossover frequency suggests that the CHI2PEC0 system needed longer relaxation times at lower temperatures, as a consequence of a slightly more elastic behavior (Wu, Therriault & Heuzey, 2018). This behavior is qualitatively similar to that one previously found for single CHI solutions (Calero et al., 2010). However, the values of G' and G'' were higher in the present study since the molecular weight was almost

twice the value used in the previous study. In contrast, CHI0PEC3 systems presented a predominantly viscous behavior (G´´ > G´) in the whole frequency range (Figure 7.1b and 7.1d), indicating a liquid-like behavior at both temperatures.

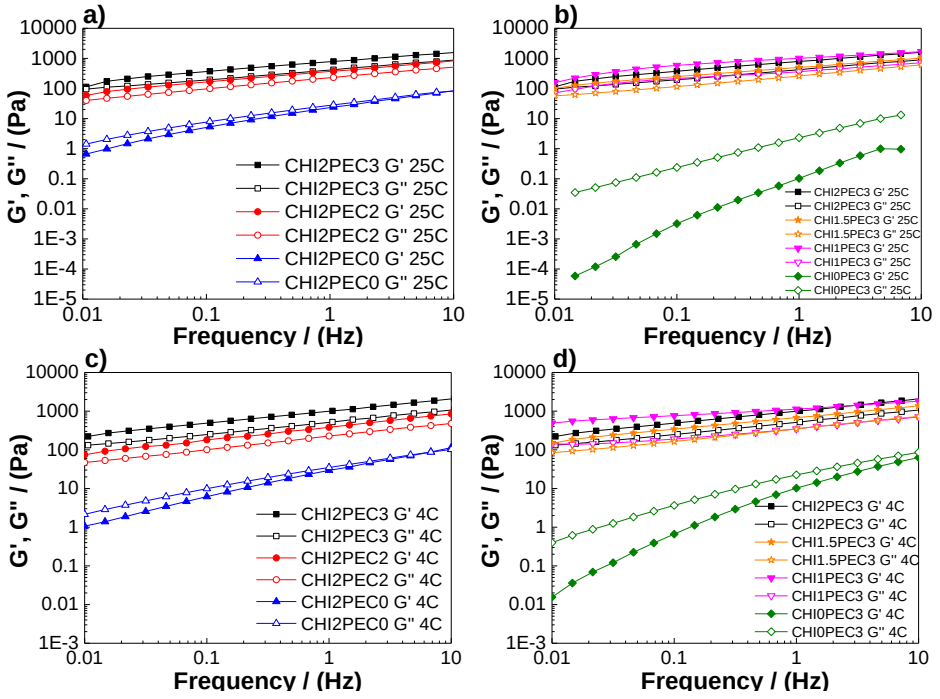

Figure 7.1. Elastic (G′) and viscous (G″) moduli as a function of frequency from 0.01- 10 Hz: (a) and (c) for chitosan-pectin hydrogels with 2% chitosan at 25 and 4°C, respectively; (b) and (d) for chitosan-pectin hydrogels with 3% pectin at 25 and 4 °C, respectively.

On the other hand, binary systems containing both biopolymers, chitosan and pectin (Figure 7.1a-d), showed a weak gel-like behavior, with G´ values higher than G´´, regardless of the frequency and

temperature analyzed. The similar and moderate frequency dependence shown by both moduli, for every chitosan/pectin system is typical of weak gels with non-covalent bonding among the components of the formulation (Liu &Ciftci, 2021). It is worth noting that a gel-like behavior typically results in proper stability to maintain dimensional firmness during deposition on the printing bed (Montoya et al., 2021).

In this sense, parameters *a* and *b* from the power law model for G′ were used to predict gel firmness. The power law coefficient, *a*, represents the magnitude of G′ at a frequency of 1 Hz, and the power law exponent, *b*, indicates the dependence of the elastic modulus on frequency, where an exponent value equal to zero means that G′ does not depend on frequency (Resch & Daubert, 2002). Power law parameters are shown in Table 7.1 as a function of the hydrogel composition and temperature. As may be observed, an increase in pectin content led to an increase in parameter *a* giving rise to an enhancement of the gel strength, either at 25 or 4 °C. Moreover, a high level of gel strength was maintained at the highest pectin content even if the chitosan content was reduced from 2 to 1%. As for parameter *b*, results revealed that when pectin concentration increased and chitosan

concentration decreased, b parameter decreased, resulting in less frequency-dependent hydrogels. Therefore, the increase of pectin led to a stronger hydrogel (Liu et al., 2019). Moreover, comparing the same hydrogels at different temperatures, 4 and 25 °C, no significant differences ($p > 0.05$) were generally observed for parameters a and b. The exceptions were found at the lowest concentrations of chitosan (CHI1PEC3 and CHI0PEC3) that showed lower values for parameter b at low temperature. In any case, parameter b ranged between 0.18 and 0.36, indicating a relatively marked frequency dependence. This response was reported to correspond to a weak gel behavior (Manzoor et al., 2020).

In order to determine the linear viscoelastic range (LVR), stress sweep tests at 25 °C and 4 °C were carried out, which provide information on the unperturbed structure of the system. To delimit the LVR, the critical strain (γ_c) was determined, and values are shown in Table 7.2. Results revealed significant differences ($p < 0.05$) between single and binary systems, since a decrease of critical strain was observed for the latter, suggesting that the hydrogel network had lower deformation capacity due to the interactions between chitosan and pectin (Perez-Puyana et al., 2020). Chitosan may act as an efficient cross-linker

in pectin systems at acidic pH, promoting an upward evolution in the viscoelastic moduli of samples (Marudova, MacDougal & Ring, 2004). Additionally, electrostatically stabilized complexes are formed in the presence of both biopolymers, where also hydrogen bonding and hydrophobic interactions may play a role (Rashidova et al., 2004).

Table 7.1. The effect of chitosan and pectin concentration on *a* coefficient and *b* exponent of the power law model for the storage modulus in the frequency sweep of the hydrogels at 25 and 4 °C.

T (°C)	Sample	*a* (Pa·Hz^b)	*b*	R^2
25	**CHI2PEC0**	20.1 ± 1.1$^{a, A}$	0.677 ± 0.015$^{a, A}$	0.9922
	CHI2PEC2	340 ± 19$^{b, B}$	0.360 ± 0.008$^{b, B}$	0.9992
	CHI2PEC3	759 ± 3$^{c, C}$	0.328 ± 0.001$^{b, BC}$	0.9980
	CHI1.5PEC3	485 ± 18$^{b, B}$	0.300 ± 0.011$^{bc, C}$	0.9992
	CHI1PEC3	725 ± 130$^{c, C}$	0.236 ± 0.013$^{c, D}$	0.9977
	CHI0PEC3	0.0938 ± 0.0002$^{a, A}$	1.580 ± 0.059$^{d, E}$	0.9858
4	**CHI2PEC0**	26.9 ± 0.4^{A}	0.676 ± 0.001^{A}	0.9959
	CHI2PEC2	381 ± 4^{B}	0.346 ± 0.003^{BC}	0.9991
	CHI2PEC3	1233 ± 37^{D}	0.303 ± 0.011^{BC}	0.9998
	CHI1.5PEC3	753 ± 81^{C}	0.295 ± 0.011^{C}	0.9996
	CHI1PEC3	1209 ± 68^{D}	0.176 ± 0.005^{F}	0.9965
	CHI0PEC3	8.90 ± 0.49^{A}	1.125 ± 0.022^{G}	0.9835

$^{A-D}$Two means followed by the same letter in the same column are not significantly ($p > 0.05$) different according to the Tukey's multiple range test.

In addition, regarding G′ values at 1 Hz (G'_1) shown in Table 7.3 for the LVR, significant differences ($p < 0.05$) were observed for the hydrogels tested at 25 °C. Thus, the single systems (CHI0PEC3 and CHI2PEC0) showed the lowest G′ values, between 0.11 and 22.96 Pa, respectively. No significant ($p > 0.05$) differences were observed between G'_1 values at 25 °C and 4 °C for CHI0PEC3, CHI2PEC0, and CHI2PEC2 hydrogels. However, G'_1 for CHI1PEC3, CHI1.5PEC3 and CHI2PEC3 samples showed a significant increase ($p < 0.05$) with increasing temperature from 4°C to 25 °C, especially for CHI1PEC3 hydrogels. Therefore, an increase in hydrogel stiffness was driven by a higher proportion of pectin (Cernencu et al., 2019).

The predominantly viscous response observed for CHI0PEC3 and CHI2PEC0 systems can be confirmed with the values of tanδ at 1 Hz ($\tan\delta_1$) that are higher than unity for these two systems at 25 °C and 4 °C. In contrast, all the binary chitosan-pectin hydrogels presented $\tan\delta_1$ values lower than 1, indicative of a predominantly elastic behavior. Among chitosan-pectin hydrogels, no significant difference ($p > 0.05$) was observed for $\tan\delta_1$, displaying values around 0.5. Therefore, considering that hydrogels exhibited small critical strain values ($\gamma_c < 0.05$)

and moderately low loss tangent values ($tan\delta_1$> 0.1), chitosan-pectin hydrogels can be considered "weak gels" (Manzoor et al., 2020). It is worth mentioning that these gels have the capacity to flow without fracture, recover their structure, and achieve the properties required for 3D printing (Pieczywek et al., 2021).

Table 7.2. Critical strain (γ_c), and values for G′ at 1 Hz (G'_1), and tanδ at 1 Hz ($tan\delta_1$) within the linear viscoelastic range for the hydrogels tested at 25 °C and 4 °C.

T (°C)	Sample	γ_c	G'_1 (Pa)	$tan\delta_1$
25	**CHI2PEC0**	$0.392 \pm 0.016^{a, A}$	$23.0 \pm 1.4^{a, A}$	$1.20 \pm 0.03^{a, A}$
	CHI2PEC2	$0.034 \pm 0.002^{b, B}$	$257 \pm 18^{b, B}$	$0.64 \pm 0.03^{a, AB}$
	CHI2PEC3	$0.037 \pm 0.004^{b, B}$	$763 \pm 41^{c, F}$	$0.54 \pm 0.01^{a, AB}$
	CHI1.5PEC3	$0.033 \pm 0.001^{b, B}$	$486 \pm 21^{d, CD}$	$0.53 \pm 0.04^{a, AB}$
	CHI1PEC3	$0.025 \pm 0.001^{b, B}$	$599 \pm 31^{e, DE}$	$0.39 \pm 0.04^{a, B}$
	CHI0PEC3	$0.752 \pm 0.137^{c, C}$	$0.114 \pm 0.010^{a, A}$	$21.52 \pm 0.92^{b, C}$
4	**CHI2PEC0**	0.333 ± 0.006^{A}	29.4 ± 0.3^{A}	1.201 ± 0.016^{A}
	CHI2PEC2	0.0243 ± 0.001^{B}	417 ± 62^{BC}	0.590 ± 0.003^{AB}
	CHI2PEC3	0.0380 ± 0.0008^{B}	1023 ± 52^{G}	0.505 ± 0.009^{AB}
	CHI1.5PEC3	0.0218 ± 0.0008^{B}	660 ± 21^{EF}	0.498 ± 0.008^{AB}
	CHI1PEC3	0.0231 ± 0.0004^{B}	1023 ± 93^{G}	0.301 ± 0.006^{B}
	CHI0PEC3	0.295 ± 0.013^{A}	11.3 ± 1.1^{A}	2.103 ± 0.085^{D}

$^{A-G}$Two means followed by the same letter in the same column are not significantly ($p > 0.05$) different according to the Tukey's multiple range test.

Temperature sweep tests from 25 to 80 °C were carried out at 1 Hz to analyze the effect of temperature on the rheological behavior of the hydrogels. As shown in Figure 7.2a, G´´ values were higher than G´ for chitosan hydrogels without pectin (CHI2PEC0) at low temperatures, indicating a fluid-like viscoelastic behavior until the crossover point was reached around 58 °C. From that temperature on, hydrogels exhibited a predominantly elastic response (i.e. G´ became higher than G´´), due to the formation of chitosan clusters by hydrophobic interactions (Tang et al., 2007). In contrast, in absence of chitosan, pectin systems (CHI0PEC3) exhibited a viscous behavior, with G´´ values clearly higher than G´ in the whole range of temperatures, as shown in Figure 7.2b. In any case, these two single systems showed mechanical spectra corresponding to polymer solutions below the threshold for the critical gel behavior.

Regarding chitosan-pectin systems (Figure 7.2a and 7.2b), all samples showed higher values of G´ than G´´, reflecting the elastic behavior of the samples in the range between 25 and 80 °C. Moreover, all chitosan-pectin systems presented nearly constant values of both moduli between 25 and 58 °C, suggesting that no difference was expected when printing at room or physiological temperature. However, for

temperatures above 58 °C, all chitosan-pectin hydrogels, except CHI2PEC2, presented an increase of both moduli until 80 °C.

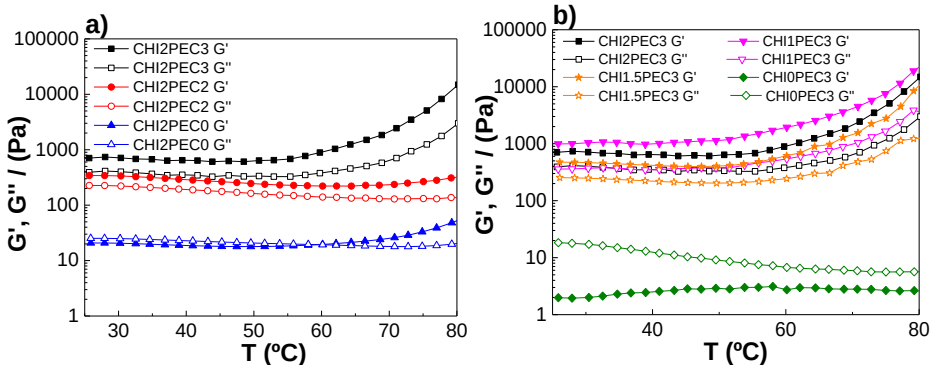

Figure 7.2. Elastic (G′) and viscous (G″) moduli as a function of temperature from 25 to 80 °C for (a) chitosan-pectin hydrogels with 2% chitosan and (b) chitosan-pectin hydrogels with 3% pectin.

7.4.1.2. Flow properties

Additionally, the flow behavior of chitosan-pectin hydrogels was determined, and flow curves are displayed in Figure 7.3. All chitosan-pectin hydrogels with 2 % chitosan presented a similar shear-thinning behavior at 25 °C (Figure 7.3a) and 4 °C (Figure 7.3c), with a marked decrease of viscosity as shear rate increased, clearly describing a power law decay region and showing a tendency towards a zero-shear limiting viscosity at low shear rate. Once again, the single CHI solution (CHI2PEC0) displayed a similar shear thinning response, although showing higher viscosity values than those found previously (due to the

highest molecular weight) (Calero et al., 2010). Moreover, flow properties were dependent on pectin concentration; when pectin concentration increased, viscosity also increased. However, binary systems containing 3 % pectin did not reflect any apparent influence of chitosan concentration on the flow curves, neither at 25 °C (Figure 7.3b) nor at 4 °C (Figure 7.3d).

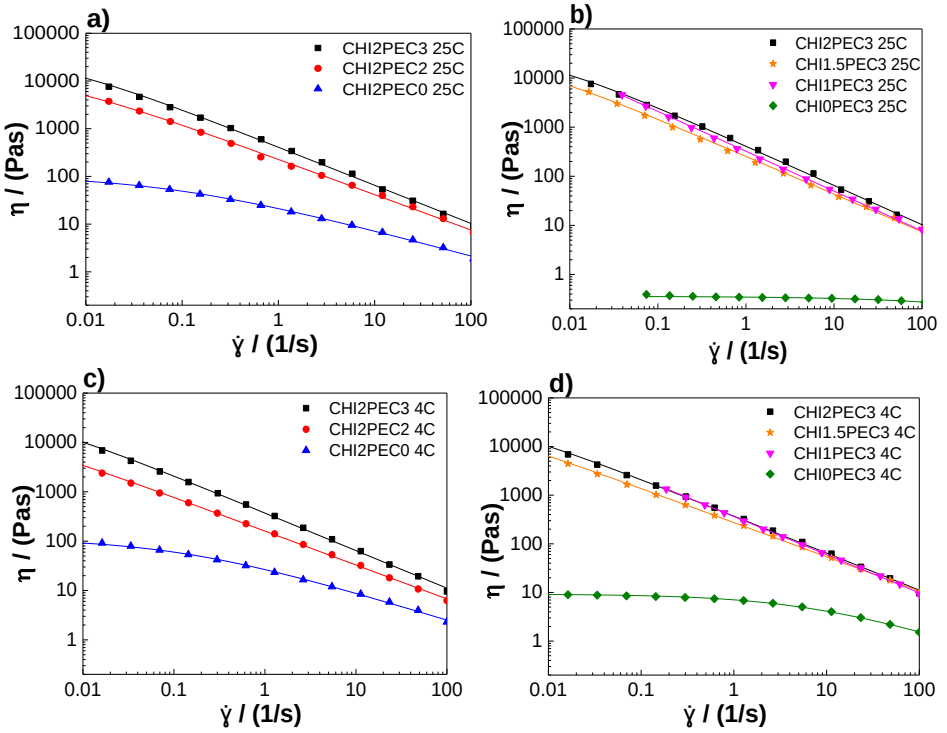

Figure 7.3. Steady state flow curves of chitosan-pectin hydrogels: a) and c) for chitosan-pectin hydrogels with 2% chitosan at 25 and 4 °C, respectively; b) and d) for chitosan-pectin hydrogels with 3% pectin. Lines reproduce the fitting to the Williamson model.

In contrast, pectin hydrogels without chitosan were found to be independent on shear rate at 25 °C, indicating a Newtonian fluid behavior, whereas at 4 °C a decrease of viscosity was observed at high shear rates, indicating a non-Newtonian shear-thinning behavior.

Moreover, the viscosity at 4 °C increased ten times with respect to the viscosity at 25 °C, as also reported by other authors (Birch et al., 2015; Chen et al., 2014). It is worth mentioning that the shear thinning behavior of the hydrogels facilitates their flow during 3D printing. Upon hydrogel ejection from the nozzle of the 3D printer (25°C) and its deposition on the printer bed (4 °C), shear rate undergoes a sudden decrease which entails a remarkable increase in the viscosity of the shear-thinning hydrogel, leading to an enhancement of the dimensional stability of the 3D printed film(Schwab et al., 2020).

Flow curves were fitted to Williamson model and fitting parameters are presented in Table 7.3. Concerning the zero-shear rate viscosities for the hydrogels at 25 °C, an increase from 19.7 to 1523 kPa·s was observed following this increasing sequence: CHI2PEC2 < CHI2PEC3 < CHI1.5PEC3 < CHI1PEC3, indicating that, when the amount of pectin increased and that of chitosan decreased, the formation of

polymer aggregates was promoted (Norcino et al., 2018; Tsianou et al., 1999). Regarding the effect of temperature, no significant difference ($p < 0.05$) was observed between the values of the zero-shear rate viscosity at 25 and 4 °C. Regarding the viscosity in the 3D printing process, taking into consideration that the nozzle diameter used was 0.84 mm, with a printing velocity of 2.8 mm/s, the shear rate can be calculated. The estimated value for the shear rate at the nozzle was between 42 and 60 s^{-1}, corresponding to a viscosity between 12 and 23 Pa·s for all binary systems. Bearing in mind these results, viscosity during 3D printing decreased 10^3 times compared to the zero-shear rate viscosity.

These results are in accordance with the empirical ink viscosities reported during 3D printing, which are in a range from 0.5 to 20 Pa·s at high shear rates (10^2-10^3 s^{-1}), while the range moves from 10^2 to 10^3 Pa·s at lower shear rates (≤ 0.1 s^{-1}) (Chen et al., 2019; Robinson et al., 2015; Tian et al., 2017). While all binary systems follow the criteria for high shear rates, only CHI2PEC2 and CHI1.5PEC3 binary systems comply with the requirement at low shear rates (i.e., viscosity lower than 10^3 Pa·s).

Table 7.3. Zero-shear rate viscosity (η_0), characteristic time (λ), flow index (n) and correlation coefficient (R^2) of Williamson model for chitosan-pectin hydrogels at 25 and 4 °C.

T (°C)	Sample	η_0 (Pa·s)	λ (s)	n	R^2
25	**CHI2PEC0**	113.84 ± 15.43$^{a, A}$	14.2 ± 1.0$^{a, A}$	0.448 ± 0.016$^{a, A}$	0.999
	CHI2PEC2	19658 ± 2287$^{a, AB}$	431 ± 116$^{b, B}$	0.266 ± 0.008$^{b, BCD}$	0.999
	CHI2PEC3	29432 ± 7419$^{a, ABC}$	198 ± 74$^{a, AB}$	0.191 ± 0.008$^{b, CD}$	0.999
	CHI1.5PEC3	36336 ± 9625$^{a, ABC}$	1040 ± 135$^{c, C}$	0.265 ± 0.022$^{b, BCD}$	0.999
	CHI1PEC3	152729 ± 31136$^{b, D}$	2621 ± 57$^{d, F}$	0.204 ± 0.018$^{b, CD}$	0.999
	CHI0PEC3	0.501 ± 0.137$^{a, A}$	0.0009 ± 0.0004$^{a, A}$	0.674 ± 0.133$^{c, E}$	0.970
4	**CHI2PEC0**	115.71 ± 8.58^{A}	8.75 ± 0.91^{A}	0.438 ± 0.013^{A}	0.999
	CHI2PEC2	37051 ± 1973^{ABC}	2632 ± 222^{F}	0.305 ± 0.007^{BC}	0.999
	CHI2PEC3	48159 ± 6715^{BC}	570 ± 124^{B}	0.249 ± 0.010^{CD}	0.999
	CHI1.5PEC3	64136 ± 7242^{C}	2131 ± 198^{E}	0.288 ± 0.007^{BC}	0.999
	CHI1PEC3	207319 ± 28281^{E}	1544 ± 282^{D}	0.168 ± 0.001^{D}	0.999
	CHI0PEC3	8.050 ± 1.237^{A}	0.119 ± 0.028^{A}	0.374 ± 0.023^{AB}	0.999

$^{a-b,\ A-E}$Two means followed by the same letter in the same column are not significantly ($p > 0.05$) different according to the Tukey's multiple range test.

In order to select the most suitable system for 3D printing applications, the following features can be considered: (i) Systems containing 3% pectin showed apparent viscosities higher than 1000 Pa·s at low shear rates (< 0.1 s^{-1}); (ii) Higher concentrations of pectin with lower concentrations of chitosan showed pectin aggregation and clustering and, thus, heterogeneity; (iii) There was no significant difference in the rheological behavior among the rest of chitosan-pectin hydrogels. Therefore, taking all these factors into account, CHI2PEC2 hydrogels were selected for 3D printing.

7.4.2. CHI2PEC2 hydrogel characterization

The FTIR spectra of chitosan, pectin and CHI2PEC2 are shown in Figure 7.4. Both chitosan and pectin showed bands at 3000 - 3600 cm^{-1}, associated with O-H bonds in both polymers and to N-H bonds in chitosan, and bands between 1150 and 890 cm^{-1} associated with the C-O-C of the saccharide ring (Rashidova et al., 2004). The differences were observed in the range between 1300 and 1750 cm^{-1}. Regarding chitosan spectrum, the band at 1644 cm^{-1}, attributed to C=O stretching; a band at 1558 cm^{-1}, associated to NH_2 bending; and two bands at 1418 and 1376 cm^{-1}, corresponding to CH_3 deformation, were observed (Barbosa et al.,

2019; Mauricio-Sánchez et al., 2018). For pectin spectrum, a band at 1738 cm^{-1}, assigned to C=O of the ester bonds, and the band at 1604 cm^{-1}, associated with the asymmetric stretching vibration of COO^- were observed (Priyadarshi, Kim & Rhim, 2021). Some displacements of these bands were observed for CHI2PEC2. In particular, the band related to the ester group in pectin shifted from 1738 cm^{-1} to 1732 cm^{-1} in CHI2PEC2. Moreover, the absorption band corresponding to C=O stretching at 1644 cm^{-1} for chitosan and at 1604 cm^{-1} for pectin shifted to 1628 cm^{-1} for CHI2PEC2. All these band displacements indicate physical interactions by hydrogen bonding between both biopolymers.

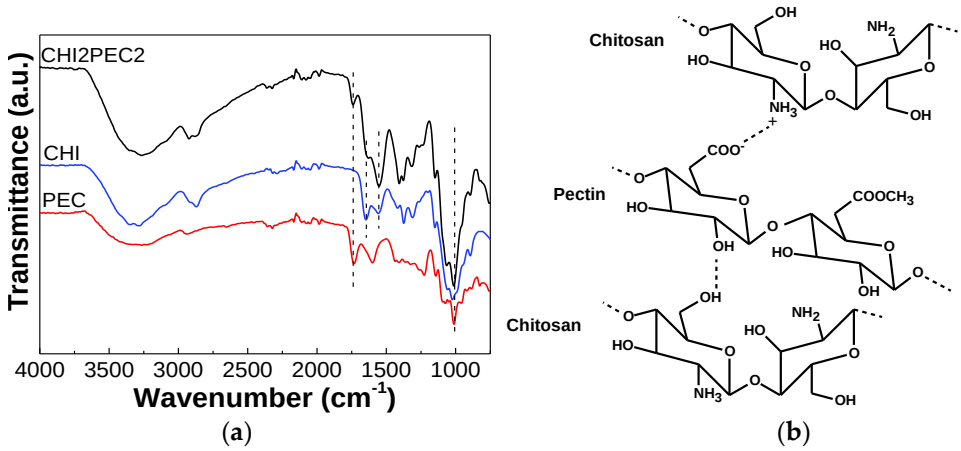

Figure 7.4.a) FTIR spectra of neat chitosan (CHI), neat pectin (PEC) and the hydrogel with 2 wt % chitosan and 2 wt % pectin (CHI2PEC2) and b) representation of the interactions between chitosan and pectin.

In order to evaluate the hydrogel adhesiveness to a biological surface, mucoadhesion analysis was carried out and the force displacement curve of one of the CHI2PEC2 replicates is shown in Figure 7.5. At the beginning of the test, when the sample is getting closer to the mucin disk, the force decreased due to the force applied to attach the hydrogel to the mucin disk. A significant increase of the force was observed as the hydrogel started to detach from the mucin disk due to the exerted force done. From then on, the force started to decrease. The maximum detachment force (F_{max}) and the work of adhesion (W_{ad}) were calculated from the mucoadhesion analysis. The values found for F_{max} and W_{ad} were 0.21 ± 0.02 N and 0.36 ± 0.03 N mm, respectively. These values are higher than those obtained for other polysaccharide systems (F_{max} = 0.093 N and W_{ad}= 0.029 N mm) for wound dressing applications (Singh, Sharma & Dhiman, 2013).

Therefore, chitosan-pectin hydrogel showed excellent mucoadhesive properties, which are essential requirements for wound dressing materials in order to be adhered to the wound site to protect it from the external environment. This mucoadhesive capacity is associated with –OH and $–NH_2$ groups in the biopolymers, which could be linked to

mucins by hydrogen bonding; furthermore, as acidic pH was used for the hydrogel preparation, the amino groups of chitosan were protonated and, thus, strong electrostatic interactions could be formed with the anionic groups of mucin (Sahatsapan et al., 2018). Since pectin and mucin are anionic compounds, hence, electrostatic repulsion charges might result in an uncoiling of polymer chains and facilitate chain entanglement and bond formation (Russo et al., 2016).

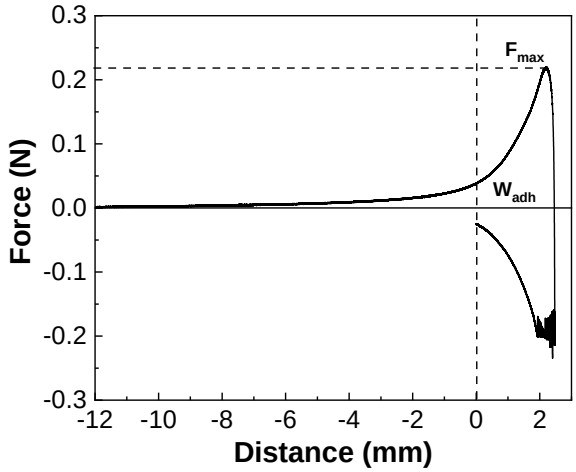

Figure 7.5. Force displacement curve of one replicate of CHI2PEC2 hydrogel in the mucoadhesion analysis.

Additionally, texture profile analysis (TPA) can provide information related to the hardness, adhesiveness, and cohesiveness of the hydrogels, which are of great relevance to analyze their handleability for 3D printing (Janarthanan et al., 2020). In this regard,

hardness, which is the maximum force required to produce the first deformation, showed a value of 5.9 ± 0.2 g. Adhesiveness is related to the capacity of a gel to adhere on a surface and, thus, higher adhesiveness values indicate that the gel needs shorter time to bond to the surface (Villanueva et al., 2019). In the case of the CHI2PEC2 system, the adhesiveness value found was 8.7 ± 0.5 g·s. This adhesiveness, as well as the hardness observed for CHI2PEC2 hydrogel, was similar to values obtained for hyaluronic acid/carboxymethylcellulose systems (Russo et al., 2016). Finally, cohesiveness is related to the strength capacity of a gel to maintain its own structure when subjected to a compressive stress (Bhattacharyya et al., 2021). CHI2PEC2 hydrogel exhibited a high cohesive value of 1.05 ± 0.04, indicative of a high capacity to maintain the three-dimensional structural integrity and, hence, to hold its structure after printing (Xia et al., 2020).

7.4.3. 3D printed CHI2PEC2 film characterization

CHI2PEC2 films were successfully printed with shape fidelity as shown in Figure 7.6. After ink deposition, the material kept the set geometry and showed mechanical integrity.

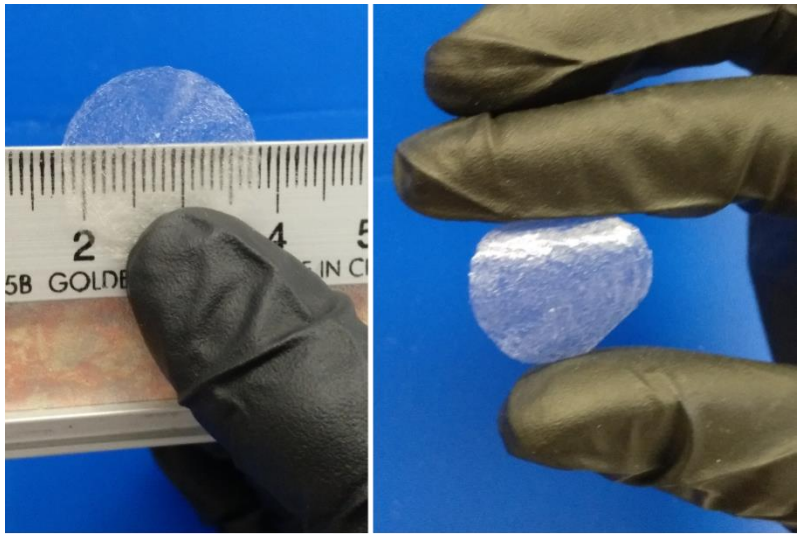

Figure 7.6. 3D printed CHI2PEC2 film after drying at room temperature.

7.4.3.1. Physicochemical properties

Swelling of CHI2PEC2 films was evaluated in phosphate buffered saline (PBS) solution (pH = 7.4) at room temperature. As can be observed in Figure 7.7, swelling increased fast up to 1250 % in the first 5 h, indicating that the samples increased more than ten times their initial weights.

Thereafter, swelling continued increasing more slowly up to 1830 % at day 7. Since pectin moieties were negatively charged with $-COO^-$ groups at pH 7.4, electrostatic repulsions were promoted and, thus, the swelling ability increased (Cesco, Valente & Paulino, 2021; Gerschenson et al., 2021). In this context, having a high swelling capacity is desirable

in order to absorb wound exudates that could slow the wound healing and macerate the nearby skin (Long et al., 2019). It is worth noting that samples kept their integrity after the 7 days of immersion.

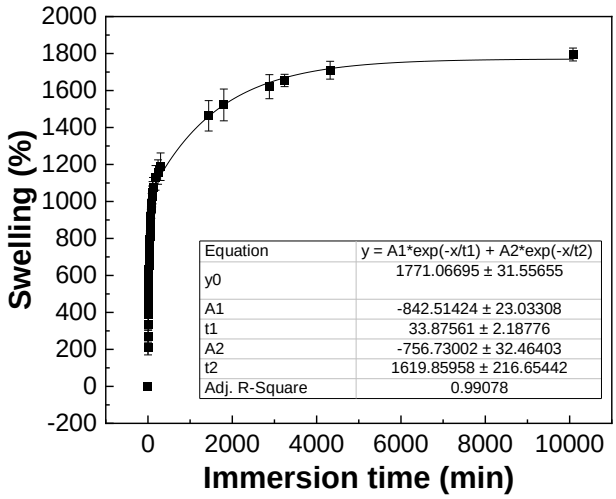

Figure 7.7. Swelling capacity of CHI2PEC2 films in PBS (pH = 7.4).

Thereafter, swelling continued increasing more slowly up to 1830 % at day 7. Since pectin moieties were negatively charged with $–COO^-$ groups at pH 7.4, electrostatic repulsions were promoted and, thus, the swelling ability increased (Cesco, Valente & Paulino, 2021; Gerschenson et al., 2021). In this context, having a high swelling capacity is desirable in order to absorb wound exudates that could slow the wound healing and macerate the nearby skin (Long et al., 2019). It is worth noting that samples kept their integrity after the 7 days of immersion.

The values of degradation degree (DD) after 1, 3, 7, 11, 15, 18 and 21 days of immersion into PBS at 37 °C are presented in Figure 7.8. No significant mass loss ($p > 0.05$) was observed up to day 7. After 7 days, a pronounced increase of DD up to 25 % was observed, but samples kept their integrity, which indicates that the interactions between chitosan and pectin were strong enough. No significant differences ($p > 0.05$) were observed between days 7 and 18, at which an increase of DD and a mass loss of 43 % were observed.

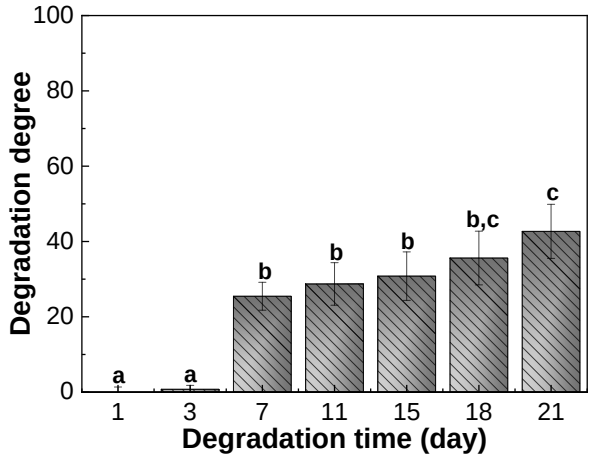

Figure 7.8. Degradation degree of CHI2PEC2 films immersed into PBS at 37 °C.

7.4.3.2. Film structure and mechanical properties

Since the hydrogel will be hydrated in the *in vivo* milieu, the films were hydrated in a 100 % humidity environment for 48 h before the test

was carried out. Stress-strain curves for CHI2PEC2 samples are shown in Figure 7.9a. As can be observed, a linear elastic behavior is observed up to 80 % of strain. There was no significant difference ($p > 0.05$) among different samples, and an average stress of 0.002 ± 0.001, 0.008 ± 0.003 and 0.14 ± 0.02 MPa was determined for a strain of 10 %, 20 % and 80 %, respectively. Furthermore, as can be observed for sample 2 in Figure 7.9b,films maintained their shape and size after a cycle of 5 compression sweeps.

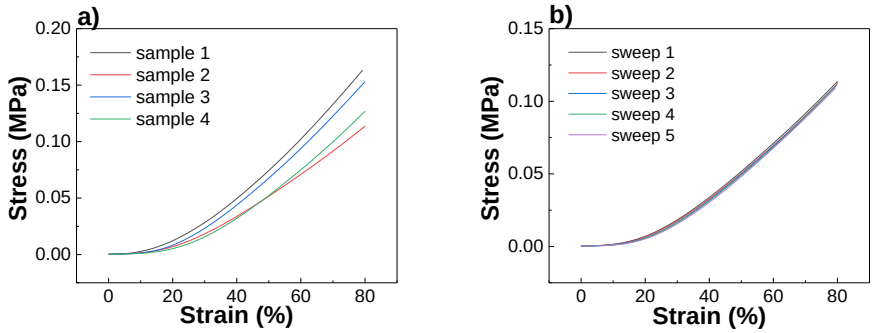

Figure 7.9. Stress-strain curves: a) for four samples of CHI2PEC2 films; b) for the sample 2 subjected to a cycle of 5 compression sweeps.

SEM analysis was performed in order to evaluate the film morphology and SEM images are shown in Figure 7.10, where cross-sections with a magnification of x1000 and x4500 are presented. As can be observed, the film showed a homogeneous structure in which different layers can be differentiated.

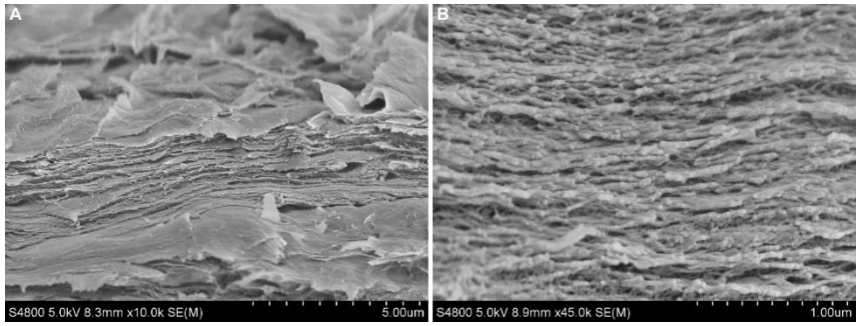

(**a**) (**b**)

Figure 7.10.SEM images of CHI2PEC2 cross-section: a) x1000 magnification and b) x4500 magnification.

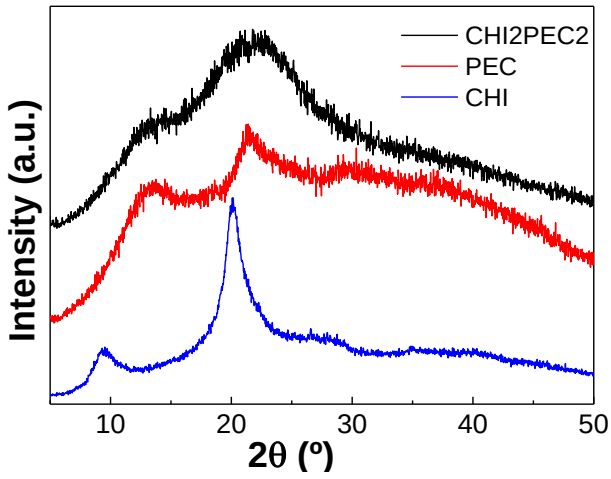

Figure 7.11. XRD diffractograms of neat chitosan (CHI), neat pectin (PEC), and CHI2PEC2 film.

Additionally, XRD measurements plotted in Figure 7.11 showed the two characteristic peaks of chitosan at 9.5° and 20.1°, and three peaks at 13.5°, 21.3° and 30° for pectin, all of them related to the semicrystalline structure of these polysaccharides (Zarandona et al., 2020). Concerning the CHI2PEC2 film, two broad peaks were observed at 13.5° and 21.8°,

revealing an amorphous structure due to the intermolecular hydrogen bonding and electrostatic interactions between chitosan and pectin (Soubhagya, Moorthi & Prabaharan, 2020).

7.5. Conclusions

Rheological analysis of hydrogels with different concentrations of chitosan and pectin was performed in order to select the optimal composition to be 3D printed and obtain dimensionally stable films. Chitosan-pectin systems showed a weak gel behavior with shear thinning flow properties. Furthermore, they showed favorable properties for 3D printing, keeping geometry and mechanical integrity after being printed at room or physiological temperatures. However, systems with high concentration of pectin presented aggregation; therefore, CHI2PEC2 hydrogel was selected as the optimal system for 3D printing. CHI2PEC2 exhibited physical interactions between chitosan and pectin, as shown by FTIR analysis, and high cohesiveness, related to the capacity of keeping shape and size after 3D printing. Likewise, high mucoadhesiveness was observed and related to the hydrogen bonding and the electrostatic interactions of chitosan and pectin with mucin. CHI2PEC2 film presents a homogeneous morphology, as shown by the SEM images of cross-

sections, and an amorphous structure revealed by XRD analysis. Furthermore, the film exhibited good properties for biomedical applications such as wound dressing since it showed a high swelling capacity, suitable for wound exudate absorption, and high strength to maintain shape and size after a cycle of compression sweeps.

Chapter

8

Pectin-chitosan films with Fe_3O_4 nanoparticles: Magnetic and electric capacity

8.1. Summary

In this chapter, chitosan-pectin films with Fe_3O_4 magnetic nanoparticles were prepared by solution casting. FTIR spectra indicated physical interactions between the matrix and nanoparticles, corroborated by DSC results. In addition, thermal characterization suggested that the interactions between chitosan, pectin and the nanoparticles resulted in a less compact structure, which influenced the mechanical properties. Regarding vibrating-sample magnetometry (VSM) and electrical analysis, chitosan-pectin films with Fe_3O_4 nanoparticles showed ferromagnetic behavior, with a dielectric constant increase as the nanoparticle concentration increased. Furthermore, films had antimicrobial activity against *Escherichia coli* (Gram -) and *Staphylococcus epidermidis* (Gram +) bacteria. Therefore, chitosan-pectin films with Fe_3O_4 magnetic nanoparticles showed promising results for active and intelligent food packaging applications.

8.2. Introduction

Packaging technologies are in continuous evolution seeking to improve the quality and freshness of food and prolonging its shelf life (Magnaghi et al., 2022). In this sense, chitosan and pectin could be suitable

materials for intelligent packaging films, since both polysaccharides are pH dependent. Under low pH conditions, positively charged chitosan and negatively charged pectin bind via ionic interactions forming a polyelectrolyte complex, resulting in an enhancement of the mechanical properties and hydrophilicity over the chitosan and pectin matrices separately (Torpol et al., 2019; Tsai et al., 2014). Few papers have reported the use of chitosan-pectin matrix for food packaging, among them, Maciel et al. (2015) prepared chitosan-pectin films with anthocyanin as a pH indicator device for intelligent food packaging, and Niu et al. (2021) added *Streptomyces coelicolor*, which improved CO_2 barrier properties of the film.

Besides the natural biopolymers, smart packaging that prolongs shelf life and provides current information about the state of the product is also gaining attention. The so-called intelligent packaging can monitor physical, chemical or biological status of the food items by detectors and sensors, from the beginning of the food supply chain until it reach to the market, giving information about the food quality and internal environment conditions of the package (Chausali, Saxena & Prasad, 2022; Pirsa, Sani & Mirtalebi, 2022). Thus, intelligent packaging can provide information of the *in situ* conditions of the food quality and freshness,

leading to a loss of dependency on food expiry dates. In this regard, metal oxides nanoparticles have a great potential for applications in food industry because of their antibacterial capacity, non-toxicity, oxygen and ethylene scavenging, and thermal stability properties (Nikolic et al., 2021). Indeed, metal oxides show sensing properties by the mechanism of adsorption and desorption with different gaseous compounds on the surface of the material, leading to changes in the electrical conductance (Galstyan et al., 2018). In this regard, Fe_3O_4 nanoparticles (NP) have been applied in many fields, such as biomedicine, cosmetics and food preservation due to its antimicrobial activity, magnetic, biocompatible and non-toxic properties (Appu et al., 2021; Yeamsuksawat, Zhao & Liang, 2021). For food applications, Fe_3O_4 nanoparticles have been used as sensors for detecting different compounds, such as heavy metals (Wu et al., 2019), caffeic acid (Abdi et al., 2020) or foodborne spoilage bacteria (Zhang et al., 2015).

In this context, the aim of the present chapter was to prepare chitosan-pectin films with Fe_3O_4 nanoparticles by solution casting. In order to assess the effect of different concentrations of Fe_3O_4 NP on the

chitosan-pectin matrix, physicochemical, thermal, structural, magnetic, electric and antimicrobial properties were measured.

8.3. Materials and methods

8.3.1. Materials

Chitosan with a molecular weight of 375 kDa and a deacetylation degree ≥ 75 % was supplied by Sigma-Aldrich, Spain. High methoxylated pectin, with a molecular weight of 472 kDa and an esterification degree of 58 %, was kindly supplied by CEAMSA, Spain. Iron oxide nanopowder (Fe_3O_4), with 50 - 100 nm size and a purification degree of 97 %, was supplied by Nanostructured & Amorphous Materials, Inc., USA. Acetic acid solution (1 N), used as solvent, was supplied by Panreac, Spain.

8.3.2. Film preparation

Chitosan-pectin films with Fe_3O_4 nanoparticles were processed by solution casting. The polymers were dissolved separately; on the one hand, the required amount of chitosan was dissolved in 1 wt % acetic acid solution by stirring for 30 min. On the other hand, Fe_3O_4 nanoparticles were dispersed in a 0.1 wt % aqueous solution of Triton 100-X by sonication for 3 h. Then, the required amount of pectin was added to the

NP aqueous solution and stirred at 67 °C. Both solutions were mixed at 8000 rpm for 10 min (Ultraturrax UT25, IKA, Germany), and air bobbles were removed by vacuum. The mixturewas placed in a petri dish to dry at room temperature. Mixture compositions are shown in Table 8.1.

Table 8.1. Composition of chitosan-pectin films with different contents of Fe_3O_4 nanoparticles.

System designation	Chitosan concentration (wt %)	Pectin concentration (wt %)	NP concentration (wt %)
Control	50.00	50.00	0
0.1NP	49.95	49.95	0.1
0.5NP	49.75	49.75	0.5
1NP	49.50	49.50	1
5NP	47.50	47.50	5
10NP	45.00	45.00	10

8.3.3. Film characterization

8.3.3.1. Fourier transform infrared (FTIR) spectroscopy

An Alpha II spectrometer (Bruker, Madrid, Spain), with a Platinum ATR accessory, was used to collect FTIR spectra of chitosan-pectin films with Fe_3O_4 nanoparticles. A total of 32 scans were performed with a resolution of 4 cm^{-1} in the wavelength between 4000 and 800 cm^{-1}.

8.3.3.2. Thermo-gravimetric analysis (TGA)

A Mettler Toledo TGA/SDTA 851 thermo-balance was used to measure the thermal stability of the samples. Dynamic scans from 25 to 900 °C were carried out at a constant rate of 10 °C/min under nitrogen atmosphere to avoid thermo-oxidative reactions.

8.3.3.3. Differential scanning calorimetry (DSC)

A Mettler Toledo DSC 822 was used to perform differential scanning calorimetry. Samples of around 3 mg were heated from -50 °C to 300 °C at a heating rate of 10 °C/min under nitrogen atmosphere to avoid oxidative reactions.

8.3.3.4. Scanning electron microscopy (SEM)

Morphology was examined by using a Hitachi S-4800 scanning electron microscope at an accelerating voltage of 15 kV. Before analysis, fractured surfaces were coated with a gold layer by sputtering with a Polaron SC502 apparatus.

Additionally, scanning electron microscopy/Energy-dispersive X-ray spectroscopy (SEM/EDX) was used to analyze the particle distribution on the samples with a Hitachi TM3000 Tabletop Microscope.).

8.3.3.5. Mechanical properties

Mechanical properties were measured with an Instron 5967 electromechanical testing system (Instron, Spain). According to ASTM D638-14 (ASTM, 2014), tests were carried out with a load cell of 500 N and a crosshead rate of 1 mm/min. Films were cut into bone shaped samples of 4.75 mm x 22.25 mm. Five samples were measured for each system. Tensile strength (TS), elongation at break (EAB) and elastic modulus (E) were measured.

8.3.3.6. Vibrating-sample magnetometry (VSM)

The magnetic properties of the films were analyzed with a MicroSense EZ7 VSM from -1.8 to 1.8 T at room temperature. The results were represented in a hysteresis loop, and remanence (M_r), magnetization saturation (M_s) and coercive field (H_c) parameters were obtained.

8.3.3.7. Electrical characterization

For the electric measurements, circular gold electrodes of 5 mm diameter were used by magnetron sputtering with a Polaron Coater SC502 onto both sides of each sample.

The electrical conductivity of the films was obtained by a 2-wire method, measured through a Keithley 487 picoammeter/voltage source with a ±10 V voltage, and the conductivity of the films (σ) was calculated by:

$$\sigma = \frac{d}{R.A}$$

where R is the resistance of the film obtained from the slope of the I–V curves, d is thickness, and A is the electrode area.

Dielectric measurements were performed using a Quadtech 1920 LCR precision meter. The capacitance (C) and the dielectric losses (tan δ) were obtained at room temperature in the frequency range of 20 Hz to 1 MHz with an applied voltage of 0.5 V. The error associated to the dielectric measurements was ~2%.

The real (ε') part of the dielectric function was calculated as:

$$\varepsilon' = \frac{C \cdot d}{\varepsilon_0 \cdot A}$$

where C is the individual sample capacity, ε_0 is the permittivity of vacuum (8.85×10^{-12} F·m^{-1}), A is the electrode area and d is the film thickness.

The real part of the conductivity of the dielectric material can be calculated from the dielectric measurements as follows:

$$\sigma'(\omega) = \varepsilon_0 \omega \varepsilon''(\omega)$$

where ε_0 is the permittivity of free space, $\omega = 2\pi f$ is the angular frequency and $\varepsilon''(\omega) = \varepsilon' \tan\delta$ is the frequency dependent imaginary part of the dielectric permittivity.

8.3.3.8. Antimicrobial analysis

To determine the inhibition capacity of films, two food pathogen were tested: the Gram-negative bacteria *Escherichia coli* and the Gram-positive bacteria *Staphylococcus epidermidis*. The bacterial pre-inoculum was prepared by using a colony from the corresponding stock and resuspended in nutrient broth (NB). After incubating overnight at 37 °C and 200 rpm, the pre-inoculum was centrifuged and the pellet was resuspended in 0.9 % NaCl aqueous solution. The optical density (OD_{600}) was measured and adjusted to 0.28 and 0.36 for *E. coli* and *S. epidermidis*, respectively.

Samples were cut in circular pieces of 10 mm diameter, placed into falcons and sterilized with ultraviolet light for 30 min. Then, 2 mL of the

final bacterial suspension was added and came into contact with the films for 2 h at 37 °C and 200 rpm. Falcons without sample were used as controls for bacterial growth.

The antimicrobial activity was tested using the colony-forming units (CFUs) assay. Ten-fold serial dilutions of the bacterial cultures of the falcons were carried out in 0.9 % NaCl aqueous solution. A volume of 10 μL was placed on spread plates of NB and colony-forming units per milliliter ($CFU \cdot mL^{-1}$) count was carried out after incubating the plates at 37 °C for 24 h. Antimicrobial activity was determined by comparing viable bacteria of each system with that incubated without any film.

8.3.4. Statistical analysis

With the purpose of determining the significant differences between measurements, analysis of variance (ANOVA) was carried out by means of SPSS software (SPSS Statictic 25.0). Tukey's multiple range test was used for multiple comparisons among different systems with a statistical significance at the $p < 0.05$ level.

8.4. Results and discussion

8.4.1. FTIR analysis

In order to evaluate the interactions among the components of the films, FTIR analysis was carried out and the spectra are shown in Figure 8.1. In control film, the characteristic bands of chitosan and pectin were observed. Among the absorption bands that chitosan and pectin share, we can found the band at 3247 cm^{-1}, associated to O-H bonds in both polymers and to N-H bonds in chitosan. Moreover, the absorption band assigned to chitosan and pectin C=O stretching bond was observed at 1633 cm^{-1}. Likewise, the bands attributed to the C-H stretching vibration and to the C-O-C of the saccharide ring of chitosan and pectin were observed between 2925 and 2850 cm^{-1} and 1150 and 890 cm^{-1}, respectively. Regarding to chitosan, the representative bands were showed at 1552 cm^{-1}, 1406 cm^{-1} and 1377 cm^{-1} corresponding to C=O stretching, NH_2 bending and CH_3 deformation. For pectin, the band associated to C=O ester bonds was observed at 1742 cm^{-1}. As observed in the previous chapter, the interactions between chitosan and pectin were physical since the bands related to C=O stretching of chitosan and pectin at 1633 cm^{-1} and to the ester bond of pectin at 1742 cm^{-1} were displaced (Zarandona et al., 2021).

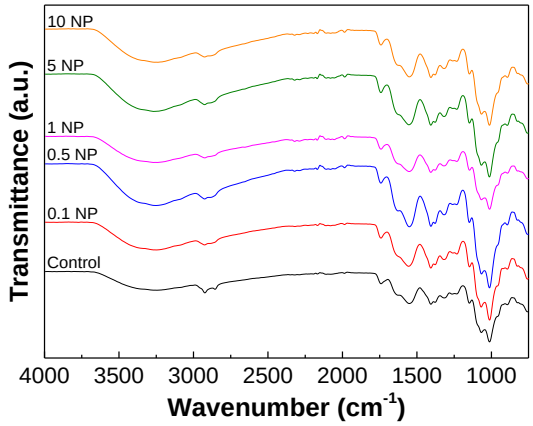

Figure 8.1. FTIR spectra of chitosan-pectin films without Fe_3O_4 nanoparticles (Control) and with different contents of Fe_3O_4 nanoparticles.

Respecting to Fe_3O_4 nanoparticles addition, some bands displacement were observed. In particular, O-H and N-H vibration band shifted to higher wavenumbers as the nanoparticle concentration increased, from 3247 cm^{-1} for control films up to 3263 cm^{-1} for 10NP. Moreover, the band associated to C-H stretching vibrations at 2853 cm^{-1} shifted to higher wavenumbers becoming a shoulder of the band at 2923 cm^{-1}. All these band displacements indicated that Fe_3O_4 nanoparticles interacted physically with chitosan-pectin matrix.

8.4.2. Thermal characterization

Thermo-gravimetric analysis (TGA) and differential scanning calorimetry (DSC) analysis were carried out in order to determine the

thermal stability of the material. Concerning TGA, derivative thermo-gravimetric curves and weight loss curves are presented in Figure 8.2a and b. Regarding neat chitosan and pectin samples (Figure 8.2a), thermal degradation was observed at 300 °C and 240 °C, respectively. For control films, 4 inflexion points were presented. The first one was observed around 68 °C, related to the water evaporation due to the moisture. The second inflection point, around 230 °C, was the greatest one and it was related to the thermal degradation of chitosan and pectin polymers. It should be noted that the thermal degradation of chitosan-pectin film happened at lower temperature than that of pure pectin and pure chitosan. This event could indicate that the ionic bonding between chitosan and pectin led to structure changes in the material (Maciel, Yoshida, & Franco, 2015). The third inflection peak was a shoulder at 283 °C, related to the chitosan that was not bonded to pectin. Finally, a slight inflection point was observed at 447 °C, related to the decomposition by-products. The addition of Fe_3O_4 nanoparticles (Figure 8.2b) caused the presence of a new inflection peak around 680 °C, which became more intense as the concentration of NP increased.

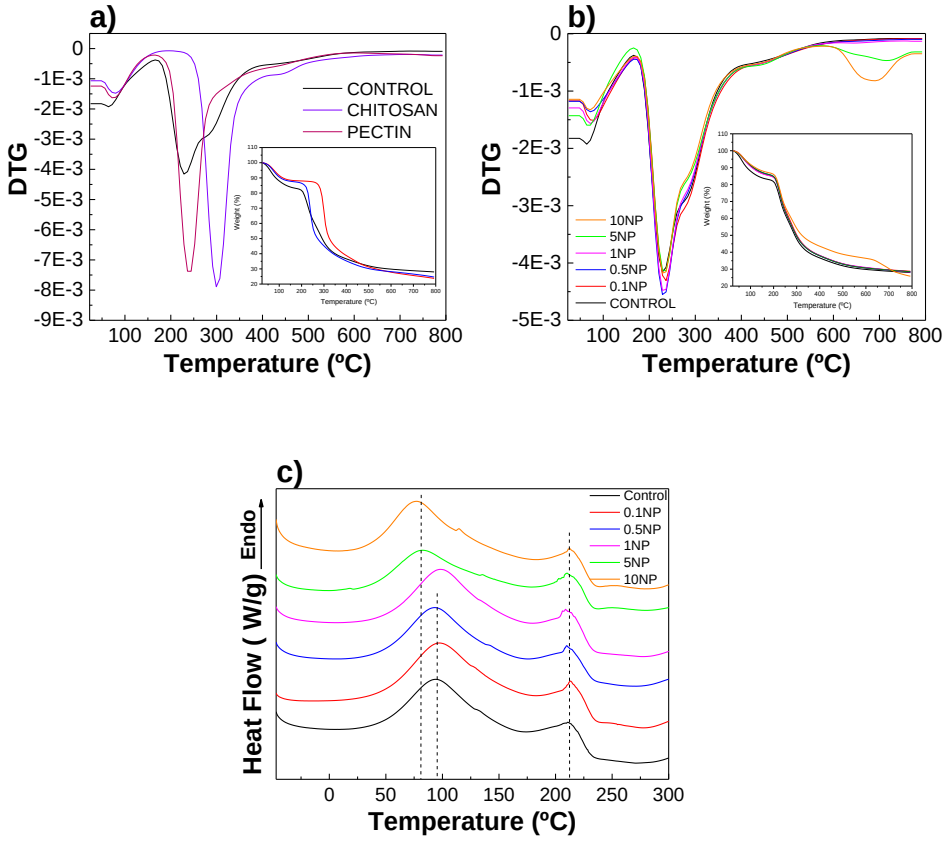

Figure 8.2. TGA of a) neat chitosan, neat pectin and control film and a) chitosan-pectin films without Fe_3O_4 nanoparticles (control) and with different contents of Fe_3O_4 nanoparticles. c) DSC analysis of chitosan-pectin films without Fe_3O_4 nanoparticles (control) and with different contents of Fe_3O_4 nanoparticles.

The endothermic peaks for the DSC thermogram of chitosan-pectin systems with Fe_3O_4 NP are shown in Figure 8.2c. Two endothermic peaks were observed for control films: the first, at 94 °C, was attributed to the film moisture, and the second, at 211 °C, was related to the entrapped water linked by hydrogen bonding with the polar groups of the

biopolymers (Pasini-Cabello et al., 2017). Regarding the films with nanoaparticles, the same endothermic peaks were observed as for the control sample, although for the samples with higher concentration of nanoparticles, 5NP and 10NP, the peak at 94 °C for control sample was shifted to lower temperatures, 82 °C and 76 °C, respectively. This displacement indicated that there were interactions between the matrix and the NP, as observed by FTIR. In addition, the shift to lower temperatures would indicate that the structure formed was less compact and, therefore, would require less energy to release the moisture.

8.4.3. Structure and mechanical properties

Morphology of the films was analyzed by SEM and the cross-section of the samples is showed in Figure 8.3. Control film presented a homogeneous structure, indicating the compatibility between chitosan and pectin. When Fe_3O_4 nanoparticles were added at low concentrations, the structure of the films remains homogeneous but, as NP concentration increased, especially for 5NP and 10NP samples, nanoparticle aggregations were observed. In particular, the nanoparticle clustering in 10NP films was bigger than in 5NP films. These results explain the

temperature decrease observed by DSC analysis, since the nanoparticle aggregations led to a less compact structure.

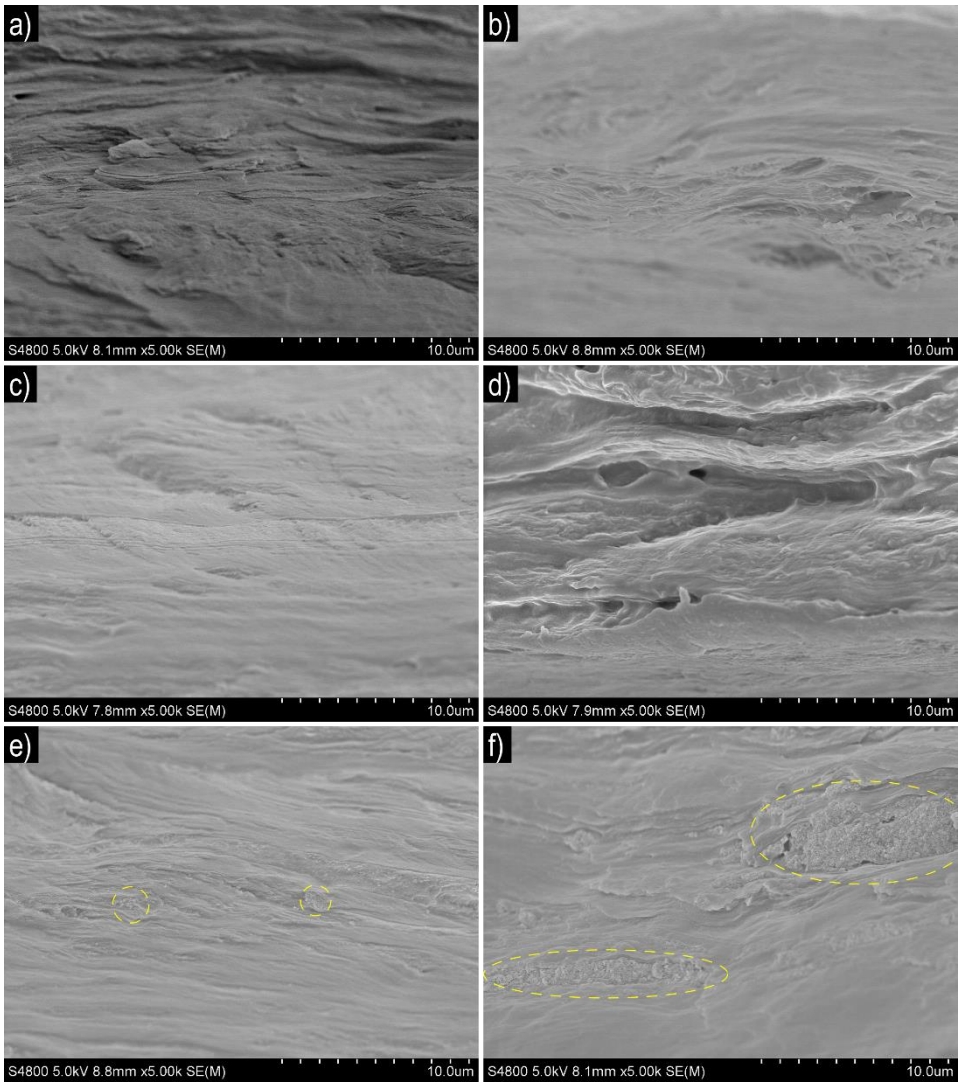

Figure 8.3. SEM images of chitosan-pectin film cross-section: a) control (0% Fe_3O_4), b) 0.1NP (0.1 % Fe_3O_4), c) 0.5NP (0.5 % Fe_3O_4), d) 1NP (1 % Fe_3O_4), e) 5NP (5 % Fe_3O_4) and, f) 10NP (10 % Fe_3O_4). Yellow dashed circles indicate nanoparticle aggregations.

The dispersion of iron on 1NP, 5NP and 10NP films surface was analyzed by SEM/EDX. As can be observed in Figure 8.4, the Fe signal in blue showed that the nanoparticles were homogeneously dispersed through the surface of the films.

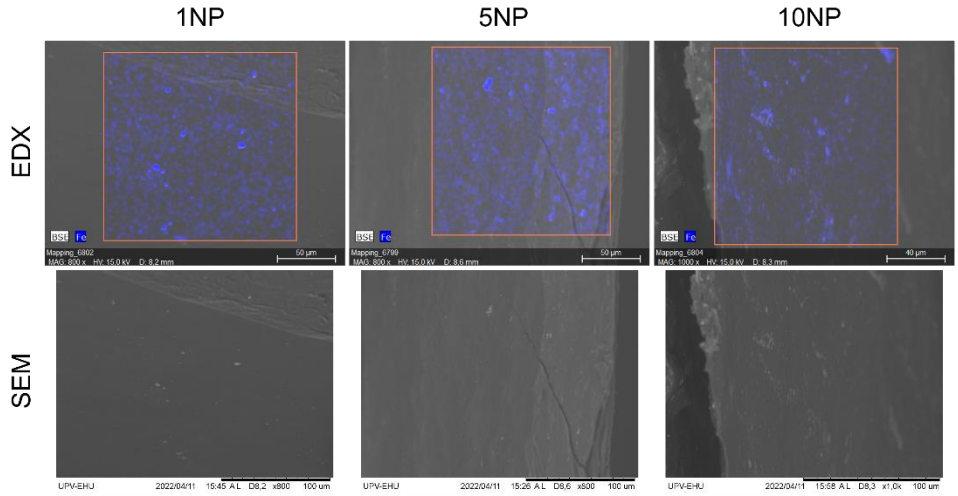

Figure 8.4. SEM/EDX images of the surface of chitosan-pectin films with 1 % Fe_3O_4 (1NP), 5 % Fe_3O_4 (5NP) and 10 % Fe_3O_4 (10NP).

Tensile strength (TS), elongation at break (EAB), and elastic modulus (E) of the films, shown in Table 8.2, have been measured in order to assess the influence of the magnetic nanoparticles on the chitosan-pectin matrix.

Regarding to control film, high values of TS were obtained, due to the strong intermolecular bonds between chitosan and pectin, which

derived into a compact structure. These values are higher than those found by other authors for chitosan-pectin films (Alakin et al., 2021). When the nanoparticles were added to the system, no significant differences ($p > 0.05$) were observed in EAB results. However, TS values decreased as the nanoparticles concentration increased, as well as E values for 5NP and 10NP, indicating the influence of nanoparticles for concentrations greater than 5 %. These results indicate that Fe_3O_4 nanoparticles affected the structure of the polymeric matrix, as observed in SEM images, hindering the interactions between chitosan and pectin chains (Salari et al., 2018).

Table 8.2. Tensile strength (TS), elongation at break (EAB) and elastic modulus (E) of chitosan-pectin films without Fe_3O_4 nanoparticles (Control) and with different contents of Fe_3O_4 nanoparticles.

Films	TS (MPa)	EAB (%)	E (MPa)
Control	47.0 ± 1.1^{a}	6.0 ± 0.5^{a}	2395 ± 52^{a}
0.1NP	43.7 ± 1.2^{b}	5.9 ± 0.2^{a}	2397 ± 18^{a}
0.5NP	43.9 ± 1.2^{b}	6.0 ± 0.6^{a}	2443 ± 27^{a}
1NP	44.0 ± 0.5^{b}	6.3 ± 0.8^{a}	2417 ± 40^{a}
5NP	40.7 ± 0.8^{c}	7.0 ± 0.5^{a}	2076 ± 58^{b}
10NP	40.1 ± 1.0^{c}	7.0 ± 0.7^{a}	2053 ± 46^{b}

[a-c]Two means followed by the same letter in the same column are not significantly ($p > 0.05$) different according to the Tukey's multiple range test.

8.4.4. Magnetic properties

Regarding magnetic properties, VSM analysis was carried out to obtain the hysteresis loops and calculate the remanence, the magnetization saturation, and the coercive field (Figure 8.5). The systems exhibited a ferromagnetic behavior, since the values of remanence and coercive field were unequal to zero (Venkateswarlu et al., 2015). As observed in Figure 8.3b, the magnetic behavior of the systems was dependent of the nanoparticle concentration. As the nanoparticle concentration increased, M_r values increased, from 0.23 emu/g (0.1NP) to 19.70 emu/g (10NP), as well as M_s values from 2.38 emu/g (0.1NP) to 206.11 emu/g (10NP). However, coercive field increased as nanoparticle concentration increased up to 0.5 % (50 Oe), and then, started to decrease until 41 Oe (10NP) as nanoparticle concentration increased. The coercive field is dependent on the nanoparticle size, as the size increases the coercivity increases until a critical particle size is reached, after which the coercivity decreases. Nevertheless, since the size of the nanoparticles in this study are the same for all samples, results may be related to the agglomeration of the nanoparticles, as described in previous works (Reinzabal et al., 2020)

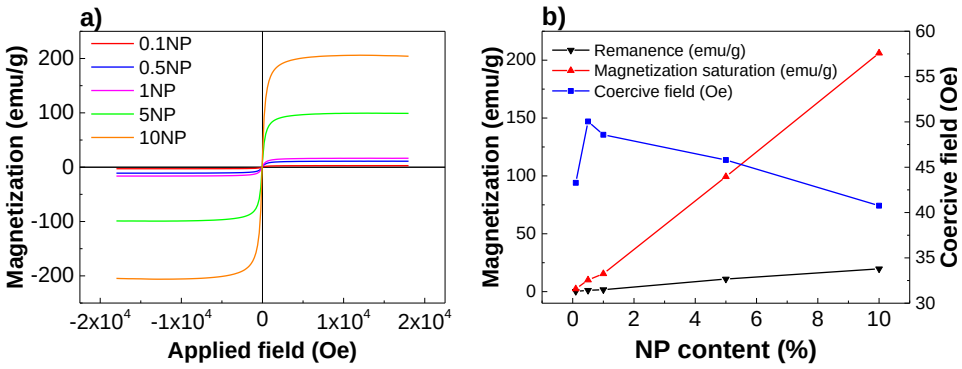

Figure 8.5. a) Hysteresis loops and b) magnetic properties (remanence, magnetization saturation, and coercive field) of chitosan-pectin films with Fe_3O_4 nanoparticles.

8.4.5. Electric characterization

Electrical conductivity of the films with Fe_3O_4 nanoparticles has been evaluated by performing I-V curves (Figure 8.6a). It can be observed that the I-V curves depend on the Fe_2O_3 content and follow Ohm's law.

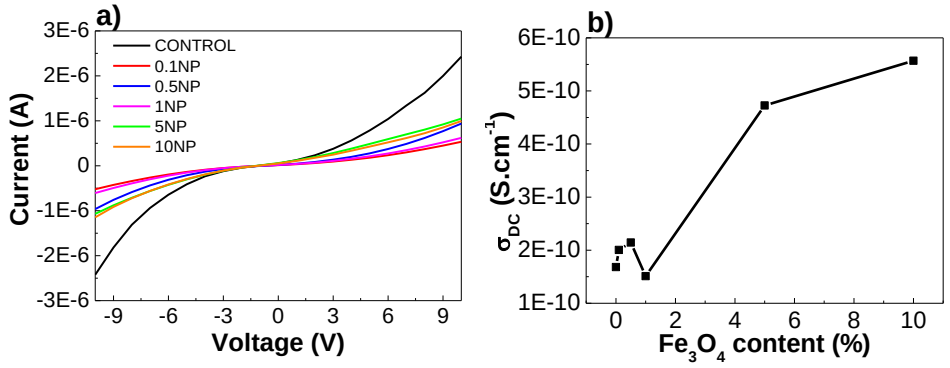

Figure 8.6. a) Current-voltage (*I-V*) curves and b) electrical conductivity value of films as a function of Fe_3O_4 content.

As can be observed in Figure 8.6b, the electrical conductivity increases strongly as a function of Fe_2O_3 content. The electrical conductivity of control film and film with 10 wt % Fe_3O_4 are $1.7x10^{-10}$ S·cm^{-1} and $5.6x10^{-12}$ S·cm^{-1}, respectively.This behavior is due to the fact that the addition of Fe_3O_4 nanoparticles increases the charge carriers where the conduction is assigned to the electron hopping.

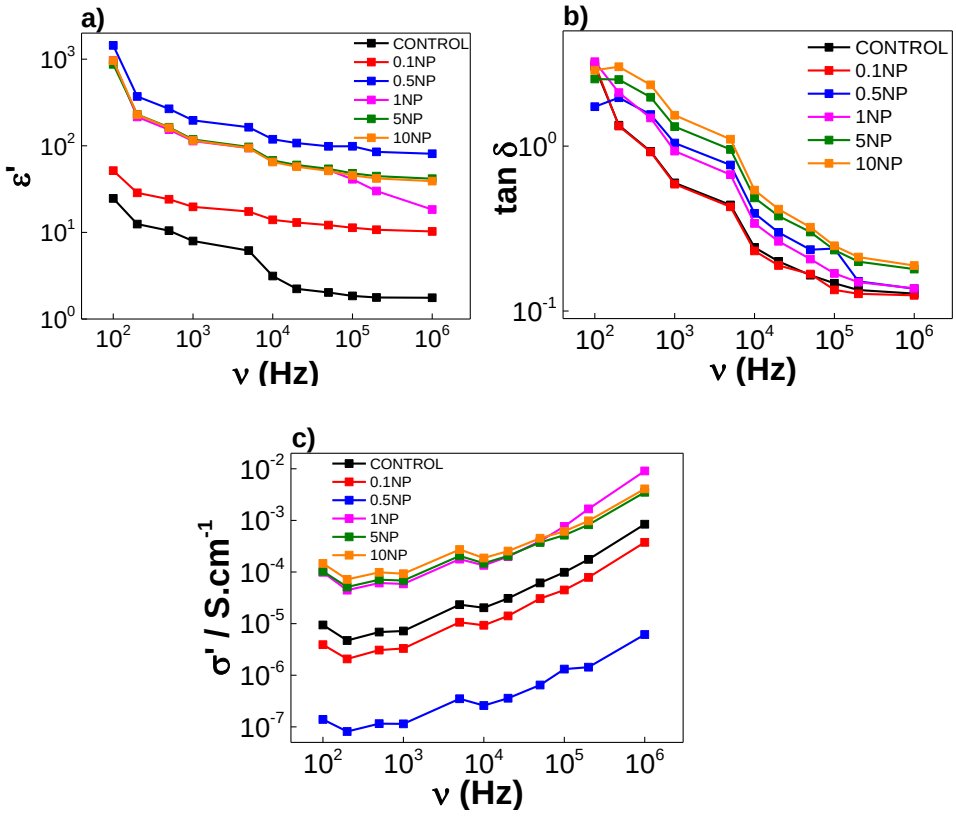

Figure 8.7. a) Real part of dielectric constant (ε´), b) dielectric losses (tan δ), and c) a.c. conductivity (σ´) of chitosan-pectin films with different contents of Fe_3O_4 nanoparticles.

Additionally, the dielectric analysis was evaluated and results are shown in Figure 8.7. The dielectric constant (Figure 8.7a) and tan δ (Figure 8.7b) depend on the frequency due to dipole relaxation. Regardless of frequency range, the dielectric constant and tan δ increase as a function of NP concentration due to polarization contributors derived from the addition of nanoparticles, mainly dominated by interfacial and spatial charge polarization. Concerning a.c. conductivity (Figure 8.7c), values increase with frequency, indicating the local contribution to the electrical conductivity. Regardless of frequency range, the addition of Fe_3O_4 nanoparticles increases the a.c. conductivity due to the charge carrier hopping.

8.4.6. Antimicrobial capacity

All films showed antimicrobial activity, as shown in Figure 8.8, although different response was observed for both bacteria. In the case of *S. epidermidis*, 10 NP films reached 43 % of inhibition, while 98 % was reached for for *E. coli*. The antimicrobial capacity of the films is driven by both chitosan and magnetic nanoparticles. The antimicrobial mechanism of chitosan is caused by the positive charge of the amino group of chitosan with the negative charges of cell membranes, affecting the loss of protein

and other intracellular components (Tuesta-Chavez et al., 2022). On the other hand, the antimicrobial effect of iron nanoparticles is related to the capacity of the nanoparticles to interact with the cell membrane and to penetrate inside the cells, causing membrane damage and inactivation of the bacteria (El-Khawaga et al., 2020). Therefore, chitosan-pectin films with Fe_3O_4 nanoparticles showed antibacterial activity due to the cooperative action of chitosan and Fe_3O_4 nanoparticles.

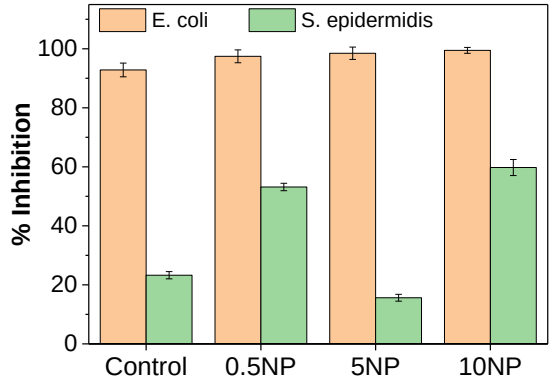

Figure 8.8. Inhibition capacity of chitosan-pectin films without Fe_3O_4 nanoparticles and with different contents of Fe_3O_4 nanoparticles against *E. coli* and *S. epidermidis* strains.

It is worth noting that Fe_3O_4 nanoparticles improved antimicrobial capacity when compared to control films. Additionally, it should be noted the difference in the inhibitory capacity of the films with respect to the two bacteria under study. This difference might be due to the different cell

walls of Gram-positive and Gram-negative bacteria. The cell wall of Gram-positive bacteria consists of an outer thick layer of peptidoglycan that acts as a layer of resistance against most inhibitory molecules, whereas the cell wall of Gram-negative bacteria has a thinner peptidoglycan layer (Salem et al., 2019).

8.5. Conclusions

The preparation of chitosan-pectin films with Fe_3O_4 magnetic nanoparticles by solution casting method led to homogeneous films. FTIR results indicated that the physical interactions between chitosan and pectin were not affected by the addition of the nanoparticles. However, the mechanical properties were influenced by Fe_3O_4 nanoparticles, due to the aggregation of the nanoparticles, as shown by SEM. The incorporation of nanoparticles also influenced the electrical, magnetic and antimicrobial properties. As the nanoparticle concentration increased, the dielectric constant, the remanence and the magnetization saturation increased. For the antimicrobial properties, the addition of the nanoaparticles increased the antimicrobial capacity of the films for pathogenic *Escherichia coli* (Gram-negative) and *Straphylococcus epidermidis* (Gram-positive) bacteria. Therefore, the incorporation of Fe_3O_4 nanoparticles into chitosan-pectin

films forming solutions could extend food shelf-life, besides functioning as a sensor for food packaging due to its electric and magnetic properties.

Chapter

9

General conclusions

In this chapter, the main conclusions of the doctoral thesis are summarized:

- EPS, valorized from natural materials from marine sources, showed good compatibility with chitosan, increasing the hydrophobic character and improving the mechanical properties of chitosan films.
- β-CD showed good capacity to form inclusion complex with 2-phenyl ethanol and it was effective avoiding the loss of bioactive during film preparation.
- The use of chitosan coatings with gallic acid led to the improvement of the shelf life of horse mackerel fillets during chilled storage, delaying microbial growth and the production of volatile amines, and becoming a promising material for active food packaging applications.
- Chitosan films were successfully processed by thermo-compression.
- The crosslinking reaction between the amino group of chitosan and the carboxyl group of citric acid led to compact films, with controlled release of *Aloe vera*.

- Chitosan-pectin hydrogels showed a weak gel behavior and shear thinning flow properties, favorable for 3D printing.
- 3D printed chitosan-pectin films were reproducible and preserved shape and size after a cycle of compression sweeps.
- The addition of Fe_3O_4 magnetic nanoparticles provided chitosan-pectin films with electrical, magnetic and antimicrobial properties, resulting in a promising material as a sensor for food quality monitoring and shelf life extension.

Chapter

10

References

Abdi, R., Ghorbani-HasanSaraei, A., Karimi-Maleh, H., Raeisi, S. N. & Karimi, F. (2020). Determining Caffeic Acid in Food Samples Using a Voltammetric Sensor Amplified by Fe_3O_4 Nanoparticles and Room Temperature Ionic Liquid. *International Journal of Electrochemical Science, 15*, 2539-2548. 10.20964/2020.03.30

Abid, M.; Cheikhrouhou, S.; Renard, C.M.G.C.; Bureau, S.; Cuvelier, G.; Attia, H. & Ayadi, M.A. (2017). Characterization of pectins extracted from pomegranate peel and their gelling properties. *Food Chemistry*, *215*, 318-325. https://doi.org/10.1016/j.foodchem.2016.07.181

Akalin, G.O., Oztuna Taner, O. & Taner, T. (2021). The preparation, characterization and antibacterial properties of chitosan/pectin silver nanoparticle films. *Polymer Bulletin*. https://doi.org/10.1007/s00289-021-03667-0

Ale, E.C.; Rojas, M.F.; Reinheimer, J.A. & Binetti, A.G. (2020). *Lactobacillus fermentum*: Could EPS production ability be responsible for functional properties? *Food Microbiology*, *90*, 103465. https://doi.org/10.1016/j.fm.2020.103465

Alemán, A., González, F., Arancibia, M.Y., López-Caballero, M.E., Montero, P. & Gómez-Guillén, M.C. (2016). Comparative study between film and coating packaging based on shrimp concentrate obtained from marine industrial waste for fish sausage preservation. *Food Control*, *70*, 325-332. https://doi.org/10.1016/j.foodcont.2016.06.007

Alishahi, A. & Aïder, M. (2012). Applications of Chitosan in the Seafood Industry and Aquaculture: A Review. *Food Bioprocess Technology, 5,* 817-830. https://doi.org/10.1007/s11947-011-0664-x

Al-Nabulsi, A., Osaili, T., Sawalha, A., Olaimat, A.N., Albiss, B.A., Mehyar, G., Ayyash, M. & Holley, R. (2020). Antimicrobial activity of chitosan coating containing ZnO nanoparticles against *E. coli* O157:H7 on the surface of white brined cheese. *International Journal of Food Microbiology, 334*, 108838. https://doi.org/10.1016/j.ijfoodmicro.2020.108838

Alsaggaf, M. S., Moussa, S. H., & Tayel, A. A. (2017). Application of fungal chitosan incorporated with pomegranate peelextract as edible coating for microbiological, chemical and sensorialquality enhancement of Nile tilapia fillets. *International Journal of Biological Macromolecules, 99,* 499-505. https://doi.org/10.1016/j.ijbiomac.2017.03.017

Al-Tayyar, N.A., Youssef, A.M. & Al-hindi, R. (2020). Antimicrobial food packaging based on sustainable Bio-based materials for reducing foodborne Pathogens: A review. *Food Chemistry, 310*, 125915. https://doi.org/10.1016/j.foodchem.2019.125915

Amato, A., Migneco, L.M., Martinelli, A., Pietrelli, L., Piozzi, A., & Francolini, I. (2018). Antimicrobial activity of catechol functionalized-chitosan versus *Staphylococcus epidermidis*. *Carbohydrate Polymers, 179*, 273-281. https://doi.org/10.1016/j.carbpol.2017.09.073

Amri, F., Husseinsyah, S., & Hussin, K. (2013). Mechanical, morphological and thermal properties of chitosan filled polypropylene composites: The

effect of binary modifying agents. *Composites Part A: Applied Science and Manufacturing*, *46*, 89-95. https://doi.org/10.1016/j.compositesa.2012.10.014

An, X., Kang, Y., & Li, G. (2019). The interaction between chitosan and tannic acid calculated based on the density functional theory. *Chemical Physics, 520,* 100-107. https://doi.org/10.1016/j.chemphys.2018.12.009

Andonegi, M., Las Heras, K., Santos-Vizcaíno, E., Igartua, M., Hernandez, R.M., de la Caba, K. & Guerrero, P. (2020). Structure-properties relationship of chitosan/collagen films with potential for biomedical applications. *Carbohydrate Polymers, 237*, 116159. https://doi.org/10.1016/j.carbpol.2020.116159

AOAC. In: Horwitz W, editor, Official methods of analysis of the Association of Official Analytical Chemists (17th ed.). Washington DC: AOAC; 2000.

Appu, M., Lian, Z., Zhao, D. & Huang, J. (2021). Biosynthesis of chitosan-coated iron oxide (Fe_3O_4) hybrid nanocomposites from leaf extracts of *Brassica oleracea* L. and study on their antibacterial potentials. *3 Biotech,11*, 271. https://doi.org/10.1007/s13205-021-02820-w

Arancibia, M.Y., Alemán, A., López-Caballero, M.E., Gómez-Guillén, M.C. & Montero, P. (2015b). Development of active films of chitosan isolated by mild extraction with added protein concentrate from shrimp waste. *Food Hydrocolloids*, *43*, 91-99. https://doi.org/10.1016/j.foodhyd.2014.05.006

Arancibia, M.Y., López-Caballero, M.E., Gómez-Guillén, M.C. & Montero, P. (2015a). Chitosan coatings enriched with active shrimp waste for shrimp

preservation. *Food Control*, *54*, 259-266. https://doi.org/10.1016/j.foodcont.2015.02.004

ASTM D 638-14 (2014). Standard test method for tensile properties of plastics. In *Annual book of ASTM standards*. Philadelphia, PA: American Society of Testing and Materials.

ASTM D523-18. (2018). Standard test method for specular gloss. In *Annual book of ATSM standards.* Philadelphia, PA: American Society for Testing and Materials.

ASTM E96-00. (2000). Standard test methods for water vapour transmission of material. *In Annual book of ASTM standards*. Philadelphia, PA: American Society for Testing and Materials.

Badawy, M.E.I., Lotfy, T.M.R. & Shawir, S.M.S. (2020). Facile synthesis and characterizations of antibacterial and antioxidant of chitosan monoterpene nanoparticles and their applications in preserving minced meat. *International Journal of Biological Macromolecules, 156*, 127-136. https://doi.org/10.1016/j.ijbiomac.2020.04.044

Bajer, D., Janczak, K. & Bajer, K. (2020). Novel Starch/Chitosan/Aloe Vera Composites as Promising Biopackaging Materials. *Journal of Polymers and the Environment, 28*, 1021-1039. https://doi.org/10.1007/s10924-020-01661-7

Balaji, A.N. & Nagarajan, K.J. (2017). Characterization of alkali treated and untreated new cellulosic fiberfrom Saharan aloe vera cactus leaves. *Carbohydrate Polymers, 174*, 200-208. https://doi.org/10.1016/j.carbpol.2017.06.065

Baniasadi, H.; Ajdary, R.; Trifol, J.; Rojas, O.J. & Seppälä, J. (2021). Direct ink writing of aloe vera/cellulose nanofibrils bio-hydrogels. *Carbohydrate Polymers*, *266*, 118114. https://doi.org/10.1016/j.carbpol.2021.118114

Barba, C., Eguinoa, A., & Maté, J. I. (2015). Preparation and characterization of ◎-cyclodextrin inclusion complexes as a tool of a controlled antimicrobial release in whey protein edible films. LWT-Food Science and Technology, 64, 1362-1369. https://doi.org/10.1016/j.lwt.2015.07.060

Barbosa, H.F.G., Francisco, D.S., Ferreira, A.P.G. & Cavalheiro, E.T.G. (2019). A new look towards the thermal decomposition of chitins and chitosans with different degrees of deacetylation by coupled TG-FTIR. *Carbohydrate Polymers, 225*, 115232. https://doi.org/10.1016/j.carbpol.2019.115232

Baron, R. D., Pérez, L. L., Salcedo, J. M., Córdoba, L. P., & Sobral P. J. A. (2017). Production and characterization of films based on blends of chitosan from blue crab (*Callinectes sapidus*) waste and pectin from Orange (*Citrus sinensis Osbeck*) peel. *International Journal of Biological Macromolecules, 98,* 676-683. https://doi.org/10.1016/j.ijbiomac.2017.02.004

Bealer, E.J., Onissema-Karimu, S., Rivera-Galletti, A., Francis, M., Wilkowski, J., Salas-de la Cruz D. & Hu, X. (2020). Protein-Polysaccharide Composite Materials: Fabrication and Applications. *Polymers, 12*, 464. https://doi.org/10.3390/polym12020464

Berger, J.; Reist, M.; Mayer, J.M.; Felt, O.; Peppas, N.A. & Gurny, R. (2004). Structure and interactions in covalently and ionically crosslinked chitosan

hydrogels for biomedical applications. *European Journal of Pharmaceutics and Biopharmaceutics*, *57*, 19-34. https://doi.org/10.1016/S0939-6411(03)00161-9

Bhattacharyya, A.; Janarthanan, G.; Tran, H.N.; Ham, H.J.; Yoon, J.H. & Noh, I. (2021). Bioink homogeneity control during 3D bioprinting of multicomponent micro/nanocomposite hydrogel for even tissue regeneration using novel twin screw extrusion system. *Chemical Engineering Journal*, *415*, 128971. https://doi.org/10.1016/j.cej.2021.128971

Binsi, P. K., Nayak, N., Sarkar, P. C., Sahu, U., Ninan, G. & Ravishankar, C. N. (2016). Comparative evaluation of gum arabic coating and vacuum packaging on chilled storage characteristics of Indian mackerel (*Rastrelliger kanagurta*). *Journal Food Scientist & Technologists*, *53(4)*, 1889-1898. https://doi.org/10.1007/s13197-015-2122-7

Birch, N.P.; Barney, L.E.; Pandres, E.; Peyton, S.R. & Schiffman, J.D. (2015). Thermal-Responsive Behavior of a Cell Compatible Chitosan/Pectin Hydrogel. *Biomacromolecules, 16*, 1837-1843. http://10.1021/acs.biomac.5b00425

Bøknæs, N., Østerberg, C., Nielsen, J. & Dalgaard, P. (2000). Influence of Freshness and Frozen Storage Temperature on Quality of Thawed Cod Fillets Stored in Modified Atmosphere Packaging. *LWT - Food Science and Technology*, *33(3)*, 244-248. https://doi.org/10.1006/fstl.2000.0634

Bonilla, F., Chouljenko, A., Reyes, V., Bechtel, P. J., King, J. M., & Sathivel, S. (2018). Impact of chitosan application technique on refrigerated catfish

fillet quality. *LWT-Food Science and Technology*, *90*, 277-282. https://doi.org/10.1016/j.lwt.2017.12.010

Božič, M., Gorgieva, S., & Kokol, V. (2012). Laccase-mediated functionalization of chitosan by caffeic and gallic acids for modulating antioxidant and antimicrobial properties. *Carbohydrate Polymers, 87(4),* 2388-2398. https://doi.org/10.1016/j.carbpol.2011.11.006

Brewer, M.S. (2011). Natural Antioxidants: Sources, Compounds, Mechanisms of Action, and Potential Applications. *Comprehensive Reviews in Food Science and Food Safety, 10(4),* 221-247. https://doi.org/10.1111/j.1541-4337.2011.00156.x

Bula, K., Klapiszewski, L., & Jesionowski, T. (2019). Effect of processing conditions and functional silica/lignin content on the properties of bio-based composite thin sheet films. *Polymer Testing*, *77*, 105911. https://doi.org/10.1016/j.polymertesting.2019.105911

Cai, L., Leng, L., Cao, A., Cheng, X., & Li, J. (2018). The effect of chitosan-essential oils complex coating on physicochemical, microbiological, and quality change of grass carp (*Ctenopharyhgodon idella*) fillets. *Journal of Food Safety*, *38*, 12399. https://doi.org/10.1111/jfs.12399

Calero, N.; Muñoz, J.; Ramírez, P. & Guerrero, A. (2010). Flow behaviour, linear viscoelasticity and surface properties of chitosan aqueous solutions. *Food Hydrocolloids*, *24*, 659-666. https://doi.org/10.1016/j.foodhyd.2010.03.009

Casadidio, C., Peregrina, D.V., Gigliobianco, M.R., Deng, S., Censi R. & Di Martino, P. (2019). Chitin and Chitosans: Characteristics, Eco-Friendly

Processes, and Applications in Cosmetic Science. *Marine Drugs, 17*, 369. https://doi.org/10.3390/md17060369

Castillo, L. A., Farenzena, S., Pintos, E., Rodríguez, M. S., Villar, M. A., García, M. A., & López, O. V. (2017). Active films based on thermoplastic corn starch and chitosan oligomer for food packaging applications. *Food Packaging and Shelf Life, 14*, 128-136. https://doi.org/10.1016/j.fpsl.2017.10.004

Cazón, P. & Vázquez, M. (2020) Mechanical and barrier properties of chitosan combined with other components as food packaging film. *Environmental Chemistry Letters, 18*, 257-267. https://doi.org/10.1007/s10311-019-00936-3

Cernencu, A.I.; Lungu, A.; Stancu, I.C.; Serafim, A.; Heggset, E.; Syverud, K. & Iovu, H. (2019). Bioinspired 3D printable pectin-nanocellulose ink formulations. *Carbohydrate Polymers*, *220*, 12-21. https://doi.org/10.1016/j.carbpol.2019.05.026

Cesco, C.T.; Valente, A.J.M. & Paulino, A.T. (2021). Methylene Blue Release from Chitosan/Pectin and Chitosan/DNA Blend Hydrogels. *Pharmaceutics, 13*, 842. https://doi.org/10.3390/pharmaceutics13060842

Chang, S.H., Chen C.H. & Tsai, G.J. (2020). Effects of Chitosan on *Clostridium perfringens* and Application in the Preservation of Pork Sausage. *Marine Drugs, 18*, 70. https://doi.org/10.3390/md18020070

Chang, X.L., Wang, C, Feng, Y. & Liu, Z. (2006). Effects of heat treatments on the stabilities of polysaccharides substances and barbaloin in gel juice

from *Aloe vera* Miller. *Journal of Food Engineering, 75(2)*, 245-251. https://doi.org/10.1016/j.jfoodeng.2005.04.026

Chanwitheesuk, A., Teerawutgulrag, A., Kilburn, J.D. & Rakariyatham, N. (2007). Antimicrobial gallic acid from Caesalpinia mimosoides Lamk. *Food Chemistry*, *100(3)*, 1044-1048. https://doi.org/10.1016/j.foodchem.2005.11.008

Charles, A.L., Abdillah, A.A., Saraswati, Y.R., Sridhar, K., Balderamos, C., Masithah, E.D. & Alamsjah, M.A. (2021). Characterization of freeze-dried microencapsulation tuna fish oil with arrowroot starch and maltodextrin. *Food Hydrocolloids, 112*, 106281. https://doi.org/10.1016/j.foodhyd.2020.106281

Charve, J. & Reineccius, G. A. (2009). Encapsulation Performance of Proteins and Traditional Materials for Spray Dried Flavors. Journal of Agricultural and Food Chemistry, 57(6), 2486-2492. https://doi.org/10.1021/jf803365t

Chausali, N., Saxena, J. & Prasad, R. (2022). Recent trends in nanotechnology applications of bio-based packaging. *Journal of Agriculture and Food Research, 7*, 100257. https://doi.org/10.1016/j.jafr.2021.100257

Chen, G., Ali, F., Dong, S., Yin, Z., Li, S., & Chen, Y. (2018). Preparation, characterization and functional evaluation of chitosan-based films with zein coatings produced by cold plasma. *Carbohydrate Polymers, 202,* 39-46. https://doi.org/10.1016/j.carbpol.2018.08.122

Chen, Q.J., Zhou, L.L., Zou, J.Q., & Gao, X. (2019). The preparation and characterization of nanocomposite film reinforced by modified cellulose

nanocrystals. *International Journal of Biological Macromolecules, 132(1)*, 1155-1162. https://doi.org/10.1016/j.ijbiomac.2019.04.063

Chen, X.; Yue, Z.; Winberg, P.C.; Dinoro, J.N.; Hayes, P.; Beirne, S. & Wallace, G.G. (2019). Development of rhamnose-rich hydrogels based on sulfated xylorhamno-uronic acid toward wound healing applications. *Biomaterials Science*, *7*, 3497. https://doi.org/10.1039/C9BM00480G

Chen, Y.; Zhang, J.G.; Sun, H.J. & Wei, Z.J. (2014). Pectin from Abelmoschus esculentus: Optimization of extraction and rheological properties. *International Journal of Biological Macromolecules*, *70*, 498-505. https://doi.org/10.1016/j.ijbiomac.2014.07.024

Crizel, T.M., Rios, A.O., Alves, V.D., Bandarra, N., Moldão-Martins, M., & Flôres, S.H. (2018). Biodegradable Films Based on Gelatin and Papaya Peel Microparticles with Antioxidant Properties. *Food Bioprocess Technology*, *11*, 536-550. https://doi.org/10.1007/s11947-017-2030-0

Croisiee, F. & Jérôme, C. (2013). Chitosan-based biomaterials for tissue engineering. *European Polymer Journal*, *49*, 780-792. https://doi.org/10.1016/j.eurpolymj.2012.12.009

da Rocha, M., Alemán, A., Romani, V. P., López-Caballero, M. E., Gómez-Guillén, M. C., Montero, P. & Prentice, C. (2018). Effects of agar films incorporated with fish protein hydrolysate or clove essential oil on flounder (*Paralichthys orbignyanus*) fillets shelf-life. *Food Hydrocolloids*, *81*, 351-363. https://doi.org/10.1016/j.foodhyd.2018.03.017

De Mey, E., De Maere, H., Paelinck, H. & Fraeye, I. (2015). Volatile N-nitrosamines in Meat Products: Potential Precursors, Influence of

Processing and Mitigation Strategies. *Critical Reviews in Food Science and Nutrition, 57(13),* 2909-2923. https://doi.org/10.1080/10408398.2015.1078769

de Oliveira, J.M.; Amaral, S.A. & Burkert, C.A.V. (2018). Rheological, textural and emulsifying properties of an exopolysaccharide produced by *Mesorhizobium loti* grown on a crude glycerol-based medium. *International Journal of Biological Macromolecules*, *120*, 2180-2187. https://doi.org/10.1016/j.ijbiomac.2018.06.158

de Souza, F.C.B.; de Souza, R.F.B.; Drouin, B.; Mantovani, D. & Moraes, Â.M. (2019). Phosphorylation of chitosan to improve osteoinduction of chitosan/xanthan-based scaffolds for periosteal tissue engineering *International Journal of Biological Macromolecules*, *132*, 178-189. https://doi.org/10.1016/j.ijbiomac.2019.12.004

Dehouche, N., Idres, C., Kaci, M., Zembouai, I. & Bruzaud, S. (2020). Effects of various surface treatments on Aloe Vera fibers used as reinforcement in poly(3-hydroxybutyrate-co-3-hydroxyhexanoate) (PHBHHx) biocomposites. *Polymer Degradation and Stability*, *175*, 109131. https://doi.org/10.1016/j.polymdegradstab.2020.109131

Delbarre-Ladrat, C.; Sinquin, C.; Lebellenger, L.; Zykwinska, A. & Colliec-Jouault, S. (2014). Exopolysaccharides produced by marine bacteria and their applications as glycosaminoglycan-like molecules. *Frontiers in Chemistry*, *2*, 85. https://doi.org/10.3389/fchem.2014.00085

Demir, D.; Ceylan, S.; Göktürk, D. & Bölgen, N. (2021). Extraction of pectin from albedo of lemon peels for preparation of tissue engineering scaffolds. *Polymer Bulletin*, *78*, 2211-2226. https://doi.org/10.1007/s00289-020-03208-1

Deshmukh, A.R., Aloui, H., Khomlaem, C., Negi, A., Yun, J.-H., Kim, H.-S. & Kim, B.S. (2021). Biodegradable films based on chitosan and defatted *Chlorella* biomass: Functional and physical characterization. *Food Chemistry*, *337*, 127777. https://doi.org/10.1016/j.foodchem.2020.127777

Di Filippo, M.F.; Panzavolta, S.; Albertini, B.; Bonvicini, F.; Gentilomi, G.A.; Ramona Orlacchio, R.; Passerini, N.; Bigi, A. & Dolci, L.S. (2020). Functional properties of chitosan films modified by snail mucus extract. *International Journal of Biological Macromolecules*, *143*, 126-135. https://doi.org/10.1016/j.ijbiomac.2019.11.230

Ebadi, Z., Khodanazary, A., Hosseini, S.M., & Zanguee, N. (2019). The shelf life extension of refrigerated *Nemipterus japonicus* fillets by chitosan coating incorporated with propolis extract. *International Journal of Biological Macromolecules*, *139*, 94-102. https://doi.org/10.1016/j.ijbiomac.2019.07.204

El Knidri, H., El Khalfaouy, R., Laajeb, A., Addaou, A., & Lahsini, A. (2016). Eco-friendly extraction and characterization of chitin and chitosan from the shrimp shell waste via microwave irradiation. *Process Safety and Environmental Protection*, *104*, 395-405. https://doi.org/10.1016/j.psep.2016.09.020

El-hamahmy, M. A. M., ElSayed, A. I., & Odero, D. C. (2017). Physiological effects of hot water dipping, chitosan coating and gibberellic acid on shelf-life and quality assurance of sugar snap peas (*Pisum sativum* L. var.

macrocarpon). *Food Packaging and Shelf Life*, *11*, 58-66. https://doi.org/10.1016/j.fpsl.2016.12.002

El-Khawaga, A.M.; Farrag, A.A.; Elsayed, M.A.; El-Sayyad, G.S. & El-Batal, A.I. (2021). Antimicrobial and Photocatalytic Degradation Activities of Chitosan-coated Magnetite Nanocomposite. *Journal of Cluster Science, 32,* 1107-1119. https://doi.org/10.1007/s10876-020-01869-6

Estupiñán, M.; Hernández, I.; Saitua, E.; Bilbao, M.E.; Mendibil, I.; Ferrer, J. & Alonso-Sáez, L. (2020). Novel *Vibrio* spp. strains producing omega-3 fatty acids isolated from coastal seawater. *Marine Drugs*, *18*(2), 99. https://doi.org/10.3390/md18020099

Etxabide, A., Coma, V., Guerrero, P., Gardrat, C., & de la Caba, K. (2017). Effect of cross-linking in surface properties and antioxidant activity of gelatin films incorporated with a curcumin derivative. *Food Hydrocolloids, 66,* 168-175. https://doi.org/10.1016/j.foodhyd.2016.11.036

EUR-Lex-32005R2074, 2005. Commission Regulation (EC) No 2074/2005 of 5 December 2005. https://eur-lex.europa.eu/eli/reg/2005/2074/oj Accessed on 15 April 2022.

Ezquerra-Brauer, J. M., Miranda, J. M., Cepeda, A., Barros-Velázquez, J., & Aubourg, S. P. (2016). Effect of jumbo squid (*Dosidicus gigas*) skin extract on the microbial activity in chilled mackerel (*Scomber scombrus*). *LWT - Food Science and Technology 72,* 134-140. https://doi.org/10.1016/j.lwt.2016.04.024

Fernández-Pan, I., Maté, J.I., Gardrat, C. & Coma, V. (2015). Effect of chitosan molecular weight on the antimicrobial activity and release rate of

carvacrol-enriched films. Food Hydrocolloids, 51, 60-68. https://doi.org/10.1016/j.foodhyd.2015.04.033

Finore, I.; Di Donato, P.; Mastascusa, V.; Nicolaus, B. & Poli, A. (2014). Fermentation technologies for the optimization of marine microbial exopolysaccharide production. *Marine Drugs*, *12*, 3005–3024. https://doi.org/10.3390/md12053005

Fischetti, T.; Celikkin, N.; Negrini, N.C.; Farè, S. & Swieszkowski, W. (2020). Tripolyphosphate-Crosslinked Chitosan/Gelatin Biocomposite Ink for 3D Printing of Uniaxial Scaffolds *Frontiers in Bioengineering and Biotechnology*, *8*, 400. https://doi.org/10.3389/fbioe.2020.00400

Flórez, M., Guerra-Rodríguez, E., Cazón, P. & Vázquez, M. (2022). Chitosan for food packaging: Recent advances in active and intelligent films. *Food Hydrocolloids*, *124*, 107328. https://doi.org/10.1016/j.foodhyd.2021.107328

Freeman, D. J., Falkiner, F. R. & Keane, C. T. (1989). New method for detecting slime production by coagulase negative staphylococci. Journal of Clinical Pathology, 42, 872-874. 10.1136/jcp.42.8.872

Galstyan, V., Bhandari, M. P., Sberveglieri, V., Sberveglieri, G. & Comini, E. (2018). Metal Oxide Nanostructures in Food Applications: Quality Control and Packaging. *Chemosensors*, *6*, 16. https://doi.org/10.3390/chemosensors6020016

Galvis-Sánchez, A. C., Castro, M. C. R., Biernacki, K., Gonçalves, M. P., & Souza, H. K. S. (2018). Natural deep eutectic solvents as green plasticizers for chitosan thermoplastic production with controlled/desired mechanical

and barrier properties. *Food Hydrocolloids, 82*, 478-489. https://doi.org/10.1016/j.foodhyd.2018.04.026

García-Martínez, J.; Acinas, S.G.; Massana, R. & Rodriguez-Valera, F. (2002). Prevalence and microdiversity of *Alteromonas macleodii*-like microorganisms in different oceanic regions. *Environmental Microbiology*, *4(1)*, 42-50. https://doi.org/10.1046/j.1462-2920.2002.00255.x

Gawish, S.M., Abo El-Ola, S.M., Ramadan, A.M & Abou El-Kheir, A.A. (2012). Citric acid used as a crosslinking agent for the grafting of chitosan onto woolen fabric. *Journal of Applied Polymer Science*, 123, 3345-3353. https://doi.org/10.1002/app.33873

Gerschenson, L.N.; Fissore, E.N.; Rojas, A.M.; Encalada, A.M.I.; Zukowski, E.F. & Coelho, R.A.H. (2021). Pectins obtained by ultrasound from agroindustrial by-products. *Food Hydrocolloids*, *118*, 106799. https://doi.org/10.1016/j.foodhyd.2021.106799

Ghaderi-Ghahfarokhi, M., Barzegar, M., Sahari, M.A., Gavlighi, H.A. & Gardini, F. (2017). Chitosan-cinnamon essential oil nano-formulation: Application as a novel additive for controlled release and shelf life extension of beef patties. *International Journal of Biological Macromolecules, 102*, 19-28. https://doi.org/10.1016/j.ijbiomac.2017.04.002

Ghasemlou, M.; Khodaiyan, F.; Oromiehie, A. & Yarmand, M.S. (2011). Development and characterisation of a new biodegradable edible film made from kefiran, an exopolysaccharide obtained from kefir grains. *Food Chemistry*, *127(4)*, 1496-1502. https://doi.org/10.1016/j.foodchem.2011.02.003

Gomes, G.M., Bigon, J.P., Montoro, F.E. & Lona, L.M.F. (2019). Encapsulation of N,N-diethyl-*meta*-toluamide (DEET) via miniemulsion polymerization for temperature controlled release. *Journal of Applied Polymer Science, 136(9),* 47139. https://doi.org/10.1002/app.47139

Gómez-Estaca, J., Aleman, A., Lòpez-Caballero, M.E., Baccan, G.C., Montero, P. & Gómez-Guillén, M.C. (2019). Bioaccessibility and antimicrobial properties of a shrimp demineralization extract blended with chitosan as wrapping material in ready-to-eat raw salmon. *Food Chemistry*, *276*, 342-349. https://doi.org/10.1016/j.foodchem.2018.10.031

Grande-Tovar, C.D.; Serio, A.; Delgado-Ospina, J.; Paparella, A.; Rossi, C. & Chaves-López, C. (2018). Chitosan films incorporated with *Thymus capitatus* essential oil: mechanical properties and antimicrobial activity against degradative bacterial species isolated from tuna (*Thunnus* sp.) and swordfish (*Xiphias gladius*). *Journal of Food Science and Technology*, *55,* 4256-4265. https://doi.org/10.1007/s13197-018-3364-y

Gudjónsdóttir, M., Gacutan Jr., M.D., Mendes, A.C., Chronakis, I.S., Jespersen, L. & Karlsson, A.H. (2015). Effects of electrospun chitosan wrapping for dry-ageing of beef, as studied by microbiological, physicochemical and low-field nuclear magnetic resonance analysis. *Food Chemistry*, *184*, 167-175. https://doi.org/10.1016/j.foodchem.2015.03.088

Guerrero, P., Muxika, A., Zarandona, I. & de la Caba, K. (2019). Crosslinking of chitosan films processed by compression molding. *Carbohydrate Polymers*, *206*, 820-826. https://doi.org/10.1016/j.carbpol.2018.11.064

Gutiérrez, T.J. & González, G. (2017). Effect of Cross-Linking with *Aloe vera* Gel on Surface and Physicochemical Properties of Edible Films Made from Plantain Flour. *Food Biophysics, 12*, 11-22. https://doi.org/10.1007/s11483-016-9458-z

Hafsa, J., ali Smach, M., Khedher, M.R.B., Charfeddine, B., Limem, K., Majdoub, H. & Rouatbi, S. (2016). Physical, antioxidant and antimicrobial properties of chitosan films containing *Eucalyptus globulus* essential oil. *LWT - Food Science and Technology, 68*, 356-364. https://doi.org/10.1016/j.lwt.2015.12.050

Haghighi, H., Licciardello, F., Fava, P., Siesler, H.W. & Pulvirenti, A. (2020). Recent advances on chitosan-based films for sustainable food packaging applications. *Food Packaging and Shelf Life, 26*, 100551. https://doi.org/10.1016/j.fpsl.2020.100551

Hanahan, D. (1983) Studies on transformation of *Escherichia coli* with plasmids. Journal of Molecular Biology, 166(4), 557-580. https://doi.org/10.1016/S0022-2836(83)80284-8

Hann, S.Y.; Cui, H.; Esworthy, T.; Miao, S.; Zhou, X.; Lee, S.J.; Fisher, J.P. & Zhang, L.G. (2019). Recent advances in 3D printing: vascular network for tissue and organ regeneration. *Translational Research*, *211*, 46-63. https://doi.org/10.1016/j.trsl.2019.04.002

Hernandez, H.L.; Souza, J.W. & Appel, E.A. (2021). A Quantitative Description for Designing the Extrudability of Shear-Thinning Physical Hydrogels. *Macromolecular Bioscience*, *21*, 2000295. https://doi.org/10.1002/mabi.202000295

Hinton, T.J.; Jallerat, Q.; Palchesko, R.N.; Park, J.H.; Grodzicki, M.S.; Shue, H.J.; Ramadan, M.H.; Hudson, A.R. & Feinberg, A.W. (2015). Three-dimensional printing of complex biological structures by freeform reversible embedding of suspended hydrogels. *Science Advances*, *1*, e150075. https://doi.org/10.1126/sciadv.1500758

Hou, Y., Shavandi, A., Carne, A., Bekhit, A. A., Ng, T. B., Cheung, R. C. F., & Bekhit, A. E. A. (2016). Marine shells: potential opportunities for extraction of functional and health-promoting materials. *Environmental Science and Technology*, *46*(11-12), 1047-1116. https://doi.org/10.1080/10643389.2016.1202669

Hu, H., Yao, X., Qin, Y., Yong, H. & Liu, J. (2020). Development of multifunctional food packaging by incorporating betalains from vegetable amaranth (*Amaranthus tricolor L.*) into quaternary ammonium chitosan/fish gelatin blend films. *International Journal of Biological Macromolecules*, *159*, 675-684. https://doi.org/10.1016/j.ijbiomac.2020.05.103

Hu, Z. & Gänzle, M.G. (2018). Challenges and opportunities related to the use of chitosan as a food preservative. *Journal of Applied Microbiology*, *126(5)*, 1318-1331. https://doi.org/10.1111/jam.14131

Huang, C. Y., Kuo, C. H., Wu, C. H., Ku, M. W., & Chen, P. W. (2018). Extraction of crude chitosans from squid (*Illex argentinus*) pen by a compressional puffing-pretreatment process and evaluation of their antibacterial activity. *Food Chemistry*, *254*, 217-223. https://doi.org/10.1016/j.foodchem.2018.02.018

Huang, M., Wang, H., Xu, X., Lu, X., Song, X. & Zhou, G. (2020). Effects of nanoemulsion-based edible coatings with composite mixture of rosemary extract and ε-poly-L-lysine on the shelf life of ready-to-eat carbonado chicken. *Food Hydrocolloids*, *102*, 105576. https://doi.org/10.1016/j.foodhyd.2019.105576

Huss, H.H. (2013). Fresh fish quality and quality changes. FAO Fisheries Series No 29 - Primary Source. Nabu Press.

Indurkar, A.; Pandit, A.; Jain, R. & Dandekar, P. (2021). Plant-based biomaterials in tissue engineering. *Bioprinting*, *21*, e00127. https://doi.org/10.1016/j.bprint.2020.e00127

Irawan, A., Barleany, D. R., Jayanudin, Yulvianti, M., Maulana, R. C. & Fitriani, L. Y. (2019). Chitosan active films containing red ginger extract for shelf-life extention and quality retention of milkfish (*chanos chanos*). *AIP Conference Proceedings 2085*, 020032. https://doi.org/10.1063/1.5095010

Isfahani, F.R., Tavanai, H. & Morshed, M. (2017). Release of Aloe vera from Electrospun Aloe vera-PVA Nanofibrous Pad. *Fibers and Polymers, 18 (2)*, 264-271. https://doi.org/10.1007/s12221-017-6954-9

Istúriz-Zapata, M. A., Hernandez-Lopez, M., Correa-Pacheco, Z. N. & Barrera-Necha, L. L. (2020). Quality of cold-stored cucumber as affected by nanostructured coatings of chitosan with cinnamon essential oil and cinnamaldehyde. *LWT-Food Science and Technology*, *123*, 109089. https://doi.org/10.1016/j.lwt.2020.109089

Iturriaga, L., Olabarrieta, I., Castellan, A., Gardrat, C., Coma, V. (2014). Active naringin-chitosan films: Impact of UV irradiation. *Carbohydrate Polymers*, *110*, 374-381. https://doi.org/10.1016/j.carbpol.2014.03.062

Jahromi, H. K., Farzin, A., Hasanzadeh, E., Barough, S. E., Mahmoodi, N., Najafabadi, M. R. H., Farahani, M. S., Mansoori, K., Shirian, S. & Ai, J. (2020). Enhanced sciatic nerve regeneration by poly-L-lactic acid/multi-wall carbon nanotube neural guidance conduit containing Schwann cells and curcumin encapsulated chitosan nanoparticles in rat. *Materials Science & Engineering C, 109*, 110564. https://doi.org/10.1016/j.msec.2019.110564

Janarthanan, G.; Shin, H.S.; Kim, I.G.; Ji, P.; Chung, E.J.; Lee, C. & Noh, I. (2020). Self-crosslinking hyaluronic acid–carboxymethylcellulose hydrogel enhances multilayered 3D-printed construct shape integrity and mechanical stability for soft tissue engineering. *Biofabrication*, *12*, 045026. https://doi.org/10.1088/1758-5090/aba2f7

Jha, P. (2020). Effect of grapefruit seed extract ratios on functional properties of corn starch-chitosan bionanocomposite films for active packaging. *International Journal of Biological Macromolecules, 163*, 1546-1556. https://doi.org/10.1016/j.ijbiomac.2020.07.251

Ji, F.; You, L.; Wang, L.; Liu, Z.; Zhang, Y. & Lv, S. (2016). Layer-by-layer assembled chitosan-based antibacterial films with improved stability under alkaline conditions. *Industrial & Engineering Chemistry Research***,** *55*, 10664-10670. https://doi.org/10.1021/acs.iecr.6b02080

Jiang, Y., Yu, L., Hu, Y., Zhu, Z., Zhuang, C., Zhao, Y. & Zhong, Y. (2020). The preservation performance of chitosan coating with different

molecular weight on strawberry using electrostatic spraying technique. *International Journal of Biological Macromolecules, 151*, 278-285. https://doi.org/10.1016/j.ijbiomac.2020.02.169

Kanatt, S.R., & Makwana, S.H. (2020). Development of active, water-resistant carboxymethyl cellulose-poly vinyl alcohol-*Aloe vera* packaging film. *Carbohydrate Polymers, 227*, 115303. https://doi.org/10.1016/j.carbpol.2019.115303

Karoui, R. & Hassoun, A. (2017). Efficiency of Rosemary and Basil Essential Oils on the Shelf-Life Extension of Atlantic Mackerel (*Scomber scombrus*) Fillets Stored at 2°C. *Journal of AOAC International, 100(2)*, 335-344. https://doi.org/10.5740/jaoacint.16-0410

Kim, D.; Lee, J. & Kim, G. **(**2020**).** Biomimetic gelatin/HA biocomposites with effective elastic properties and 3D-structural flexibility using a 3D-printing process. *Additive Manufacturing*, *36*, 101616. https://doi.org/10.1016/J.ADDMA.2020.101616

Kuai, L., Liu, F., Ma, Y., Goff, H.D. & Zhong, F. (2020). Regulation of nano-encapsulated tea polyphenol release from gelatin films with different Bloom values. *Food Hydrocolloids*,108, 106045. https://doi.org/10.1016/j.foodhyd.2020.106045

Kumar, S., Mukherjee, A. & Dutta, J. (2020). Chitosan based nanocomposite films and coatings: Emerging antimicrobial food packaging alternatives. *Trends in Food Science & Technology, 97*, 196-209. https://doi.org/10.1016/j.tifs.2020.01.002

Kurek, M., Hlupić, L., Elez Garofulić, I., Descours, E., Ščetar, M., Galić, K. (2019). Comparison of protective supports and antioxidative capacity of two bio-based films with revalorised fruit pomaces extracted from blueberry and red grape skin. *Food Packaging and Shelf Life*, *20*, 100315. https://doi.org/10.1016/j.fpsl.2019.100315

Lamarra, J., Giannuzzi, L., Rivero, S. & Pinotti, A. (2017). Assembly of chitosan support matrix with gallic acid-functionalized nanoparticles. *Materials Science and Engineering C, 79*, 848-859. https://doi.org/10.1016/j.msec.2017.05.104

Le Costaouëc, T.; Cérantola, S.; Ropartz, D.; Ratiskol, J.; Sinquin, C.; Colliec-Jouault, S. & Boisset, C. (2012). Structural data on a bacterial exopolysaccharide produced by a deep-sea *Alteromonas macleodii* strain. *Carbohydrate Polymers*, *90(1)*, 49–59. https://doi.org/10.1016/j.carbpol.2012.04.059

Leceta, I., Guerrero, P., Ibarburu, I., Dueñas, M.T. & de la Caba, K. (2013). Characterization and antimicrobial analysis of chitosan-based films. *Journal of Food Engineering, 116(4)*, 889-899. https://doi.org/10.1016/j.jfoodeng.2013.01.022

Leceta, I., Molinaro, S., Guerrero, P., Kerry, J. P., & de la Caba, K. (2015). Quality attributes of map packaged ready-to-eat baby carrots by using chitosan-based coatings. *Postharvest Biology and Technology, 100,* 142-150. https://doi.org/10.1016/j.postharvbio.2014.09.022

Leceta, I., Urdanpilleta, M., Zugasti, I., Guerrero, P., & de la Caba, K. (2018). Assessment of gallic acid-modified fish gelatin formulations to

optimize the mechanical performance of films. *International Journal of Biological Macromolecules, 120,* 2131-2136. https://doi.org/10.1016/j.ijbiomac.2018.09.081

Lee, J.S., Jahurul, M.H.A., Pua, V.C., Shapawi, R. & Chan, P.T. (2019). Effects of chitosan and ascorbic acid coating on the chilled tilapia fish (*Oreochromis niloticus*) fillet. *Journal of Physics: Conference Series, 1358*, 012009. https://doi.org/10.1088/1742-6596/1358/1/012009

Lee, J.K., Patel, S.K.S., Sung, B.H. & Kalia, V.C. (2020). Biomolecules from municipal and food industry wastes: An overview. *Bioresource Technology, 298*, 122346. https://doi.org/10.1016/j.biortech.2019.122346

Lekjing, S. (2016). A chitosan-based coating with or without clove oil extends the shelf life of cooked pork sausages in refrigerated storage. *Meat Science, 111,* 192-197. https://doi.org/10.1016/j.meatsci.2015.10.003

Li, G.-B., Wang, J. & Kong, X.-P. (2020). Coprecipitation-based synchronous pesticide encapsulation with chitosan for controlled spinosad release. *Carbohydrate Polymers, 249*, 116865. https://doi.org/10.1016/j.carbpol.2020.116865

Li, Q.; Xu, S.; Feng, Q.; Dai, Q.; Yao, L.; Zhang, Y.; Gao, H.; Dong, H.; Chen, D. & Cao, X. (2021). 3D printed silk-gelatin hydrogel scaffold with different porous structure and cell seeding strategy for cartilage regeneration. *Bioactive Materials*, *6*, 3396-3410. https://doi.org/10.1016/j.bioactmat.2021.03.013

Liang, J., Yan, H., Zhang, J., Dai, W., Gao, X., Zhou, Y., Wan, X. & Puligundla, P. (2017). Preparation and characterization of antioxidant

edible chitosan films incorporated with epigallocatechin gallate nanocapsules. Carbohydrate Polymers, 171, 300-306. 10.1016/j.carbpol.2017.04.081

Limchoowong, N., Sricharoen, P., Techawongstien, S., & Chanthai, S. (2016). An iodine supplementation of tomato fruits coated with an edible film of the iodide-doped chitosan. *Food Chemistry, 200,* 223-229. https://doi.org/10.1016/j.foodchem.2016.01.042

Liu, J.; Sun, L.; Xu, W.; Wang, Q.; Yu, S. & Sun, J. (2019). Current advances and future perspectives of 3D printing natural-derived biopolymers. *Carbohydrate Polymers*, *207*, 297-316. https://doi.org/10.1016/j.carbpol.2018.11.077

Liu, L. & Ciftci, O.N. (2021). Effects of high oil compositions and printing parameters on food paste properties and printability in a 3D printing food processing model. *Journal of Food Engineering*, *288*, 110135. https://doi.org/10.1016/j.jfoodeng.2020.110135

Liu, M., Zhou, Y., Zhang, Y., Yu, C. & Cao, S. (2013). Preparation and structural analysis of chitosan films with and without sorbitol. *Food Hydrocolloids, 33(2)*, 186-191. https://doi.org/10.1016/j.foodhyd.2013.03.003

Liu, Y.; Yu, Y.; Liu, C.; Regenstein, J.M.; Liu, X. & Zhou, P. (2019). Rheological and mechanical behavior of milk protein composite gel for extrusion-based 3D food printing *LWT*, *102*, 338-346. https://doi.org/10.1016/j.lwt.2018.12.053

Liudvinaviciute, D., Rutkaite, R., Bendoraitiene, J., Klimaviciute, R. (2019). Thermogravimetric analysis of caffeic and rosmarinic acid containing

chitosan complexes. *Carbohydrate Polymers*, *222*, 115003. https://doi.org/10.1016/j.carbpol.2019.115003

Long, J.; Etxeberria, A.E.; Nand, A.V.; Bunt, C.R.; Ray, S. & Seyfoddin, A. (2019). A 3D printed chitosan-pectin hydrogel wound dressing for lidocaine hydrochloride delivery. *Materials Science and Engineerong: C*, *104*, 109873. https://doi.org/10.1016/j.msec.2019.109873

Lopes, C., Antelo, L. T., Franco-Uría, A., Alonso, A. A., & Pérez-Martín, R. (2018). Chitin production from crustacean biomass: Sustainability assessment of chemical and enzymatic processes. *Journal of Cleaner Production, 172,* 4140-4151. https://doi.org/10.1016/j.jclepro.2017.01.082

López-Caballero, M. E., Gómez-Guillén, M. C., Pérez-Mateos, M., & Montero, P. (2005). A chitosan-gelatin blend as a coating for fish patties. *Food Hydrocolloids*, *19(2)*, 303-311. https://doi.org/10.1016/j.foodhyd.2004.06.006

López-Caballero, M., Álvarez Torres, M., Sánchez-Fernández, J., & Moral, A. (2002). Photobacterium phosphoreum isolated as a luminescent colony from spoiled fish, cultured in model system under controlled atmospheres. *European Food Research and Technology*, *215(5)*, 390-395. https://doi.org/10.1007/s00217-002-0575-1

López-Caballero, M.E, Sánchez-Fernández, J. & Moral, A. (2001). Growth and metabolic activity of Shewanella putrefaciens maintained under different CO_2 and O_2 concentrations. *International Journal of Food Microbiology*, *64(3)*, 277-287. https://doi.org/10.1016/S0168-1605(00)00473-6

López-Caballero, M.E., Martínez-Alvarez, O., Gómez-Guillén, M.C. & Montero, P. (2006). Effect of natural compounds alternative to commercial antimelanosics on polyphenol oxidase activity and microbial growth in cultured prawns (Marsupenaeus tiger) during chilled storage. *European Food Research and Technology*, *223*, 7-15. DOI:10.1007/s00217-005-0049-3

López-Pérez, M. & Rodriguez-Valera, F. (2016). Pangenome evolution in the marine bacerium *Alteromonas. Genome Biology and Evolution*, *8(5)*, 1556-1570. https://doi.org/10.1093/gbe/evw098

Lu, Y., Li, L., Yang, F. & Zhang, H. (2013). Application of chitosan composite film to sliced fresh Channa argus for shelf life extension. *Advanced Materials Research*, *781-784*, 1550-1557. https://doi.org/10.4028/www.scientific.net/AMR.781-784.1550

Luchese, C.L.; Abdalla, V.F.; Spada, J.C. & Tessaro, I.C. (2018). Evaluation of blueberry residue incorporated cassava starch film as pH indicator in different simulants and foodstuffs. *Food Hydrocolloids*, 82, 209-218. https://doi.org/10.1016/j.foodhyd.2018.04.010

Lun'kov, A.P., Shagdarova, B.T., Zhikova, Y.V., Il'ina, A.V., & Varlamov, V.P. (2018). Properties of functional films based on chitosan derivative with gallic acid. *Applied Biochemistry and Microbiology*, *54*, 484-490. https://doi.org/10.1134/S0003683818050137

Bruschi, M.L. Strategies to Modify the Drug Release from Pharmaceutical Systems. In M.L. Bruschi (Eds.), Mathematical models of drug release, Sawston: Woodhead Publishing, 2015, pp. 63-86. https://doi.org/10.1016/B978-0-08-100092-2.00005-9

Ma, T.; Lv, L.; Ouyang, C.; Hu, X.; Liao, X.; Song, Y. & Hu, X. (2021). Rheological behavior and particle alignment of cellulose nanocrystal and its composite hydrogels during 3D printing. *Carbohydrate Polymers*, *253*, 117217. https://doi.org/10.1016/j.carbpol.2020.117217

Ma, X., Qiao, C., Wang, X., Yao, J. & Xu, J. (2019). Structural characterization and properties of polyols plasticized chitosan films. *International Journal of Biological Macromolecules, 135*, 240-245. https://doi.org/10.1016/j.ijbiomac.2019.05.158

Maciel, V.B.V., Yoshida, C.M.P. & Franco, T.T. (2015). Chitosan/pectin polyelectrolyte complex as a pH indicator. *Carbohydrate Polymers, 132*, 537-545. https://doi.org/10.1016/j.carbpol.2015.06.047

Maghami, M., Motalebi, A.A. & Anvar, S.A.A. (2019). Influence of chitosan nanoparticles and fennel essential oils (*Foeniculum vulgare*) on the shelf life of *Huso huso* fish fillets during the storage. *Food Science and Nutrition*, 7, 3030-3041. https://doi.org/10.1002/fsn3.1161

Magnaghi, L.R., Zanoni, C., Alberti, G., Quadrelli, P. & Biesuz, R. (2022). Towards intelligent packaging: BCP-EVOH@ optode for milk freshness measurement. *Talanta, 241*, 123230. https://doi.org/10.1016/j.talanta.2022.123230

Mahendiran, B.; Muthusamy, S.; Sampath, S.; Jaisankar, S.N.; Popat, K.C.; Selvakumar, R. & Krishnakumar, G.S. (2021). Recent trends in natural polysaccharide based bioinks for multiscale 3D printing in tissue regeneration: A review. *International Journal of Biological Macromolecules*, *183*, 564-588. https://doi.org/10.1016/j.ijbiomac.2021.04.179

Manzoor, M.; Singh, J.; Bandral, J.D.; Gani, A. & Shams, R. (2020). Food hydrocolloids: Functional, nutraceutical and novel applications for delivery of bioactive compounds. *International Journal of Biological Macromolecules*, *165*, 554-567. https://doi.org/10.1016/j.ijbiomac.2020.09.182

Martínez, O., Salmerón, J., Epelde, L., Vicente, M.S., & de Vega, C. (2018). Quality enhancement of smoked sea bass (*Dicentrarchus labrax*) fillets by adding resveratrol and coating with chitosan and alginate edible films. *Food Control, 85*, 168-176. https://doi.org/10.1016/j.foodcont.2017.10.003

Martínez-Alvarez, O., Chamorro, S. & Brenes, A. (2015). Protein hydrolysates from animal processing by-products as a source of bioactive molecules with interest in animal feeding: A review. *Food Research International, 73*, 204-212. https://doi.org/10.1016/j.foodres.2015.04.005

Marudova, M.; MacDougal, A.J. & Ring, S.G. (2004). Pectin–chitosan interactions and gel formation. *Carbohydrate Research, 339*, 1933-1939. https://doi.org/10.1016/j.carres.2004.05.017

Matet, M., Heuzey, M.-C., Pollet, E., Ajji, A. & Averous, L. (2013). Innovative thermoplastic chitosan obtained by thermo-mechanical mixing with polyol plasticizers. *Carbohydrate Polymers, 95(1)*, 241-251. https://doi.org/10.1016/j.carbpol.2013.02.052

Mauricio-Sánchez, R.A.; Salazar, R.; Luna-Bárcenas, J.G. & Mendoza-Galván, A. (2018). FTIR spectroscopy studies on the spontaneous neutralization of chitosan acetate films by moisture conditioning. *Vibrational Spectroscopy*, *94*, 1-6. https://doi.org/10.1016/j.vibspec.2017.10.005

Meena, R.A.A., Banu, J.R., Kannah, R.Y., Yogalakshmi, K.N. & Kumar, G. (2020). Biohythane production from food processing wastes - Challenges and perspectives. *Bioresource Technology, 298*, 122449. https://doi.org/10.1016/j.biortech.2019.122449

Mendes, A. C. & Pedersen, G. A. (2021). Perspectives on sustainable food packaging: is bio-based plastics a solution? *Trends in Food Science & Technology, 112*, 839-846. https://doi.org/10.1016/j.tifs.2021.03.049

Merz, B., Capello, C., Leandro, G.C., Moritz, D.E., Monteiro, A.R. & Valencia, G.A. (2020). A novel colorimetric indicator film based on chitosan, polyvinyl alcohol and anthocyanins from jambolan (*Syzygium cumini*) fruit for monitoring shrimp freshness. *International Journal of Biological Macromolecules, 153*, 625-632. https://doi.org/10.1016/j.ijbiomac.2020.03.048

Minh, N.C., Cuong, N.H., Phuong, P.T.D., Schwarz, S., Stevens, W.F., Hoa, N.V. & Trung, T.S. (2017). Swelling-assisted reduction of chitosan molecular weight in the solid state using hydrogen peroxide. Polymer Bulletin, 74, 3077-3087. https://doi.org/10.1007/s00289-016-1880-3

Minh, N.C., Nguyen, V.H., Schwarz, S., Stevens, W.F. & Trung, T.S. (2019). Preparation of water soluble hydrochloric chitosan from low molecular weight chitosan in the solid state. International Journal of Biological Macromolecules, 121, 718-726. https://doi.org/10.1016/j.ijbiomac.2018.10.130

Miranda, J. M., Carrera, M., Pastén, A., Vega-Gálvez, A., Barros-Velázquez, J. & Aubourg, S. P. (2018). The Impact of Quinoa (*Chenopodium*

quinoa Willd.) Ethanolic Extracts in the Icing Medium on Quality Loss of Atlantic Chub Mackerel (*Scomber colias*) Under Chilling Storage. *European Journal Lipid Science and Technology, 120*, 1800280. https://doi.org/10.1002/ejlt.201800280

Mirón-Mérida, V.A., Yáñez-Fernández, J., Montañez-Barragán, B., & Huerta, B.E.B. (2019). Valorization of coffee parchment waste (Coffea arabica) as a source of caffeine and phenolic compounds in antifungal gellan gum films. *LWT-Food Science and Technology, 101,* 167-174. https://doi.org/10.1016/j.lwt.2018.11.013

Mohamed, S.S.; Amer, S.K.; Selim, M.S. & Rifaat, H.M. (2018). Characterization and applications of exopolysaccharide produced by marine *Bacillus altitudinis* MSH2014 from Ras Mohamed, Sinai, Egypt. *Egyptian Journal of Basic and Applied Science*, *5(4)*, 204-209. https://doi.org/10.1016/j.ejbas.2018.05.009

Montoya, J.; Medina, J.; Molina, A.; Gutiérrez, J.; Rodríguez, B. & Marín, R. (2021). Impact of viscoelastic and structural properties from starch-mango and starch-arabinoxylans hydrocolloids in 3D food printing. *Additive Manufacturing*, *39*, 101891. https://doi.org/10.1016/j.addma.2021.101891

Muxika, A., Etxabide, A., Uranga, J., Guerrero, P., & de la Caba, K. (2017). Chitosan as a bioactive polymer: Processing, properties and applications. *International Journal of Biological Macromolecules, 105*, 1358-1368. https://doi.org/10.1016/j.ijbiomac.2017.07.087

Nasrollahzadeh, M., Sajjadi, M., Iravani, S. & Varma, R.S. (2021). Starch, cellulose, pectin, gum, alginate, chitin and chitosan derived (nano) materials for sustainable water treatment: A review. *Carbohydrate Polymers, 251*, 116986. https://doi.org/10.1016/j.carbpol.2020.116986

Negm, N.A.; Hefni, H.H.H.; Abd-Elaal, A.A.A.; Badr, E.A. & Kana, M.T.H.A. (2020). Advancement on modification of chitosan biopolymer and its potential applications. *International Journal of Biological Macromolecules, 152*, 681-702. https://doi.org/10.1016/j.ijbiomac.2020.02.196

Nikolic, M. V., Vasiljevic, Z. Z., Auger, S. & Vidic, J. (2021). Metal oxide nanoparticles for safe active and intelligent food packaging. *Trends in Food Science & Technology*, *116*, 655-668. https://doi.org/10.1016/j.tifs.2021.08.019

Niu, X., Liu, A., Liu, C., Zhang, C., Low, S. S. & Show, P. L. (2021). Small Laccase from *Streptomyces coelicolor* catalyzed chitosan-pectin blending film for hazardous gas removal. *Environmental Technology & Innovation 23*, 101690. https://doi.org/10.1016/j.eti.2021.101690

Norcino, L.B.; de Oliveira, J.E.; Moreira, F.K.V.; Marconcini, J.M. & Mattoso, L.H.C. (2018). Rheological and thermo-mechanical evaluation of bio-based chitosan/pectin blends with tunable ionic cross-linking. *International Journal of Biological Macromolecules*, *118*, 1817-1823. https://doi.org/10.1016/j.ijbiomac.2018.07.027

Ochoa-Yepes, O., Di Giogio, L., Goyanes, S., Mauri, A., & Fama, L. (2019). Influence of process (extrusion/thermo-compression, casting) and lentil protein content on physicochemical properties of starch films.

Carbohydrate Polymers, 208, 221-231. https://doi.org/10.1016/j.carbpol.2018.12.030

Olatunde, O. O. & Benjakul, S. (2018). Nonthermal Processes for Shelf-Life Extension of Seafoods: A Revisit. *Comprehensive Reviews in Food Science and Food Safety*, *17*, 892-904. https://doi.org/10.1111/1541-4337.12354

Oryan, A., Kamali, A., Moshiri, A., Baharvand, H., & Daemi, H. (2018). Chemical crosslinking of biopolymeric scaffolds: Current knowledge and future directions of crosslinked engineered bone scaffolds. *International Journal of Biological Macromolecules, 107*, 678-688. https://doi.org/10.1016/j.ijbiomac.2017.08.184

Otero, L., Pérez-Mateos, M., Holgado, F., Márquez-Ruiz, G. & López-Caballero, M.E. (2019). Hyperbaric cold storage: Pressure as an effective tool for extending the shelflife of refrigerated mackerel (*Scomber scombrus*, L.). *Innovative Food Science and Emerging Technologies*, *51*, 41-50. https://doi.org/10.1016/j.ifset.2018.05.003

Oucif, H., Miranda, J.M., Mehidi, S.A., Abi-Ayad, S.M.E.A., Barros-Velázquez, J. & Aubourg, S.P. (2018). Effectiveness of a combined ethanol-aqueous extract of alga *Cystoseira compressa* for the quality enhancement of a chilled fatty fish species. *European Food Research and Technology, 244(2)*, 291-299. https://doi.org/10.1007/s00217-017-2955-6

Ozaki, M.M., Munekata, P.E.S., Lopes, A.S., do Nascimento, M.S., Pateiro, M., Lorenzo, J.M. & Pollonio, M.A.R. (2020). Using chitosan and radish powder to improve stability of fermented cooked sausages. *Meat Science, 167*, 108165. https://doi.org/10.1016/j.meatsci.2020.108165

Pachapur, V. L., Guemiza, K., Rouissi, T., Sarma, S. J., & Brar, S. K. (2015). Novel biological and chemical methods of chitin extraction from crustacean waste using saline water. *Journal of Chemical Technology and Biotechnology, 91*(8), 2331-2339. https://doi.org/10.1002/jctb.4821

Paparella, A., Mazzarrino, G., Chaves-López, C., Rossi, C., Sacchetti, G., Guerrieri, O., & Serio, A. (2016). Chitosan boosts the antimicrobial activity of *Origanum vulgare* essential oil in modified atmosphere packaged pork. *Food Microbiology, 59,* 23-31. https://doi.org/10.1016/j.fm.2016.05.007

Pasini Cabello, S.D., Ochoa, N.A., Takara, E.A., Mollá, S. & Compañ, V. (2017). Influence of Pectin as a green polymer electrolyte on the transport properties of Chitosan-Pectin membranes. *Carbohydrate Polymers, 157*, 1759-1768. 10.1016/j.carbpol.2016.11.061

Pastor, C., Sánchez-González, L., Chiralt, A., Cháfer, M., & González-Martínez, C. (2013). Physical and antioxidant properties of chitosan and methylcellulose based films containing resveratrol. *Food Hydrocolloids, 30(1)*, 272-280. https://doi.org/10.1016/j.foodhyd.2012.05.026

Pereira, R., Tojeire, A., Vaz, D.C., Mendes, A. & Bártolo, P. (2011). Preparation and Characterization of Films Based on Alginate and Aloe Vera. *International Journal of Polymer Analysis and Characterization, 16*, 449-464. https://doi.org/10.1080/1023666X.2011.599923

Perez-Puyana, V.; Rubio-Valle, J.F.; Jiménez-Rosado, M.; Guerrero, A. & Romero, A. (2020). Chitosan as a potential alternative to collagen for the development of genipin-crosslinked scaffolds, *Reactive and Functional*

Polymers, *146*, 104414. https://doi.org/10.1016/j.reactfunctpolym.2019.104414

Pieczywek, P.M.; Cieśla, J.; Płaziński, W. & Zdunek, A. (2021). Aggregation and weak gel formation by pectic polysaccharide homogalacturonan. *Carbohydrate Polymers*, *256*, 117566. https://doi.org/10.1016/j.carbpol.2020.117566

Pinzon, M.I., Garcia, O.R. & Villa, C.C. (2018). The influence of *Aloe vera* gel incorporation on the physicochemical and mechanical properties of banana starch-chitosan edible films. *Journal of the Science of Food Agriculture, 98*, 4042-4049. https://doi.org/10.1002/jsfa.8915

Pirsa, S., Sani, I. K. & Mirtalebi, S. S. (2022). Nano-biocomposite based color sensors: Investigation of structure, function, and applications in intelligent food packaging. *Food Packaging and Shelf Life, 31*, 100789. https://doi.org/10.1016/j.fpsl.2021.100789

Prajapati, A.K., Das, S. & Mondal, M.K. (2020). Exhaustive studies on toxic Cr(VI) removal mechanism from aqueous solution using activated carbon of *Aloe vera* waste leaves. *Journal of Molecular Liquids, 307*, 112956. https://doi.org/10.1016/j.molliq.2020.112956

Priyadarshi, R., Sauraj, Kumar, B., Deeba, F., Kulshreshtha, A., & Negi, Y. S. (2018). Chitosan films incorporated with Apricot (*Prunus armeniaca*) kernel essential oil as active food packaging material. *Food Hydrocolloids, 85*, 158-166. https://doi.org/10.1016/j.foodhyd.2018.07.003

Priyadarshi, R.; Kim, S.M & Rhim, J.W. (2021). Pectin/pullulan blend films for food packaging: Effect of blending ratio *Food Chemistry*, *347*, 129022. https://doi.org/10.1016/j.foodchem.2021.129022

Qin, Y., Liu, Y., Yuan, L., Yong, H. & Liu, J. (2019). Preparation and characterization of antioxidant, antimicrobial and pH-sensitive films based on chitosan, silver nanoparticles and purple corn extract. *Food Hydrocolloids, 96*, 102-111. https://doi.org/10.1016/j.foodhyd.2019.05.017

Quitral, V., Donoso, M.L., Ortiz, J., Herrera, M.V., Araya, H. & Aubourg, S. P. (2009). Chemical changes during the chilled storage of Chilean jack mackerel (*Trachurus murphyi*): Effect of a plant-extract icing system. *LWT - Food Science and Technology, 42(8),* 1450-1454. https://doi.org/10.1016/j.lwt.2009.03.005

Raghavendra, G.M., Jung, J., Kim, D., & Seo, J. (2016). Microwave assisted antibacterial chitosan-silver nanocomposite films. *International Journal of Biological Macromolecules*, *84*, 281-288. https://doi.org/10.1016/j.ijbiomac.2015.12.026

Rahman, S., Carter, P. & Bhattarai, N. (2017). Aloe Vera for Tissue Engineering Applications. *Journal of Functional Biomaterials, 8(1)*, 6. https://doi.org/10.3390/jfb8010006

Ramírez-Guerra, H.E., Castillo-Yañez, F.J., Montaño-Cota, E.A., Ruíz-Cruz, S., Marquez-Rios, E., Canizales-Rodriguez, Torres-Arreola, W., Montoya-Camacho, N. & Ocaño-Higuera, V.M. (2018). Protective effect of an edible tomato plant extract/chitosan coating on the quality and shelf life

of sierra fish fillets. *Journal of Chemistry* 2018, 2436045. https://doi.org/10.1155/2018/2436045

Rasente, R.Y., Imperiale, J.C., Lázaro-Martínez, J.M., Gualco, L., Oberkersch, R., Sosnik, A. & Calabrese, G.C. (2016). Dermatan sulfate/chitosan polyelectrolyte complex with potential application in the treatment and diagnosis of vascular disease. *Carbohydrate Polymers, 144*, 362-370. https://doi.org/10.1016/j.carbpol.2016.02.046

Rashidova, S. Sh.; Milusheva, R. Yu.; Semenova, L.N.; Mukhamedjanova, M.Yu.; Voropaeva, N.L.; Vasilyeva, S.; Faizieva, R. & Ruban, I.N. (2004). Characteristics of Interactions in the Pectin–Chitosan System. *Chromatographia*, *59*, 779-782. https://doi.org/10.1365/s10337-004-0289-6

Raspo, M.A., Gomez, C.G., & Andreatta A.E. (2018). Optimization of antioxidant, mechanical and chemical physical properties of chitosan-sorbitol-gallic acid films by response surface methodology. *Polymer Testing, 70,* 180-187. https://doi.org/10.1016/j.polymertesting.2018.07.003

Reizabal, A., Costa, C. M., Pereira, N., Pérez-Álvarez, L., Vilas-Vilela, J.-L. & Lanceros-Méndez, S. (2020). Silk Fibroin Based Magnetic Nanocomposites for Actuator Applications. *Advanced Engineering Materials, 22*, 2000111. https://doi.org/10.1002/adem.202000111

Resch, J.J. & Daubert, C.R. (2002). Rheological and physicochemical properties of derivatized whey protein concentrate powders *International Journal of Food Properties*, *5(2)*, 419-434. https://doi.org/10.1081/JFP-120005795

Reyes, J. E., Tabilo-Munizaga, G., Pérez-Won, M., Maluenda, D. & Roco, T. (2015). Effect of high hydrostatic pressure (HHP) treatments on microbiological shelf-life of chilled Chilean jack mackerel (*Trachurus murphyi*). *Innovative Food Science and Emerging Technologies*, *29*, 107-112. https://doi.org/10.1016/j.ifset.2015.01.010

Riezk, A.; Raynes, J.G.; Yardley, V.; Murdan, S. & Croft, S. L. (2020). Activity of chitosan and its derivatives against *Leishmania major* and *Leishmania mexicana in vitro*. *Antimicrobial Agents and Chemotherapy*, *64*, e01772-19. doi: 10.1128/AAC.01772-19

Rinaudo, M. (2006). Chitin and chitosan: Properties and applications. Progress in Polymer Science, 31(7), 603-632. https://doi.org/10.1016/j.progpolymsci.2006.06.001

Robinson, S.S.; O'Brien, K.W.; Zhao, H.; Peele, B.N.; Larson, C.M.; MacMurray, B.C.; Van Meerbeek, I.M.; Dunham, S.N. & Shepherd, R.F. (2015). Integrated soft sensors and elastomeric actuators for tactile machines with kinesthetic sense. *Extreme Mechanics Letters*, *5*, 47-53. https://doi.org/10.1016/j.eml.2015.09.005

Roca, C.; Lehmann, M.; Torres, C.A.V; Baptista, S.; Gaudê Ncio, S.P.; Freitas, F. & Reis, M.A.M. (2016). Exopolysaccharide production by a marine *Pseudoalteromonas* sp. strain isolated from Madeira Archipelago ocean sediments. *New Biotechnology*, *33(4)*, 460-466. https://doi.org/10.1016/j.nbt.2016.02.005

Rodríguez, O., Losada, V., Aubourg, S.P. & Barros-Velázquez, J. (2005). Sensory, microbial and chemical effects of a slurry ice system on horse

mackerel (*Trachurus trachurus*). *Journal of the Science of Food and Agriculture, 85(2)*, 235-242. https://doi.org/10.1002/jsfa.1960

Rougeaux, H., Pichon, R., Kervarec, N., Raguénès, G.H.C. & Guezennec, J.G. (1996). Novel bacterial exopolysaccharides from deep-sea hydrothermal vents. Carbohydrate Polymimers, 31(4), 237-242. https://doi.org/10.1016/S0144-8617(96)00079-3

Roy, S. & Rhim J.W. (2020). Preparation of carbohydrate-based functional composite films incorporated with curcumin. *Food Hydrocolloids*, *98*, 105302. https://doi.org/10.1016/j.foodhyd.2019.105302

Rui, L., Xie, M., Hu, B., Zhou, L., Yin, D., & Zeng, X. (2017). A comparative study on chitosan/gelatin composite films with conjugated or incorporated gallic acid. *Carbohydrate Polymers, 173,* 473-481. https://doi.org/10.1016/j.carbpol.2017.05.072

Russo, E.; Selmin, F.; Baldassari, S.; Gennari, C.G.M.; Caviglioli, G.; Cilurzo, F.; Minghetti, P. & Parodi, B. (2016). A focus on mucoadhesive polymers and their application in buccal dosage forms. *Journal of Drug Delivery Science and Technology*, *32*, 113-125. https://doi.org/10.1016/j.jddst.2015.06.016

Sabbah, M., Di Pierro, P., Cammarota, M., Dell'Olmo, E., Arciello, A., & Porta, R. (2019). Development and properties of new chitosan-based films plasticized with spermidine and/or glycerol. *Food Hydrocolloids*, *87*, 245-252. https://doi.org/10.1016/j.foodhyd.2018.08.008

Sahana, T.G. & Rekha, P.D. (2019). A bioactive exopolysaccharide from marine bacteria *Alteromonas sp.* PRIM-28 and its role in cell proliferation

and wound healing *in vitro*. *International Journal of Biological Macromolecules*, *131*, 10-18. https://doi.org/10.1016/j.ijbiomac.2019.03.048

Sahatsapan, N.; Rojanarata, T.; Ngawhirunpat, T.; Opanasopit, P. & Tonglairoum, P. (2018). 6-Maleimidohexanoic acid-grafted chitosan: A new generation mucoadhesive polymer. *Carbohydrate Polymers*, *202*, 258-264. https://doi.org/10.1016/j.carbpol.2018.08.119ç

Sahraee, S., Milani, J.M., Regenstein, J.M. & Kafil, H.S. (2019). Protection of foods against oxidative deterioration using edible films and coatings: A review. *Food Bioscience, 32*, 100451. https://doi.org/10.1016/j.fbio.2019.100451

Salari, M.; Khiabani, M.S.; Mokarram, R.R.; Ghanbarzadeh, B. & Kafil, H.S. (2018). Development and evaluation of chitosan based active nanocomposite films containing bacterial cellulose nanocrystals and silver nanoparticles. *Food Hydrocolloids, 84*, 414-423. https://doi.org/10.1016/j.foodhyd.2018.05.037

Salem, D.M.S.A.; Ismail, M.M. & Aly-Eldeen, M.A. (2019). Biogenic synthesis and antimicrobial potency of iron oxide (Fe_3O_4) nanoparticles using algae harvested from the Mediterranean Sea, Egypt. *Egyptian Journal of Aquatic Research, 45*, 197-204. https://doi.org/10.1016/j.ejar.2019.07.002

Sánchez-González, L.; Chafer, M.; Chiralt, A. & Gonzalez-Martinez, C. (2010). Physical properties of edible chitosan films containing bergamot essential oil and their inhibitory action on *Penicillium italicum*. *Carbohydrate Polymers*, *82*, 277-283. https://doi.org/10.1016/j.carbpol.2010.04.047

Santos, V.P., Marques, N.S.S., Maia, P.C.S.V., de Lima, M.A.B., Franco L.O. & de Campos-Takaki, G.M. (2020). Seafood Waste as Attractive Source of Chitin and Chitosan Production and Their Applications. *International Journal of Molecular Science, 21*, 4290. https://doi.org/10.3390/ijms21124290

Sarjit, A., Wang, Y. & Dykes, G.A. (2015). Antimicrobial activity of gallic acid against thermophilic *Campylobacter* is strain specific and associated with a loss of calcium ions. *Food Microbiology*, *46*, 227-233. https://doi.org/10.1016/j.fm.2014.08.002

Schwab, A.; Levato, R.; D'Este, M.; Piluso, S.; Eglin, D. & Malda, J. (2020). Printability and Shape Fidelity of Bioinks in 3D Bioprinting. *Chemical Reviews*, *120*, 10850-10877. https://doi.org/10.1021/acs.chemrev.0c00084

Sedaghat, F., Yousefzadi, M., Toiserkani, H., & Najafipour, S. (2017). Bioconversion of shrimp waste *Penaeus merguiensis* using lactic acid fermentation: An alternative procedure for chemical extraction of chitin and chitosan. *International Journal of Biological Macromolecules, 104,* 883-888. https://doi.org/10.1016/j.ijbiomac.2017.06.099

Selim, M.S.; Amer, S.K.; Mohamed, S.S.; Mounier, M.M., & Rifaat, H.M. (2018). Production and characterisation of exopolysaccharide from *Streptomyces carpaticus* isolated from marine sediments in Egypt and its effect on breast and colon cell lines. *Journal of Genetic Engineering and Biotechnololy*, *16(1)*, 23-28. https://doi.org/10.1016/j.jgeb.2017.10.014

Serrano-León, J. S., Bergamaschi, K. B., Yoshida, C. M. P., Saldaña, E., Selani, M. M., Rios-Mera, J. D., Alencar, S. M., & Contreras-Castillo, C. J. (2018). Chitosan active films containing agro-industrial residue extracts

for shelf life extension of chicken restructured product. *Food Research International, 108*, 93-100. https://doi.org/10.1016/j.foodres.2018.03.031

Sharma, S. & Tiwari, S. (2020). A review on biomacromolecular hydrogel classification and its applications. *International Journal of Biological Macromolecules, 162*, 737-747. https://doi.org/10.1016/j.ijbiomac.2020.06.110

Shavandi, A., Hu, Z., Teh, S. S., Zhao, J., Carne, A., Bekhit, A., & Bekhit, A. E. D. A. (2017). Antioxidant and functional properties of protein hydrolysates obtained from squid pen chitosan extraction effluent. *Food Chemistry, 227,* 194-201. https://doi.org/10.1016/j.foodchem.2017.01.099

Shin, C.S., Kim, D.Y. & Shin, W.S. (2019). Characterization of chitosan extracted from Mealworm Beetle (*Tenebrio molitor, Zophobas morio*) and Rhinoceros Beetle (*Allomyrina dichotoma*) and their antibacterial activities. *International Journal of Biological Macromolecules, 125*, 72-77. https://doi.org/10.1016/j.ijbiomac.2018.11.242

Shokri, S., Parastouei, K., Taghdir, M. & Abbaszadeh, S. (2020). Application an edible active coating based on chitosan- *Ferulago angulata* essential oil nanoemulsion to shelf life extension of Rainbow trout fillets stored at 4 °C. *International Journal of Biological Macromolecules, 153*, 846-854. https://doi.org/10.1016/j.ijbiomac.2020.03.080

Singh, B.; Sharma, S. & Dhiman, A. (2013). Design of antibiotic containing hydrogel wound dressings: Biomedical properties and histological study of wound healing. *International Journal of Pharmaceutics, 457*, 82-91. https://doi.org/10.1016/j.ijpharm.2013.09.028

Sone, I., Skåra, T. & Olsen, S. H. (2019). Factors influencing post-mortem quality, safety and storage stability of mackerel species: a review. *European Food Research and Technology, 245,* 775-791. https://doi.org/10.1007/s00217-018-3222-1

Soubhagya, A.S.; Moorthi, A. & Prabaharan, M. (2020). Preparation and characterization of chitosan/pectin/ZnO porous films for wound healing *International Journal of Biological Macromolecules*, *157*, 135-145. https://doi.org/10.1016/j.ijbiomac.2020.04.156

Souza, V.G.L., Pires, J.R.A., Vieira, E.T., Coelhoso, I.M., Duarte, M.P. & Fernando, A.L. (2019). Activity of chitosan-montmorillonite bionanocomposites incorporated with rosemary essential oil: From *in vitro* assays to application in fresh poultry meat. *Food Hydrocolloids, 89*, 241-252. https://doi.org/10.1016/j.foodhyd.2018.10.049

Sullivan, D.J., Cruz-Romero, M.C., Hernandez, A.B., Cummins, E., Kerry, J.P. & Morris, M.A. (2020). A novel method to deliver natural antimicrobial coating materials to extend the shelf-life of European hake (*Merluccius merluccius*) fillets. *Food Packaging and Shelf Life, 25*, 100522. https://doi.org/10.1016/j.fpsl.2020.100522

Tabernero, A. & Cardea, S. (2020). Supercritical carbon dioxide techniques for processing microbial exopolysaccharides used in biomedical applications. *Materials Science and Engineering: C*, *112*, 110940. https://doi.org/10.1016/j.msec.2020.110940

Talón, E., Trifkovic, K.T., Nedovic, V.A., Bugarski, B.M., Vargas, M., Chiralt, A. & González-Martínez, C. (2017). Antioxidant edible films based

on chitosan and starch containing polyphenols from thyme extracts. *Carbohydrate Polymers, 157*, 1153-1161. https://doi.org/10.1016/j.carbpol.2016.10.080

Tan, S., Zhong, C. & Langrish, T. (2020). Encapsulation of caffeine in spray-dried micro-eggs for controlled release: The effect of spray-drying (cooking) temperature. *Food Hydrocolloids, 108*, 105979. https://doi.org/10.1016/j.foodhyd.2020.105979

Tang, Y.F.; Du, Y.M.; Hu, X.W.; Shi, X.W. & Kennedy, J.F.. (2007). Rheological characterisation of a novel thermosensitive chitosan/poly(vinyl alcohol) blend hydrogel. *Carbohydrate Polymers*, *67*, 491-499. https://doi.org/10.1016/j.carbpol.2006.06.015

Tapeh, S.M.T., Baei, M.S., & Keshel, S.H. (2021). Synthesis of thermogel modified with biomaterials as carrier for hUSSCs differentiation into cardiac cells: Physicomechanical and biological assessment. *Materials Science & Engineering C, 119*, 111517. https://doi.org/10.1016/j.msec.2020.111517

Tian, K.; Bae, J.; Bakarich, S.E.; Yang, C.; Gately, R.D.; Spinks, G.M.; in het Panhuis, M.; Suo, Z. & Vlassak, J.J. (2017). 3D Printing of Transparent and Conductive Heterogeneous Hydrogel–Elastomer Systems. *Advanced Materials*, *29*, 1604827. https://doi.org/10.1002/adma.201604827

Torpol, K., Sriwattana, S., Sangsuwan, J., Wiriyacharee, P. & Prinyawiwatkul, W. (2019). Optimising chitosan-pectin hydrogel beads containing combined garlic and holy basil essential oils and their

application as antimicrobial inhibitor. *International Journal of Food Science and Technology, 54*, 2064-2074. https://doi.org/10.1111/ijfs.14107

Torres-Giner, S., Wilkanowicz, S., Melendez-Rodriguez, B. & Lagaron, J.M. (2017). Nanoencapsulation of *Aloe vera* in Synthetic and Naturally Occurring Polymers by Electrohydrodynamic Processing of Interest in Food Technology and Bioactive Packaging. *Journal of Agricicultural and Food Chemistry, 65*, 4439-4448. https://doi.org/10.1021/acs.jafc.7b01393

Tsai, R.-Y., Chen, P.-W., Kuo, T.-Y., Lin, C.-M., Wang, D.-M., Hsien, T.-Y. & Hsieh H.-J. (2014). Chitosan/pectin/gum Arabic polyelectrolyte complex: Process-dependent appearance, microstructure analysis and its application. *Carbohydrate Polymers, 101*, 752-759. 10.1016/j.carbpol.2013.10.008

Tsianou, M.; Kjøniksen, A.L.; Thuresson, K. & Nyström, B. (1999). Light Scattering and Viscoelasticity in Aqueous Mixtures of Oppositely Charged and Hydrophobically Modified Polyelectrolytes. *Macromolecules*, *32*, 2974-2982. https://doi.org/10.1021/ma981619c

Tuesta-Chavez, T.; Monteza, J.; Jaimes, M.I.S.; Ruiz-Pacco, G.A.; Changanaqui, K.; Espinoza-Suarez, J.B.; Alarcon, H.; Osorio-Anaya, A.M.; Valderrama-Negrón, A.C. & Sotomayor, M.D.P.T. (2022). Characterization and evaluation of antioxidant and antimicrobial capacity of prepared liquid smoke-loaded chitosan nanoparticles. *Journal of Food Engineering, 319*, 110912. https://doi.org/10.1016/j.jfoodeng.2021.110912

Valencia-Sullca, C., Atarés, L., Vargas, M., & Chiralt, A. (2018). Physical and antimicrobial properties of compression-molded cassava starch-

chitosan films for meat preservation. *Food and Bioprocess Technology*, *11*(7), 1339-1349. https://doi.org/10.1007/s11947-018-2094-5

Venkateswarlu, S., Kumar, B. N., Prathima, B., Anitha, K. & Jyothi, N.V.V. (2015). A novel Green synthesis of Fe_3O_4-Ag core shell recyclable nanoparticles using *Vitis vinifera* stem extract and its enhanced antibacterial performance. *Physica B*, *457*, 30-35. https://doi.org/10.1016/j.physb.2014.09.007

Villanueva, J.G.V.; Huertas, P.A.S.; Galan, F.S.; Rueda, R.J.E.; Triana, J.C.B. & Rodriguez, J.P.C. (2019). Bio-adhesion evaluation of a chitosan-based bone bio-adhesive. *International Journal of Adhesion and Adhesives*, *92*, 80-88. https://doi.org/10.1016/j.ijadhadh.2019.04.009

Vincent, P.; Pignet, P.; Talmont, F.; Bozzi, L.; Fournet, B.; Guezennec, J.; Jeanthon, C. & Prieur D. (1994). Production and characterization of an exopolysaccharide excreted by a deep-sea Alvinella pompejana. *Applied and Environmental Microbiology*, *60*, 4134–4141. https://doi.org/10.1128/aem.60.11.4134-4141.1994

Wang, X., Yong, H., Gao, L., Li, L., Jin, M., & Liu, J. (2019). Preparation and characterization of antioxidant and pH-sensitive films based on chitosan and black soybean seed coat extract. *Food Hydrocolloids*, *89*, 56-66. https://doi.org/10.1016/j.foodhyd.2018.10.019

Wang, Y.; Compaoré-Sérémé, D.; Sawadogo-Lingani, H.; Coda, R.; Katina K. & Maina, N.H. (2019). Influence of dextran synthesized *in situ* on the rheological, technological and nutritional properties of whole grain pearl

millet bread. *Food Chemistry*, *285*, 221-230. https://doi.org/10.1016/j.foodchem.2019.01.126

Wood, P. & Fulcher, R. (1978) Interaction of some dyes with cereal β-glucans. Cereal Chemistry, 55(6), 952-966.

Wu, C., Li, Y., Wang, L., Hu. Y., Chen. J., Liu, D. & Ye, X. (2016). Efficacy of chitosan-gallic acid coating on shelf life extension of refrigerated pacific mackerel fillets. *Food Bioprocess Technology, 9*, 675-685. https://doi.org/10.1007/s11947-015-1659-9

Wu, C., Sun, J., Zheng, P., Kang, X., Chen, M., Li, Y., Ge, Y., Hu, Y. & Pang, J. (2019) Preparation of an intelligent film based on chitosan/oxidized chitin nanocrystals incorporating black rice bran anthocyanins for seafood spoilage monitoring. *Carbohydrate Polymers, 222*, 115006. https://doi.org/10.1016/j.carbpol.2019.115006

Wu, Q.; Therriault, D. & Heuzey, M.C. (2018) Processing and Properties of Chitosan Inks for 3D Printing of Hydrogel Microstructures. *ACS Biomaterials Science & Engineering*, 4(7), 2643-2652. https://doi.org/10.1021/acsbiomaterials.8b00415

Wu, W., Jia, M., Zhang, Z., Chen, X., Zhang, Q., Zhang, W., Li, P., & Chen, L. (2019). Sensitive, selective and simultaneous electrochemical detection of multiple heavy metals in environment and food using a lowcost Fe_3O_4 nanoparticles/fluorinated multi-walled carbon nanotubes sensor. *Ecotoxicology and Environmental Safety, 175*, 243-250. https://doi.org/10.1016/j.ecoenv.2019.03.037

Xia, H.; Ren, M.; Zou, Y.; Qin, S. & Zeng, C. (2020). Novel Biocompatible Polysaccharide-Based Eutectogels with Tunable Rheological, Thermal, and Mechanical Properties: The Role of Water *Molecules*, *25(15)*, 3314. https://doi.org/10.3390/molecules25153314

Yadav, S., Mehrotra, G.K. & Dutta, P.K. (2021). Chitosan based ZnO nanoparticles loaded gallic-acid films for active food packaging. *Food Chemistry, 334*, 127605. https://doi.org/10.1016/j.foodchem.2020.127605

Yang, X., Zhou, Y., Wang, B., Wang, F., Han, P., & Li, L. (2019). Tartary buckwheat extract and chitosan coated tilapia (*Oreochromis Niloticus*) fillets determine their shelf life. *Journal of Food Science*, *84*, 1288-1296. https://doi.org/10.1111/1750-3841.14649

Yeamsuksawat, T., Zhao, H. & Liang, J. (2021). Characterization and antimicrobial performance of magnetic Fe3O4@Chitosan@Ag nanoparticles synthesized via suspension technique. *Materials Today Communications, 28*,102481. https://doi.org/10.1016/j.mtcomm.2021.102481

Yong, H., Wang, X., Bai, R., Miao, Z., Zhang, X., Liu, J. (2019a). Development of antioxidant and intelligent pH-sensing packaging films by incorporating purple-fleshed sweet potato extract into chitosan matrix. *Food Hydrocolloids*, *90*, 216-224. https://doi.org/10.1016/j.foodhyd.2018.12.015

Yong, H., Wang, X., Zhang, X., Liu, Y., Qin, Y., & Liu, J. (2019b). Effects of anthocyanin-rich purple and black eggplant extracts on the physical, antioxidant and pH-sensitive properties of chitosan film. *Food Hydrocolloids, 94*, 93-104. https://doi.org/10.1016/j.foodhyd.2019.03.012

Yu, D., Jiang, Q., Xu, Y. & Xia, W. (2017). The shelf life extension of refrigerated grass carp (*Ctenopharyngodon idellus*) fillets by chitosan coating combined with glycerol monolaurate. *International Journal of Biological Macromolecules, 101*, 448-454. https://doi.org/10.1016/j.ijbiomac.2017.03.038

Zarandona, I., López-Caballero, M.E., Montero, M.P., Guerrero, P., de la Caba, K. & Gómez-Guillén, M.C. (2021). Horse mackerel (*Trachurus trachurus*) fillets biopreservation by using gallic acid and chitosan coatings. *Food Control, 120*, 107511. https://doi.org/10.1016/j.foodcont.2020.107511

Zarandona, I., Puertas, A. I., Dueñas, M. T., Guerrero, P. & de la Caba, K. (2020). Assessment of active chitosan films incorporated with gallic acid. *Food Hydrocolloids, 101*, 105486. https://doi.org/10.1016/j.foodhyd.2019.105486

Zarandona, I.; Bengoechea, C.; Álvarez-Castillo, E.; de la Caba, K.; Guerrero, A. & Guerrero, P. (2021). 3D Printed Chitosan-Pectin Hydrogels: From Rheological Characterization to Scaffold Development and Assessment. *Gels*, *7*, 175. https://doi.org/10.3390/gels7040175

Zarandona, I.; Estupiñán, M.; Pérez, C.; Alonso-Sáez, L.; Guerrero, P. & de la Caba, K. (2020). Chitosan Films Incorporated with Exopolysaccharides from Deep Seawater *Alteromonas* sp. *Marine Drugs*, *18(9)*, 447. https://doi.org/10.3390/md18090447

Zhang, C., Wang, Z., Li, Y., Yang, Y., Ju, X., & He, R. (2019a). The preparation and physiochemical characterization of rapeseed protein

hydrolysate-chitosan composite films. *Food Chemistry, 272,* 694-701. https://doi.org/10.1016/j.foodchem.2018.08.097

Zhang, H., Liang, Y., Li, X. & Kang, H. (2020b). Effect of chitosan-gelatin coating containing nano-encapsulated tarragon essential oil on the preservation of pork slices. *Meat Science, 166*, 108137. https://doi.org/10.1016/j.meatsci.2020.108137

Zhang, H., Ma, X., Liu, Y., Duan, N., Wu, S., Wang, Z. & Xu, B. (2015). Gold nanoparticles enhanced SERS aptasensor for the simultaneous detection of *Salmonella typhimurium* and *Staphylococcus aureus*. *Biosensors and Bioelectronics, 74*, 872-877. https://doi.org/10.1016/j.bios.2015.07.033

Zhang, H., Yun, S., Song, L., Zhang, Y., & Zhao, Y. (2017). The preparation and characterization of chitin and chitosan under large-scale submerged fermentation level using shrimp by-products as substrate. *International Journal of Biological Macromolecules, 96*, 334-339. https://doi.org/10.1016/j.ijbiomac.2016.12.017

Zhang, J., Zou, X., Zhai, X., Huang, X., Jiang, C., & Holmes, M. (2019b). Preparation of an intelligent pH film based on biodegradable polymers and roselle anthocyanins for monitoring pork freshness. *Food Chemistry, 272,* 306-312. https://doi.org/10.1016/j.foodchem.2018.08.041

Zhang, L., Li, Q., Hong, H., & Luo, Y. (2020). Prevention of protein oxidation and enhancement of gel properties of silver carp (*Hypophthalmichthys molitrix*) surimi by addition of protein hydrolysates derived from surimi processing by-products. *Food Chemistry, 316*, 126343. https://doi.org/10.1016/j.foodchem.2020.126343

Zhang, W., Li, X. & Jiang, W. (2020a). Development of antioxidant chitosan film with banana peels extract and its application as coating in maintaining the storage quality of apple. *International Journal of Biological Macromolecules, 154*, 1205-1214. https://doi.org/10.1016/j.ijbiomac.2019.10.275

Zhang, X., Liu, J., Qian, C., Kan, J., & Jin, C. (2019). Effect of grafting method on the physical property and antioxidant potential of chitosan film functionalized with gallic acid. *Food Hydrocolloids, 89,* 1-10. https://doi.org/10.1016/j.foodhyd.2018.10.023

Zhang, X., Liu, J., Yong, H., Qin, Y., Liu, J. & Jin, C. (2020c). Development of antioxidant and antimicrobial packaging films based on chitosan and mangosteen (*Garcinia mangostana L.*) rind powder. *International Journal of Biological Macromolecules, 145*, 1129-1139. https://doi.org/10.1016/j.ijbiomac.2019.10.038

Zhang, Z., Xia, G., Yang, Q., Fan, X. & Lyu, S. (2019). Effects of chitosan-based coatings on storage quality of Chinese shrimp. *Food Science and Nutrition*, 7, 4085-4094. https://doi.org/10.1002/fsn3.1275

Zhao, D.; Jiang, J.; Du, R.; Guo, S.; Ping, W.; Ling, H. & Ge, J. (2019). Purification and characterization of an exopolysaccharide from *Leuconostoc lactis* L2. *International Journal of Biological Macromolecules*, *139*, 1224-1231. https://doi.org/10.1016/j.ijbiomac.2019.08.114

Zhao, Y., Teixeira, J.S., Gänzle, M.M., & Saldaña, M.D.A. (2018). Development of antimicrobial films based on cassava starch, chitosan and

gallic acid using subcritical water technology. *The Journal of Supercritical Fluids, 137*, 101-110. https://doi.org/10.1016/j.supflu.2018.03.010

Zheng, R., Xu, X., Xing, J., Cheng, H., Zhang, S., Shen, J. & Li, J. (2020). Quality evaluation and characterization of specific spoilage organisms of Spanish mackerel by high-throughput sequencing during 0 °C cold chain logistics. *Foods*, *9(3)*, 312. https://doi.org/10.3390/foods9030312

Zivanovic, S., Chi, S. & Draughon, A. F. (2005). Antimicrobial activity of chitosan films enriched with essential oils. Journal of Food Science, 70, M45-M51. https://doi.org/10.1111/j.1365-2621.2005.tb09045.x

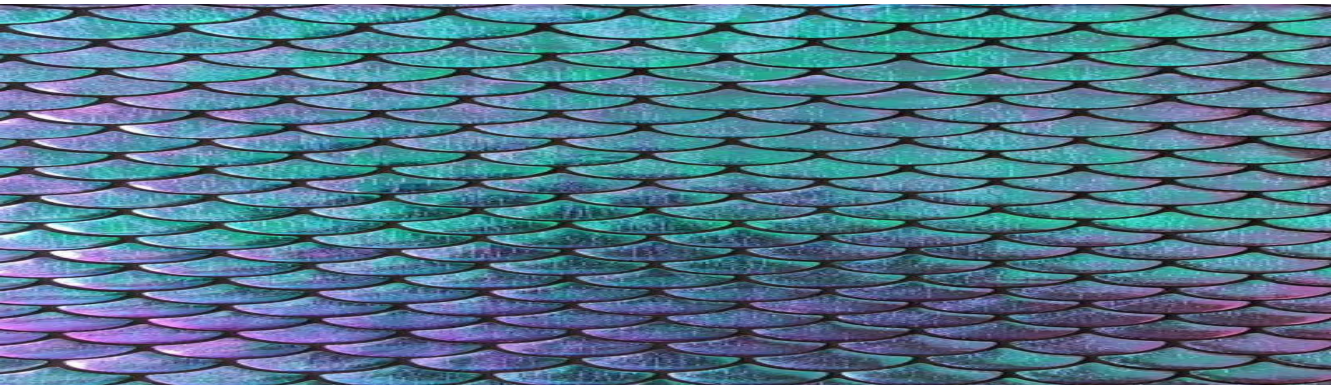

BioMat